©

Cloud screening over sea-ice and marginal ice zones: Final Report.

Issue date	*ITT no*	*client*
21/06/2017	15/211424	EUMETSAT

Document Reference
gkt050_021_DL4_1-1

	name	*Date*
Checked by Project Manager		

Editing History

Issue	*Authors*	*Date*	*Note*
1.0	G.L.Liberti	14/04/2017	First Version
1.1	G.L.Liberti, M.Sist, M.Picchiani	21/06/2017	Revised Version

Table of Content

1. Introduction

This report describes the activities carried out within the frame of the EUMETAT ITT n° 15/211424: '*Sea-ice cloud screening for Copernicus Sentinel-3 Sea and Land Surface Temperature Radiometer*'. The objective of the study was to '*recommend appropriate algorithms for the Sea and Land Surface Temperature Radiometer (SLSTR) and derive and supply the relevant auxiliary probability distribution functions.'*
A first phase of the study consisted in reviewing existing literature on the subject. This phase was documented, according with the statement of work, with a dedicated Report. Only a summary of relevant information is reported in this Final Report that is dedicated to the description of the process to generate the PDFs for the Bayesian sea ice-cloud classification algorithm.

A Bayesian approach to classify SLSTR pixels over polar oceans is presented. The approach is based on PDF's estimating the probability for a pixel, given a set of measured values for selected variables, to fall in one of the following three classes:

- Clear Ocean (SEA),
- Cloudy (CLD)
- Sea Ice (ICE).

PDF's are generated by analysing archived MODIS products. MODIS products were selected because of:

- the long available time series of two instruments,
- the complexity of the cloud detection algorithm that includes specific tests (e.g. 6.7 µm channel based one) for polar conditions
- the large validation effort that also has taken full advantage of *Aqua* being part of the A-Train.

The validity of using MODIS as proxy for SLSTR is discussed including: the different spectral response of corresponding channels and the possibility to simulate of dual view observations quasi-simultaneous (<15') *Aqua* and *Terra* co-located observations. L1 radiances and corresponding MODIS cloud detection and ice/snow products are used to build the PDF's. In addition to the observation geometry different PDF's are generated for 2.5 K width SST classes, where the SST value is taken from the *Aqua* AMSR-E product values closest in space and time.

PDF's are generated according with the following procedure:

- A first set of candidate variables to be used as input in the PDF's was defined on the basis of the results of a review of available literature on sea ice/cloud classification with instruments similar to SLSTR. In this phase, we retained variables expected to carry similar information leaving to a successive phase the comparison of classification skills.
- Based on a preliminary estimation of the practical limits for the use of multidimensional PDFs and on the redundancy, in terms of sensitivity to geophysical variables, we defined the dimensions of the PDFs, different for night-time and daytime.
- Using a limited dataset (summer and winter 2010 solstices) a preliminary set of range and class number and width for each variable was defined.
- With the above definitions, PDF's were generated sampling the whole annual cycle.
- An analysis of the PDF's statistical characteristics, of the skill in terms of classification, taking into account the need to optimize the classification procedure for operational use, was performed to define a final a set of suggested PDFs.

Examples of the PDF based classification for a set of selected SLSTR granules representing different cases are presented. The results of the classification were also compared qualitatively against current operational SLSTR cloud detection products. Ice classification results are also discussed by comparing against the sea ice 1 km concentration charts (SEAICE_ARC_SEAICE_L4_NRT_OBSERVATIONS_011_002) based on manual interpretation of satellite data (mainly SARs) produced by MET Norway and distributed through CMEMS.

To optimize and validate the classification results a set of codes that apply the PDFs to classify SLSTR granules were developed. These codes are not optimized for operational use and they will not be part of the SW that will be implemented by EUMETSAT for the operational processing. However, we evaluated that, even after the phase of optimizing the PDFs, the classification is still relatively slow in terms of computation time. In order to reduce significantly the computational burden, taking advantage of the long term and consolidated experience on the Neural Network (NN) based inversion algorithm of the team, we implemented for a subset of cases (Night-time) an alternative approach for the classification based on Neural Networks and trained on the same MODIS dataset. Some result from this additional classification method are reported.

2. Summary of literature review

As required by the Statement of Work, a Review of existing literature on sea ice/cloud detection with satellite sensors similar to SLSTR was performed. Deliverable 1 titled: '*Cloud screening over sea-ice and marginal ice zones: Review.'* contains the summary of relevant information obtained from the literature review. In particular, the selection of candidate variables, that will be discussed in the next sections, is derived from the analysis of existing literature. **Table 1** contains the number of documents (journals, technical reports, ATBD's) analysed in the review phase (not all were reported in the Deliverable 1) divided for satellite sensor.

Table 1. *Number of documents analysed in the review phase as a function of the satellite sensor*

INSTRUMENT	# DOC
AVHRR	50
MODIS	34
(A)ATSR	27
SEVIRI/GOES	10
GLI	5
VIIRS	3
MERIS	3
MISR	1
LANDSAT	1
S2-MSI	1
Others (Validation, Texture, etc)	12

3. MODIS as a proxy for SLSTR

In order to use MODIS observations as a proxy for SLSTR to produce the PDF's, it is necessary to assess the robustness of this hypothesis. In particular, we need to investigate the difference, in the measured variables due to the dissimilarity between the spectral responses of similar channels of the two instruments. In addition, this section contains the description of the approach adopted to simulate the dual view capabilities of SLSTR.

3.1 Spectral Response

Table 2 reports the corresponding MODIS channels adopted to simulate the SLSTR channels. **Figure 1** shows the corresponding spectral response function as used for RTTOV simulations. With the exception of SLSTR channel 6 (2.1 μm) the SLSTR spectral response function (SRF) generally contains the MODIS one. A larger sensitivity to atmospheric gas absorption is expected. Among the gases that could generate differences in the observed radiance water vapour is the most important one. On the other hand, we expect the differences between SRF to have limited impact on the classification, due to the relatively low water vapour amount in polar atmosphere.

During the first phase of the project when SLSTR data were not available, the only way to assess difference was by means of radiative transfer simulations. A set of available RTTOV simulation was analysed to assess quantitatively the differences between MODIS and SLSTR observations. The analysed dataset consists of 83 profiles covering a large set of climate regimes, each profile simulated for 6 different viewing angles **Figure 2** shows the difference between thermal channels and their combinations used as variables in the classification. The largest differences are observed for the channel S9. The wider SRF implies a larger sensitivity to atmospheric WV. The necessity to correct for such differences will be assessed during the test phase of the PDFs once applied to SLSTR data.

Following the availability of SLSTR an attempt to assess the differences on the basis of reported Radiances/Brightness temperatures was done. **Figure 3** shows the Channel 2 (859 nm – 250 m) image corresponding to the granule observed the 05-05-2017 at 12:35 UTC by MODIS-AQUA. The corresponding S3 SLSTR granule was observed at 12:55 UTC (**Fig.24**). **Figure 4** shows the scatterplot of corresponding observations for a set of variables used as input for the PDF's. The best linear fit parameters are reported in **Table 3.**

***Table 2**. Correspondences between SLSTR and MODIS channels*

SLSTR Channel#	λ centre (μm)	Width (μm)	MODIS Channel#	Bandwidth (μm)
S1	0.555	0.02	4	0.545–0.565
S2	0.659	0.02	1	0.620–0.670
S3	0.865	0.02	2	0.862–0.877
S4	1.375	0.015	26	1.360-1.390
S5	1.61	0.06	6	1.628–1.652
S6	2.25	0.05	7	2.105–2.155
S7	3.74	0.38	20	3.660 - 3.840
S8	10.85	0.9	31	10.78-11.280
S9	12	1	32	11.770-12.270
F1	3.74	0.38		
F2	10.85	0.9		

Table 3. *Linear fit results of the comparison between SLSTR and MODIS corresponding variables.*

Variable	Angular Coefficient	Intercept
R0.8	0.890	0.086
R1.3	1.015	0.006
R2.2	0.833	0.013
BT11-BT3.7	1.076	-1.970
BT12-BT3.7	1.074	-1.785
BT11	0.965	8.68
BT12	0.950	12.96
BT11-BT12	0.639	0.015

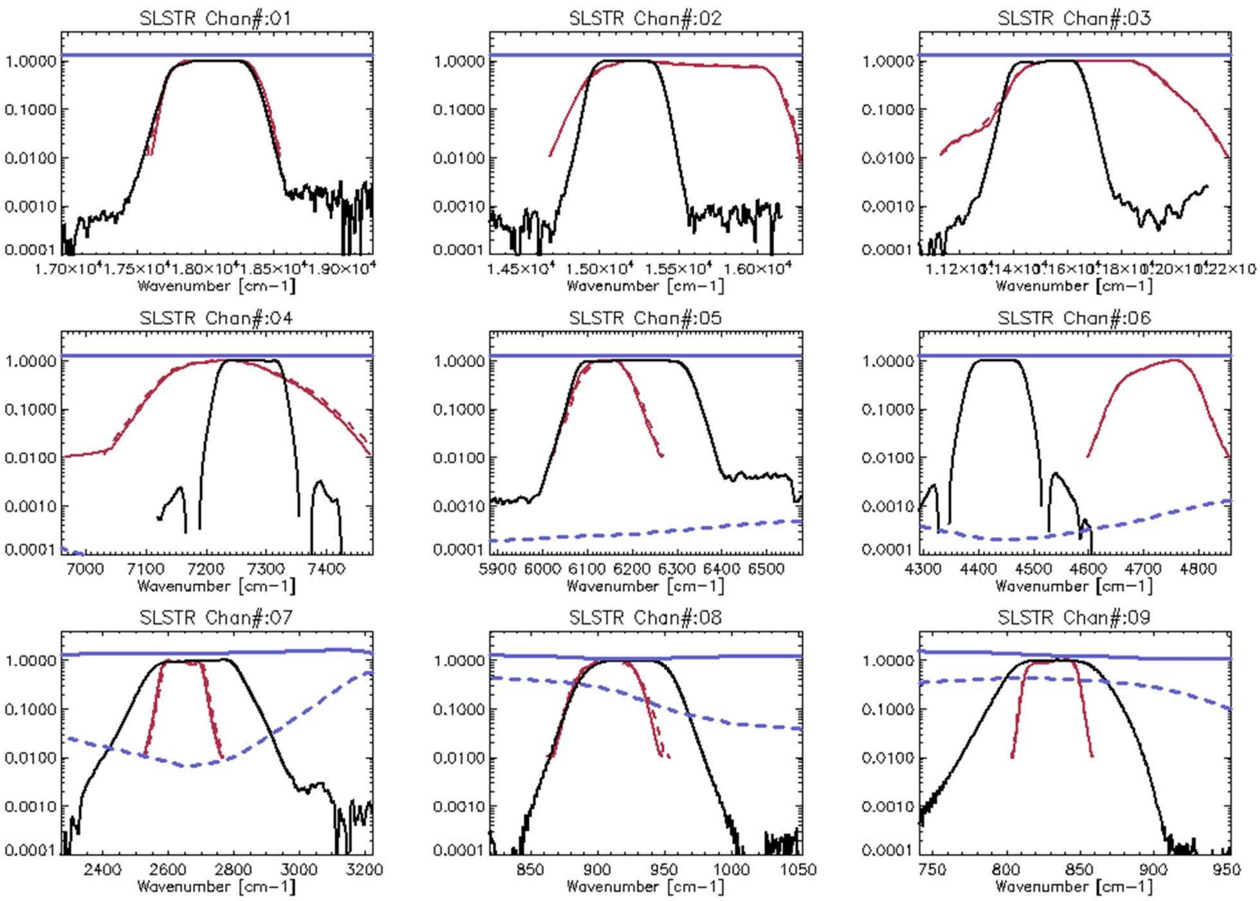

Fig.1 *Comparison between normalised spectral response function for the SLSR (black curve) and the corresponding (see Tab.2) MODIS channel (red) (continuous MODIS1, dashed MODIS2). Also plotted the complex (continuous:real, dashed: imaginary) refractive index of ice (Warren & Brandt 2008).*

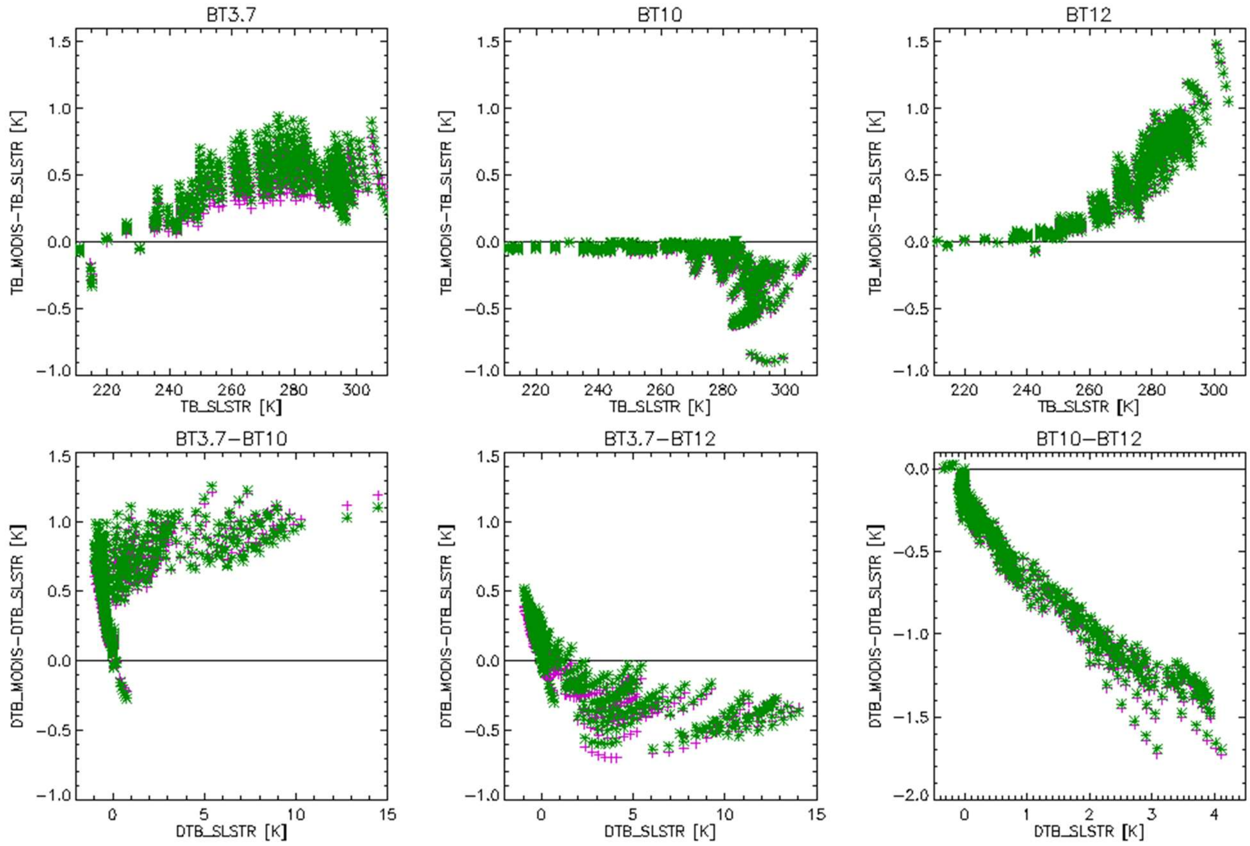

Fig.2 *Differences between simulated SLSTR Thermal channels (S7, S8 and S9) and corresponding MODIS ones.Green (MODIS2) Magenta (MODIS1)*

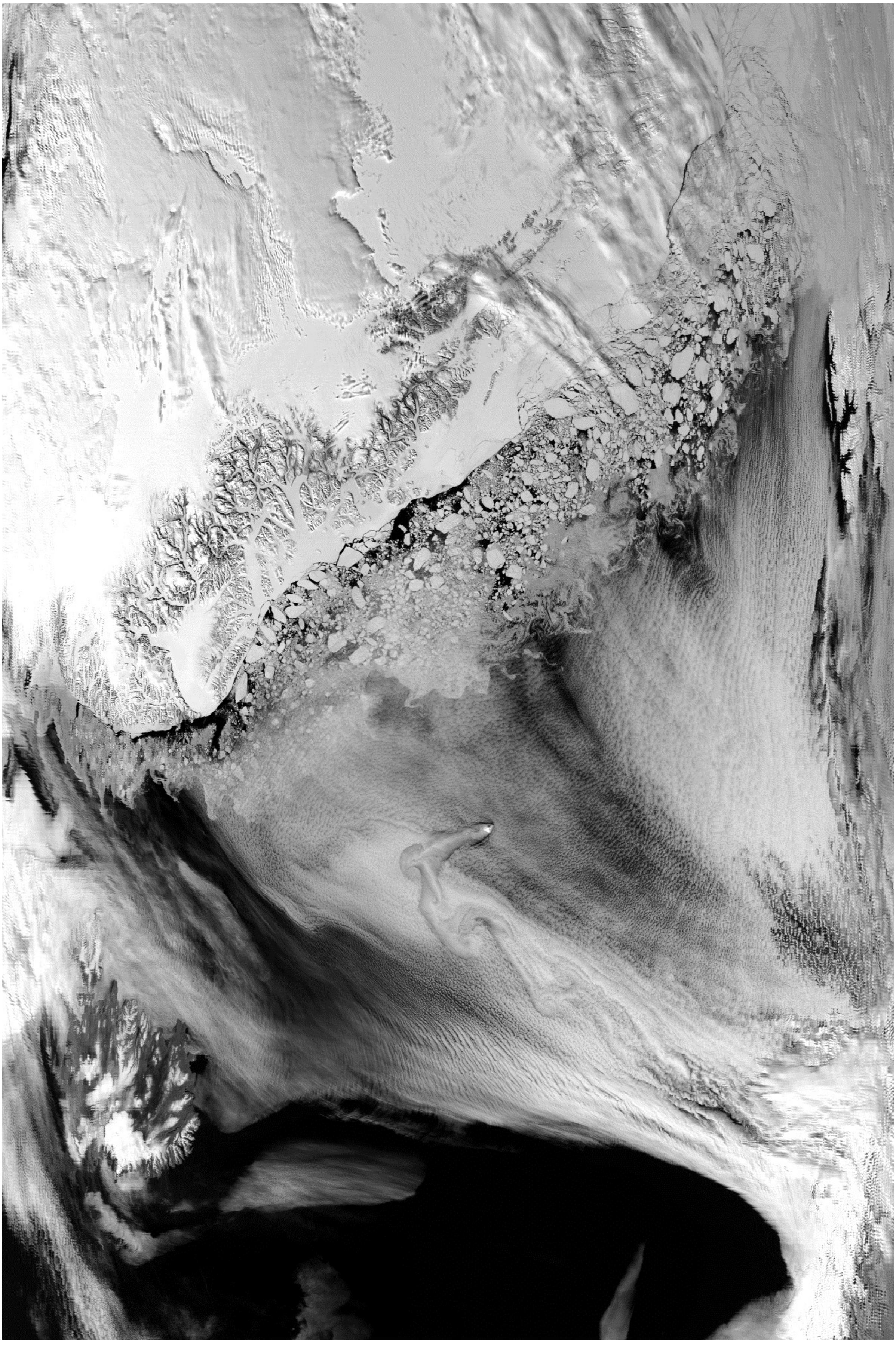

Fig.3 *MODIS AQUA Channel 2 image of the granule observed the 05-05-2017 at 12:35 UTC used for comparison against the S3 SLSTR granule observed at 12:55 UTC (Fig.24)*

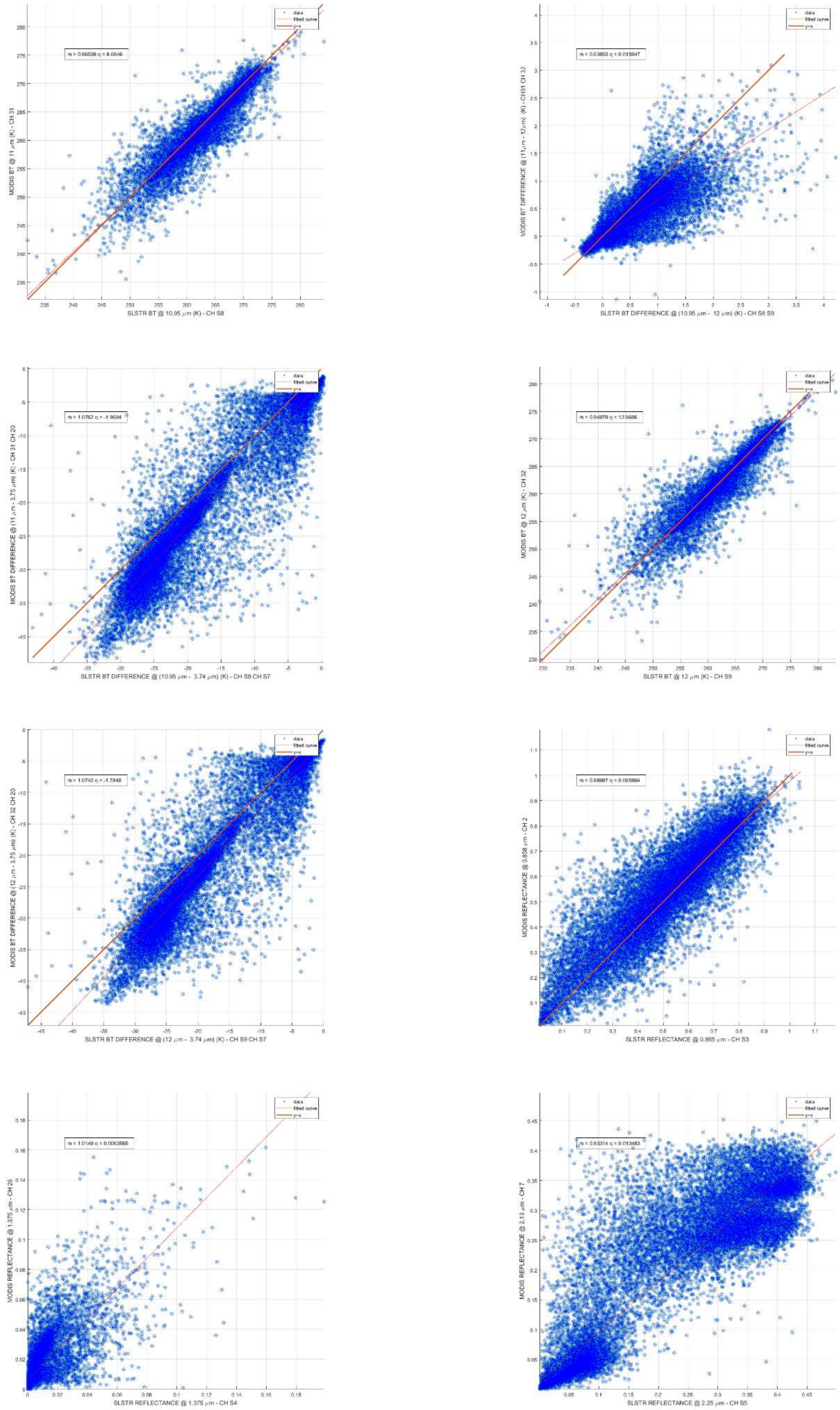

Fig.4 *Scatterplot of matching MODIS-AQUA vs SLSTR variables of interest for the PDF's generation*

3.2 Dual view

Sentinel 3 SLSTR dual view observation capability can be simulated by taking advantage of the fact that for a given longitude, at high latitudes, AQUA and TERRA satellites have an passing time that differs between 10’ and 20’ (see **fig.5**). Figure 6 shows for the day 20th December 2015 a set of 12 AQUA-TERRA partially overlapping granules with a nominal observing time difference within 15’.

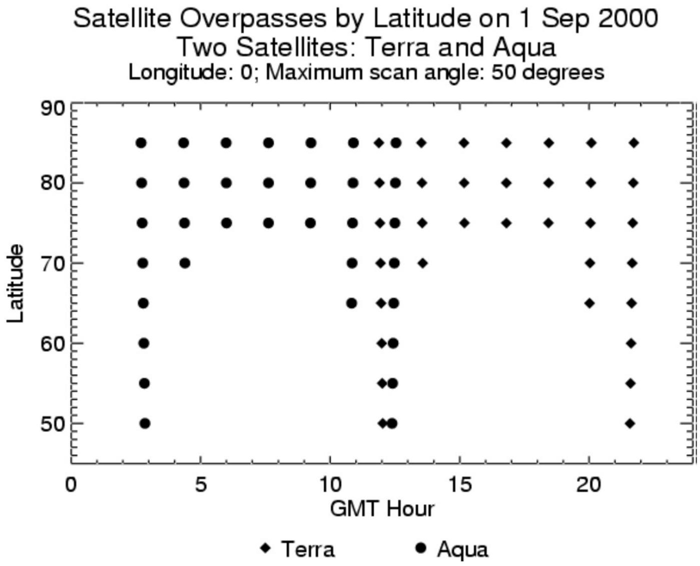

Fig.5 *Time differences between successive overpasses of the Terra and Aqua satellite as a function of latitude over the course of a 24-hour period at the Prime Meridian. Only overpasses with sensor θ_v<50° are considered (from Key et al. 2003).*

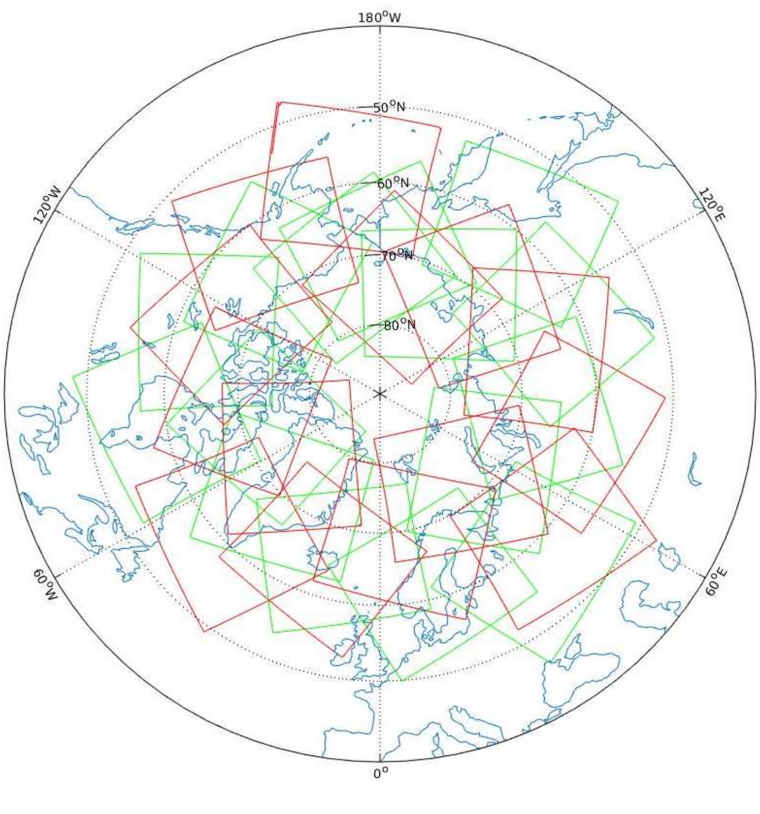

Fig.6 *20th Dec. 2015: AQUA-TERRA partially overlapping couples of granules (12) with a nominal observing time difference within 15’*

As it will detailed in the following sections, the dual view information was exploited using the same approach of Zavody et al. (2000). **Figure 7** shows the scatterplot obtained selecting only clear sky pixels (for both ACQUA and TERRA) with observation geometries compatibles with the ones characteristics of SLSTR. The two variables plotted are **BT11n-BT12n** *vs* **BT11n-BT11o**, where **n** and **o** are used to identify nadir and oblique observations respectively. Red line is drawn using the best matching couple of fitting parameters as reported in Zavody et al. 2000.

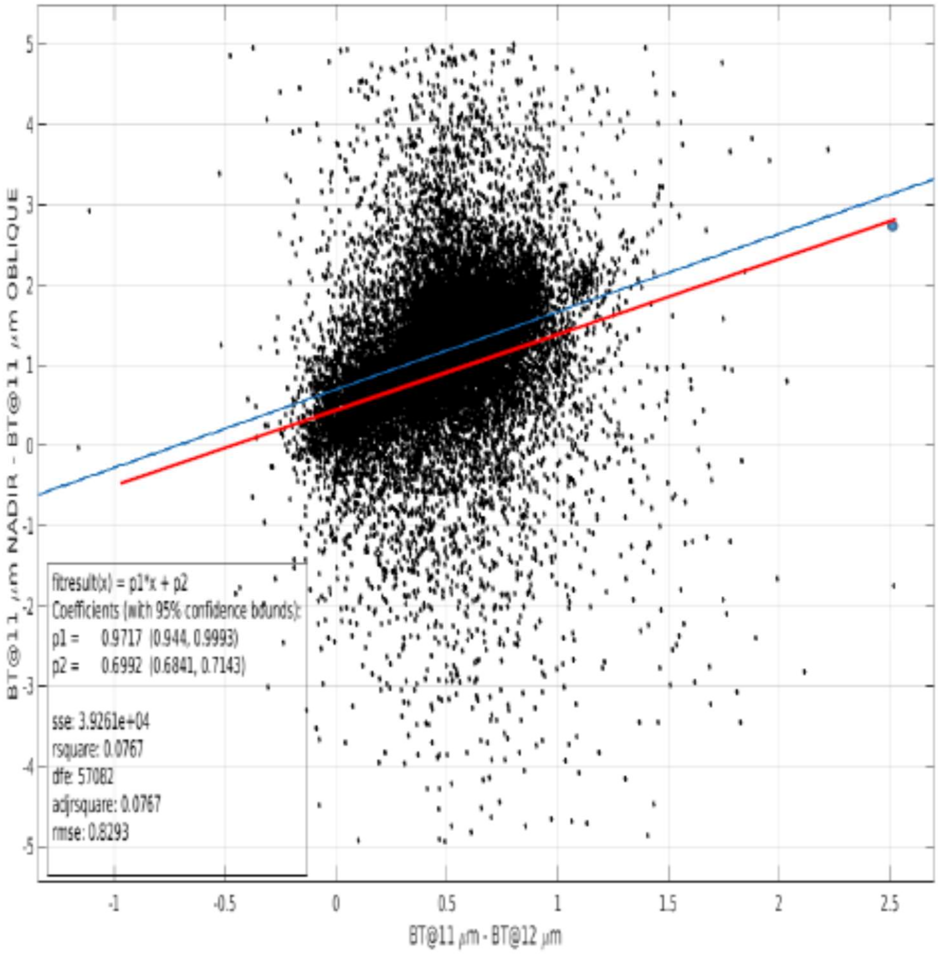

***Fig.** 7 Scatterplot of matching ACQUA and TERRA MODIS clear sky pixels with observation geometries compatibles with SLSTR ones. Variables plotted are **BT11n-BT12n** vs **BT11n-BT11o**, where **n**(adir) and **o**(blique) observations respectively. Red line is drawn using the best matching couple of fitting parameters as reported in Zavody et al. 2000.*

4. Candidate variables

About the definition of candidate variables following the conclusions in Deliverable 1 the following variables have been retained:

- **R0.8** the reflectance at 0.8 µm is expected to be low, for clear sky oceans, with relatively low contribution from molecular scattering and relatively, compared to the other SWIR window channel, large signal: these characteristics should allow to detect clouds and ice better than with channels in the visible portion of the solar spectrum. Being one of the basic channels since the first generation of VIS-IR radiometers on operational meteorological satellite a rich literature is available. Problems in the interpretation of the measurements may occur in presence of sunglint or from relatively large aerosols load.
- **R1.3** the strong absorption from WV in this band allows the detection of relatively thin cirrus even over bright surfaces as snow/sea ice. In principle, an increase of radiance in this band can be associated to occurrence of high cloud with very little ambiguity particularly over sea.
- **R1.6** the information content useful for cloud detection/classification content in this channel derives from the relatively high imaginary part of the refractive index for ice compared to the one of liquid water. Because a channel in this band is present since the second generation of VIS-IR radiometers on operational meteorological satellite a rich literature is available as a reference for the interpretation of the results.
- **R2.1** the reflectance at 2.1 µm have been added as candidate variable because there is no literature on the information content in term of sea ice/ocean/cloud classification and this study could be an occasion to document the additional (if any) information content of measurements in this band for sea-ice/cloud detection/classification. It is expected to have a strong correlation with the 1.6 µm but a lower level of the signal.
- **NDVI** the Normalized Difference Vegetation Index is included in the candidate variables as test that check the 'whiteness' of clouds.
- **NDSI** the Normalized Difference Snow Index should be sensitive not only to the presence of ice but also on its microphysical characteristics.
- **STD_R1.6** The 1.6 µm local (3x3) standard deviation was selected as unique textural variable, derived from the reflectance channels, because the 1.6 µm channel has a higher sensitivity to absorption from ice, with respect to the visible channel. In addition, the higher level of the signal, with respect to the 2.1 µm channel should allow to better distinguish between variability due to the observed scene against radiometric noise. In addition, 1.6 µm spatial variability, in terms of local (32x32) histogram test is also used in the SLSTR standard cloud detection, and this should guarantee from one point of view a continuity in the cloud detection process and also the possibility to compare the PDF with the know how derived by applying the SLSTR cloud detection.
- **BT11** The brightness temperature in the 10-11 µm atmospheric window, over ocean, particularly at high latitudes, gives the brightness temperature close the one of the emitting surface. Can be used, without large ambiguity, to detect optically thick and high clouds. On the other hand, over optically thin clouds, in presence of temperature inversion or of melting ponds over sea ice, the interpretation increases of uncertainty.
- **BT12** Same as for the TB11 except that there is a larger effect of absorption/emission from atmospheric water vapour. However, over Polar Regions, atmospheric water vapour is relatively low and the larger sensitivity to absorption from ice should result in a better detection skill.

- **BT11-BT12** The split window difference should allow the detection of relatively thin ice clouds. While over daytime the 1.3 μm channel reflectance is expected to have less ambiguity in the interpretation, during night-time this channel combination, in nadir as well as in dual view mode is the main test to retrieve this sort of clouds. In addition, because this couple of channels has been since the AVHRR-2 on operational VIS-IR imagers there is a rich literature on interpretation of this channel.
- **BT11-BT3.7** As mentioned in the review, this brightness temperature differences carries information from different physical processes (size of the condensed water particles, level of inhomogeneity of the scene) and therefore is expected to be extremely useful at least in detecting inhomogeneous scenes. A rich literature, also specific for polar region is also available for the interpretation of the information obtained from this channel combination.
- **BT12-BT3.7** As suggested by Liu et al (2004) over polar region, because of the relatively low water vapor amount and the high occurrence of ice cloud this channel combination can be more sensitive to occurrence of cloud and ice surfaces than the one using **BT11**. The skill in term of sea-ice/cloud/clear ocean classification of the two brightness temperature differences will be compared in order to select one combination for the final set of variables used to produce the PDF's.
- **STD_TB12** The local standard deviation at 12 μm has been selected as textural variable for the thermal channels instead of the one at 11 μm because over polar regions the effects due to local variability of water vapor content at the level of the 3x3 pixel area should be largely negligible compared to the relatively higher sensitivity to ice absorption.
- **STD_TB3.7** The information in terms of detection skill of the 3.7 μm local standard deviation should be compared against the one in the **STD_TB12**. Because of the non-linear radiance-temperature dependence differences are expected between the two variables. The **STD_TB3.7** is expected to be more sensitive to inhomogeneous scene, however due to the nature of the signal at 3.7 μm using this variable implies producing different PDF's daytime/night-time and even different daytime ones according with the solar illumination-observation geometry.

The above list of candidate variables should not be considered as the final one to be implemented in the operational classification algorithm. Variables expected to carry similar information are included in the list. The results of a successive phase of analysis of classification skills using different combination of variables (see below) will be used to define the final set.

This first set of candidate variables does not include the BT3.7 that was listed in the conclusions of Deliverable 1. As we mentioned in the Deliverable the use of BT3.7 as variable would include the hypothesis of estimating the reflectance contribution during daytime. Given the need to optimize the PDF's dimension and size we concluded that the information carried by the 3.7 channels will be exploited by using as classification variable the difference between the BT3.7 and the BT of the 2 channels in the 10-12 μm window.

Because of limitation in the number of dimensions of the PDF's (see Sections 6 and 7) we grouped variables carrying similar information as reported in the following list reporting also in parenthesis the corresponding SLSTR channel. Variables carrying similar information will not be at the same time in the PDF's. In addition to the need to estimate the optimum variables combination, by producing PDF's with different variables as input is also a way to have a solution in case of failure of one channel, and in case derived variable, for which and alternative solution was considered in this preliminary phase.

- **R0.8** ***(S3)***
- **R1.3** ***(S4)***
- **R1.6** ***(S5)*** **R2.1** ***(S6)*** **NDVI NDSI**
- **STD_R1.6** ***(STD_S6)***
- **BT11** ***(S9)*** **BT12** ***(S9)***
- **BT11-BT12** ***(S8-S9)***
- **BT3.7** ***(S7)*** **BT11-BT3.7** ***(S8-S7)*** **BT12-BT3.7** ***(S9-S7)***
- **STD_TB12** ***(STD_S9)*** **STD_TB3.7** ***(STD_S7)***

Concerning the dual view information content, Zavody et al (2000) introduced a cloud detection test that compares the difference between measured BT11 in the two different geometry (**n**adir and **o**blique) **BT11n-BT11o** for a given pixel, against a value predicted function of the difference **BT11n-BT12n** both measured at nadir. We adopted as unique variable taking advantage of the dual view SLSTR capabilities the variable:

DBT_DV= (BT11n-BT11o) – [a (BT11n-BT12n)+b]

Where the linear regression coefficients are obtained from the fit MODIS AQUA and TERRA matching observation (Fig. 7). In principle, dual view observations of solar reflected radiation are expected to contain useful information in terms of surface characterization, practically with the constraints in consistency, the lack of solar radiation for part of the year, the need to group observations in several observation geometry classes discourage the use of dual view information also for solar channels.

5. PDF’s Production Description.

The PDF’s for the 3 classes (**SEA/ICE/CLD**) were generated with the following procedure:

1) For each day, within the time frame 1st January - 31st December 2010 (see below the sampling strategy within the year) MODIS AQUA and TERRA granules having measurements above 60°N were acquired. The choice of 2010 to create the PDFs represents a compromise between selecting a recent year, for which other useful observations are available and selecting a period at the beginning of MODIS missions to minimize the effects of data degradation due to the aging of the instrument. The products acquired are the followings:
   - Level1B radiance (**`MOD21KM`** and **`MYD21KM`**),
   - MODIS Geolocation Fields (**`MOD03`** and **`MYD03`**),
   - Sea Ice Coverage (**`MOD29`** and **`MYD29`**)
   - Cloud Mask (**`MOD35`** and **`MYD35`**).

   Details on their use are given below. In order to produce in the shortest time PDFs representative of the annual variability in the Arctic area, the year was sampled in the following way: the first set of PDF is generated by using the first 5 days for each month. The procedure then kept updating the PDF’s by adding the successive 5 days of the month up to the end of the month. A procedure to evaluate the representativeness of the PDF was implemented by comparing single variable PDF’s as resulting from two successive steps (cycles of yearly distributed 5 days). The procedure compared overall (i.e. integrated over the parameters) single variable distribution. A convergence (i.e. a mean absolute difference

<0.1% over all classes/variables) was reached when the first 15 days of each month were analysed. However, in the successive phase of PDFs optimization we noticed (see Sect.7) that for some combination of Geometry/SST the statistics were not enough smooth and additional observations needed to be added. This occur generally for combination of SST and geometry values at the limits for their lower absolute occurrence of cases in such cases. Finally, we processed the whole 2010 year.

2) For the single view PDF's corresponding products for the same granules are analysed to:
   a) Select only pixels classified as 'sea', except the shallow sea ones (<5km from coast OR <50m deep), according with the land/sea mask reported in the MODIS products **MOD03** and **MYD03** as *Land/SeaMask* variable.
   b) **For each 'sea' pixel** determine the scene type: **DAY, NIGHT, TWILIGHT, SUNGLINT** according with the following information contained in the MODIS products MOD35 and MYD35:
      - **DAY:** day/night flag in products **MOD21KM** and **MYD21KM**.
      - **NIGHT:** day/night flag in products **MOD21KM** and **MYD21KM**.
      - **TWILIGHT:** 85°<sun zenith angle< 95° in **MOD03** and **MYD03**.
      - **SUNGLINT:** according with the sunglint flag (5th bit of cloud mask variable in products **MOD35** and **MYD35**). MODIS sunglint flag is based on a fixed value of angle (reflected sun angle, θr, lies between 0° and 36°) around the specular reflection one with no dependence from the effective surface wind speed.

      NB: PDF's are generated for 4 scene types however the SUNGLINT and TWILIGHT classes are introduced to test whether the solar channels still contain useful information. If, by successive evaluation of the classification skills, solar channels are found to not add useful information for a given scene type then the NIGHTIME PDF's will be adopted.
   c) A pixel is classified as:
      - **CLD** according to the results of cloud detection tests as reported in the product MOD29 of sea ice classification, corresponding to Ice Surface Temperature value of 50 K. NB. In the final processing chain we did not use the Cloud detection results in Cloud Mask product (MOD35/MYD35) because this product gives a confidence level while the Ice Surface Temperature cloud flag reports a conservative interpretation of the cloud detection confidence.
      - **ICE** During the day, the Sea Ice map flag, stored in the Sea_Ice_by_Reflectance variable in the MOD29/MYD29 product is used to establish whether a pixel is sea ice or clear ocean. The sea ice detection in this MODIS product is achieved using grouped criteria tests for sea ice reflectance characteristics in the visible and near-infrared regions. Criteria for sea ice are that a pixel has:

        Normalized Difference Snow Index NDSI=(CH#4-CH#6)/(CH#4+CH#6)>0.4
        Reflectance CH#2>0.11
        Reflectance CH#1>0.10.

        If a pixel passes this group of criteria tests is classified as Sea Ice in the data product. During the night if the Ice Surface Temperature in the product MOD29/MYD29 is between 210 K and 271.4 K (freezing point for sea salt water) a pixel is flagged as Sea Ice. NB Ice Surface Temperature in this product seems to be retrieved also for temperatures relatively warm.
      - **SEA** if the pixel is not classified as CLD or ICE.
   d) Define the ancillary variables associated to each pixel. The observation geometry variables are obtained from the MODIS Geolocation Fields products (**MOD03/MYD03**). The SST class is defined on the basis of the AMSRE derived SST. We discarded the hypothesis to use MODIS SST product (**MOD28** - Sea Surface Temperature) because

being derived from IR measurements, the product would not be available for cloudy pixels. The MW based SST estimation is obtained from the AMSR-E daily products (Wentz et al. 2000, 2003, 2005, 2007) distributed by Remote Sensing System (ftp://ftp.remss.com/amsre/bmaps_v07/). RSS products store only two values per day for an ascending and descending orbit in a regular grid of 2.5°x2.5°. The closest SST estimation in space and time is used. The differences due to the different spatial and temporal sampling are expected to be within the adopted width of the SST classes (2.5 K). This SST class width value has been selected according with the assumptions adopted by Pearson et al. (2014). In the successive phases of final PDF's definition and creation the value of the SST classes will be optimized. NB the AMSRE product also contain the information on sea surface sea wind, total water vapour content, precipitation and sea ice occurrence. In this phase this information is not used but in principle could be used to interpret the data or to improve the PDF's classification skills.

e) Once determined the class (**SEA/ICE/CLD**) for the analyzed pixel, the scene and the values of the ancillary data: SST (see above) and observation/illumination geometry (cosine of scattering angle for day, twilight and sun-glint scenario and air mass or path length for night-time), radiances/normalized reflectances for the MODIS channels of interest are extracted. For IR measurements, radiances are converted to brightness temperatures by the inversion of Planck's equation and applying the correction given by NASA. Normalized reflectances are converted to reflectance for daytime and sunglint scene while no conversion is applied for twilight cases.

f) From the selected observation, converted in reflectance or brightness temperature if needed, the values of the candidate PDF variables are estimated and the class, for each variable determined. Once defined the class value for each candidate classification variable, the corresponding value of frequency of occurrence *F* in the relevant PDF file (i.e. scene type, ancillary variable, class) is updated. NB. For practical reason (i.e. to allow periodic upgrade and different combinations), the first step produces files containing the combined occurrences for all candidate variables. PDF are estimated from these files.

g) The final PDF table is obtained, according to the Bayes theorem, by normalizing the value of occurrence F_{xxx} relative to each position (represented by the vector of the variables $\boldsymbol{i}$) in the grid space defined by the classification variables by the sum of occurrences for each class. For example:

$$P_{CLD}(\boldsymbol{i})=F_{CLD}(\boldsymbol{i})/(F_{CLD}(\boldsymbol{i})+F_{CLR}(\boldsymbol{i})+F_{ICE}(\boldsymbol{i}))$$

3) For the dual view case the PDF's are created with a similar procedure. . The main difference is that once opened a MODIS granule for example for TERRA the granules closest in time for ACQUA are analysed to search for combination of SLSTR allowed observation geometries. A critical issue in the production of PDF for dual view observation is the case when the classification is not consistent between the two missions: e.g TERRA gives CLD and AQUA gives SEA). To avoid arbitrary interpretation of these cases, only pixels having a consistent classification are included in the PDF, with a consequent further reduction of the database. In principle, the cases with inconsistent classification should be only due to cloud cover variability within the relatively short time interval between two TERRA-AQUA overpasses (restricted to be within 15 minutes). Cloud cover variability in Polar regions at that timescale should interest a relatively small number of cases. However, different geometry and instrument characteristics are likely to introduce further inconsistency between cloud detection results. About the requirements on observation geometry, we started with $54.9 < \theta_v < 55.1°$. Because of the relatively low number of matches, based also on the expected variability of the variable we relaxed the forward view angle condition to

53°<θ_V<57° corresponding roughly to a total range of 10% variability of the air mass around the value (1.74) at 55°. As it will be discussed below, for this case only the dual view variable is selected and stored in PDFs and it will be used, for practical reasons, as an independent variable.

The above scheme describe the classification procedure however, the main difficulty in creating the SW to produce PDF's has been to implement an efficient way to handle of multidimensional arrays in a way that they can be easily updated. Next sections (6,7) describe the two phases procedure to obtain the final PDFs set.
Finally, another critical issue encountered in this phase was the access to MODIS archive and the transfer of required data to local disks for processing.

6. PDFs generation. Phase I: preliminary definition of variables

This section describes the activities related to the generation of the PDFs. This process has been performed in two phases:

- First, a preliminary and, compatibly with the operational use, conservative definition of range and classes for each variable has been set to analyse a limited sample of cases. From the results of this first phase, taking into account limitations due to the operational use of the PDF's, a set of variables combinations, each one associated with a preliminary range and classes values, was defined.
- Secondly, according with the results of the first phase, a larger set of MODIS data was processed. The produced set of PDFs has been analysed with different approaches, including application to SLSTR data, to optimize the PDF definition and to suggest the best combination and class definition for operational use.

A preliminary activity to the production of PDF has been the definition of candidate variables and the associated range and class widths. A limiting factor for the PDFs both in the production phase as well as in their operational implementation is their dimension. The objective is to produce PDFs that can be loaded once, and then stored in memory during the processing. The issue of optimizing the number of classes, in addition to the number of variables, is therefore important.

In order to define a first set of values for range and classes, two days (21/12 and 21/06/2010) have been analysed in details. These correspond to the winter and summer solstice, although they are not expected to be representative for the extreme conditions in terms of temperature, they represent the two extreme cases in terms of solar illumination. **Table 4** summarize the characteristics of the summer/winter solstice dataset used for the preliminary definition of the variables ranges and classes.

Tab.4. *Characteristics of the summer/winter solstice dataset used for the preliminary definition of the variables ranges and classes*

	Daytime	**Night-time**
Days	21/06/2010	21/12/2010
Granules	128	128
Pixels	90733720	126421105

6.1 Single Variable Range and Classes

After each pixel was classified, relatively detailed histograms of distribution of variables values for each class and scene type were produced. In this phase, the further classification based on values of the ancillary variables (i.e. SST and illumination/observation geometry) was not performed. The idea is to have PDFs that have at least a fixed number of classes, independently from the value of the parameters, and hopefully the same range (i.e. same classes). **Fig.8** shows an example of histograms of distribution for the variable **BT11-BT12**. Each panel shows the three classes histogram for a given scene type.

Once generated the histograms for each candidate variable and each scene type, the following quantities have been estimated:

- 0.1% 0.5% 99.5% 99.9% percentile
- Min and Max value.

Fig.9 shows, for each variable (each panel) and each scene type (1 NIGHT, 2 DAY, 3 SUNGLINT, 4 TWILIGHT) the range for each class defined by:

- the Min-Max (Thinner line)
- 0.1%-99.9% percentiles (Medium line)
- 0.5%-99.5% percentiles (Thicker line)

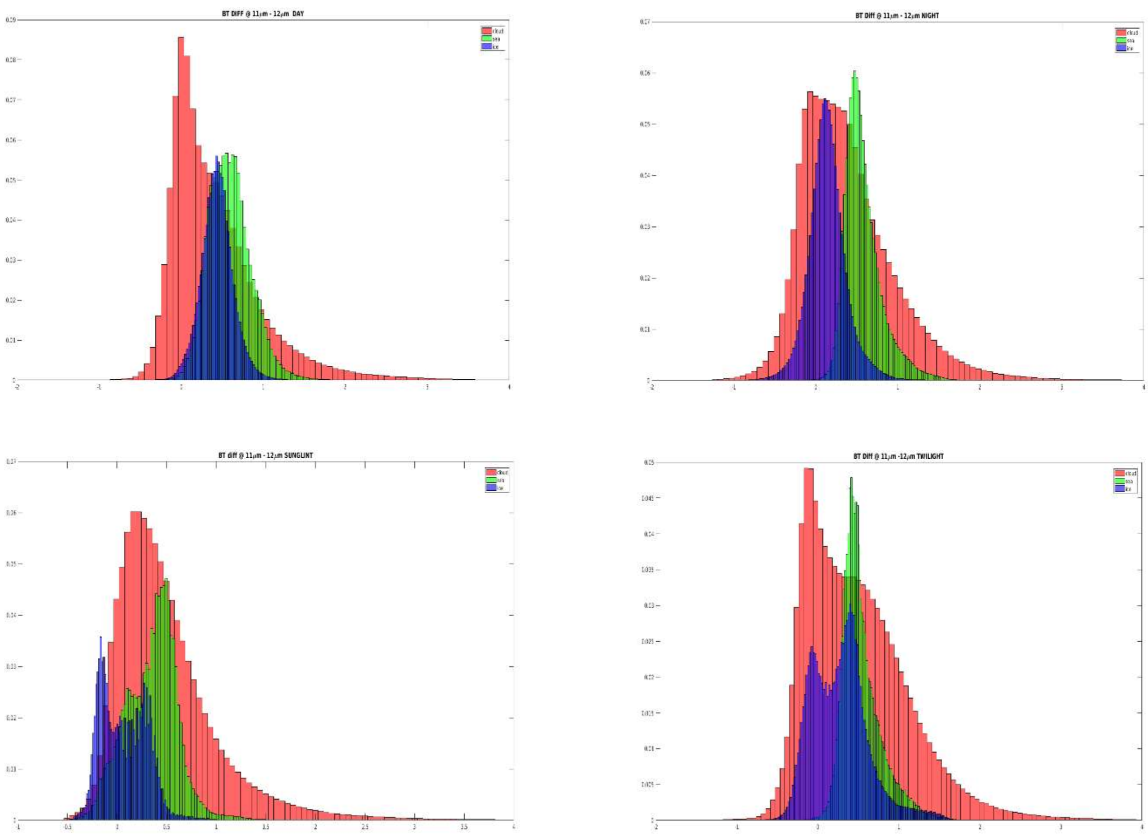

Fig.8 *Examples of histograms of distribution obtained from the summer/winter solstice dataset used for the preliminary definition of variable range and class number and widths (see text for details). The variable shown is the brightness temperature difference BT11-BT12 for different scene type (from upper to lower/left to right: DAY, NIGHT, SUNGLINT, TWILIGHT). R: CLD, B: ICE, G: SE*

For each class, the same colour code used for the histograms (**CLD**, **SEA**, **ICE**) is adopted. A first set of values to define the range for each variables for the production of the PDFs was estimated taking into account of the values of the overall 0.5%-99.5% percentiles. In addition, if part of this range was populated by a single class (e.g. R0.8 for values larger than 0.4 is populated only by cloudy pixels), the range was further restricted.

NB in this phase of further reduction of the range by compressing subranges populated by a single class we try to keep the maximum information for the ICE class. This is relatively straightforward because the Sea Ice characteristics lies for most of the variables in a subrange between the SEA and CLD classes. The rationale to keep the detail within the ICE class derives from the prospective use of the classification results to product the Sea Ice Temperature. Different types of Sea Ice are likely to require different algorithms/coefficients by not compressing the sea ice classification information in a single class we expect an ice type classification to be potentially possible.

Table 5 reports the results of this process giving for each variable the range and the class width. The min and MAX value represents respectively the upper and lower limits of the first and last class. Similarly, **Table 6** summarizes the preliminary definition of range and class widths for the parameters.

Table 5. *Preliminary definition of class limits and width for the candidate variables. [1]First class includes all valid values lower than the minimum one. [2]Last class includes all valid values larger than the maximum one.*

Variable	min[1]	MAX[2]	Width
R0.8	0.03	0.6	0.03
R1.3	0.0015	0.03	0.0015
R1.6	0.003	0.105	0.003
R2.1	0.0015	0.06	0.0015
NDVI	-0.45	0.09	0.02
NDSI	0.1	0.9	0.05
STD1.6	0.003	0.081	0.003
TB11 [K]	234	280	1
TB12 [K]	234	280	1
TB11-TB12 [K]	-0.6	1.5	0.1
TB11-TB3.7 [K]	-14 -14	-0.5 -0.5	0.5 0.1
TB12-TB3.7 [K]	-14 -14	-0.5 -0.5	0.5 0.1
STDTB12 [K]	0.3	3	0.3
STDTB3.7 [K]	0.3	3	0.3

Table 6. *Preliminary definition of class limits and width for the external parameters. [1]First class includes all valid values lower than the minimum one. [2]Last class includes all valid values larger than the maximum one. [3]First class includes all valid values that according to AMSRE products are ice contaminated.*

Parameter	Min[1]	MAX[2]	Width	
SST [°C]	-2.5[3]	17.5	2.5	AMSR-E Derived SST (and ICE occurrence)
GAMMA [°]	60	140	10	Scattering angle (Solar variables)
1/COS(θ_v)	1	2	0.1	Viewing air mass (Thermal variables)

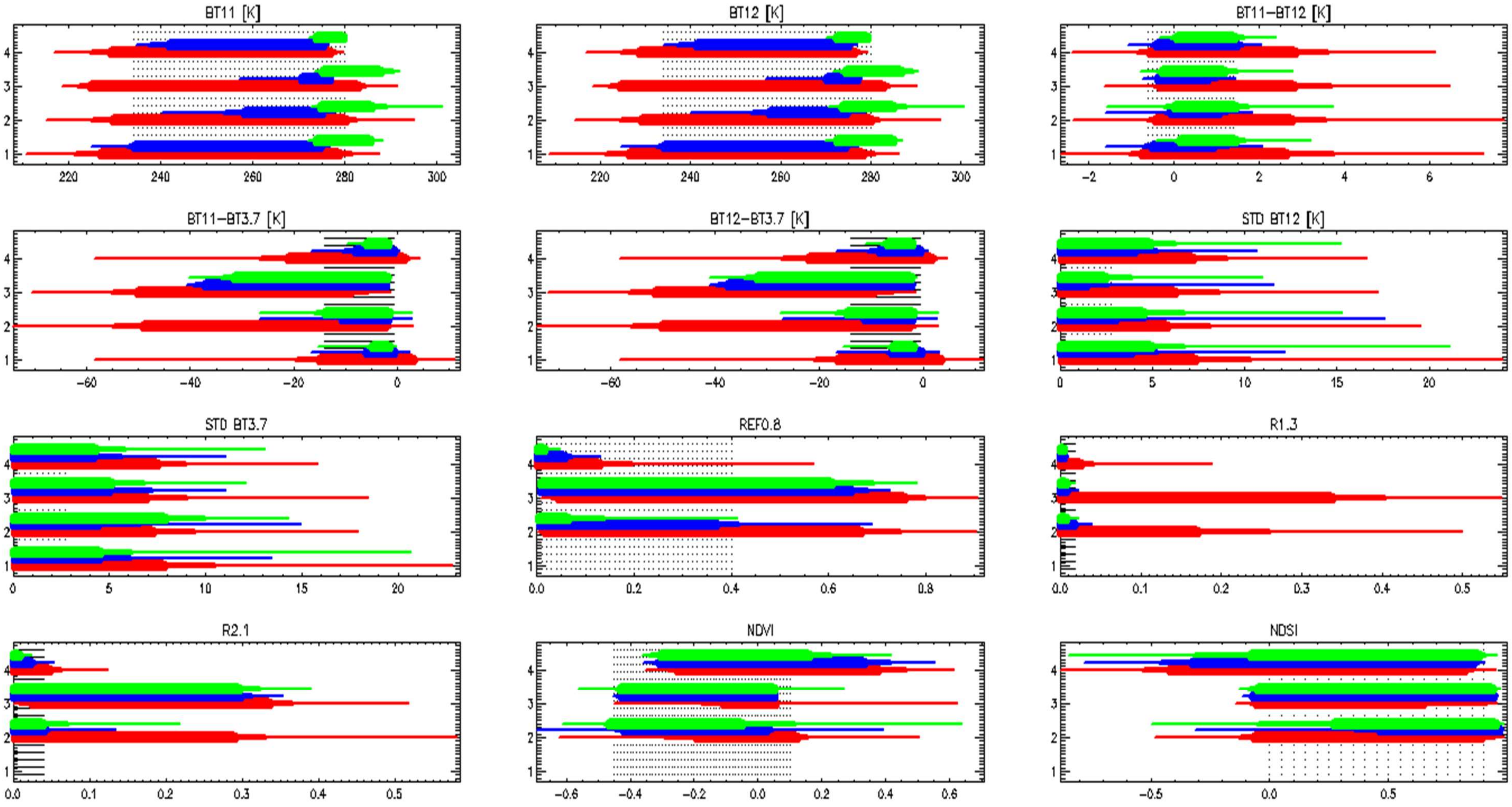

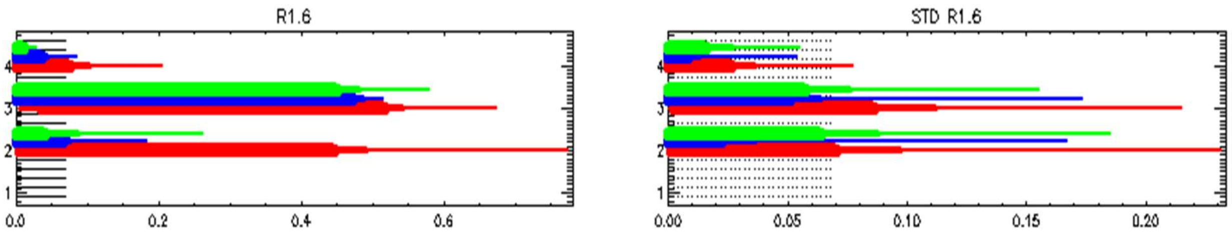

Fig.9 *Range definition: for each variable (panel), scene (1 NIGHT, 2 DAY, 3 SUNGLINT, 4 TWILIGHT) and surface type (R: CLD, B: ICE, G: SEA) range defined by:Min-Max Values (Thinner line), 0.1%-99.9% percentiles (Medium line), 0.5%-99.5% percentiles (Thicker line)*

6.2 Variables combinations

The creation of PDFs with a relatively large number of dimensions and classes (for each dimension), is limited by the computing resources and by the programming languages.

We examined two scenarios:

a) To generate separate PDFs (for each variable or by splitting variables in Solar and Thermal IR (e.g. Pearson et al 2014)) and the final PDFs estimated as a product of separate ones. This corresponds to the hypothesis that variables are independent.
b) To generate directly multidimensional PDFs.

The first scenario is easier to implement because it does not require handling a large multidimensional array. In principle, if the assumption is correct, it allows to generate and test PDFs based in all possible combinations of classification variables. However, it is evident that the assumption of independence between occurrences of radiance values is relatively weak. We tested this hypothesis by comparing, for few cases, the 'real' 2D PDF with the one obtained from the product of 1D PDF. **Fig.10** shows an example for the combination **BT11-BT12** vs **BT11.** On the left the 'real' PDF and on the right the estimated one: as expected, the two PDFs differ.

Consequently, the approach of producing multidimensional PDFs had to be adopted, despite being aware of all the issues that derive by the need to handle a multidimensional and relatively large array.

*NB. We kept the approach of independent PDFs only for the dual view variable. In fact, beside the problem of an additional dimension in the PDFs, the statistical dataset, because of the adopted geometry and temporal matching criteria, is extremely reduced compared to the daytime and night-time ones (see **Tab.9**). Dual view SLSTR observations represent a large portion of the swath and therefore we gave the priority to have a statistically significant dataset for all, single view variable.*

Producing multidimensional PDFs requires an optimization of dimensions and of the number of classes for each dimension to keep the PDFs' production and operational use in a reasonable processing time.

Because of the need to reduce the dimensions and the expected redundancy of information content in the selected variables, we defined variables' combinations, for which PDFs were generated, leaving to a successive phase the analysis of classification skills for each combination.

NB. Producing PDFs for different variables combination can be also useful in case of failure or low quality of a given channel during the instrument lifetime.

For night-time the selected variables were **BT11, BT12, BT11-BT12, BT11-BT3.7, BT12-BT3.7, STD_TB12, STD_TB3.7.**

By grouping the variables for the type of information content, we identified a minimum set of four dimensions resulting in the following list:

- **BT11** or **BT12**
- **BT11-BT12**
- **BT11-BT3.7** or **BT12-BT3.7**
- **STD_TB12** or **STD_TB3.7**

In order to generate PDFs, we considered all combinations of these variables: **Table 7** lists the combinations.

For the daytime (and consequently for TWILIGHT and SUNGLINT), we started considering a set of 8 dimensions and we grouped, with a similar approach, the variables as follows:

- **R0.8**
- **R1.3**
- **BT11-BT12**
- **STD_R1.6**
- **R1.6** or **R2.1** or **NDVI** or **NDSI**
- **BT11** or **BT12**
- **BT11-BT3.7** or **BT12-BT3.7**
- **STD_TB12** or **STD_TB3.7**

The original plan was to keep two textural variables (**STDxx**), one from the solar channel (**STD_R1.6**) and one from the thermal ones (**STD_TB12** or **STD_TB3.7**), in order to have a continuity with the night-time PDFs. However, from a preliminary set of tests, we concluded that handling PDFs with 8 dimensions was extremely critical; therefore, we reduced to a single variable carrying the information on spatial variability. **Table 8** lists the 48 variable combination tested.

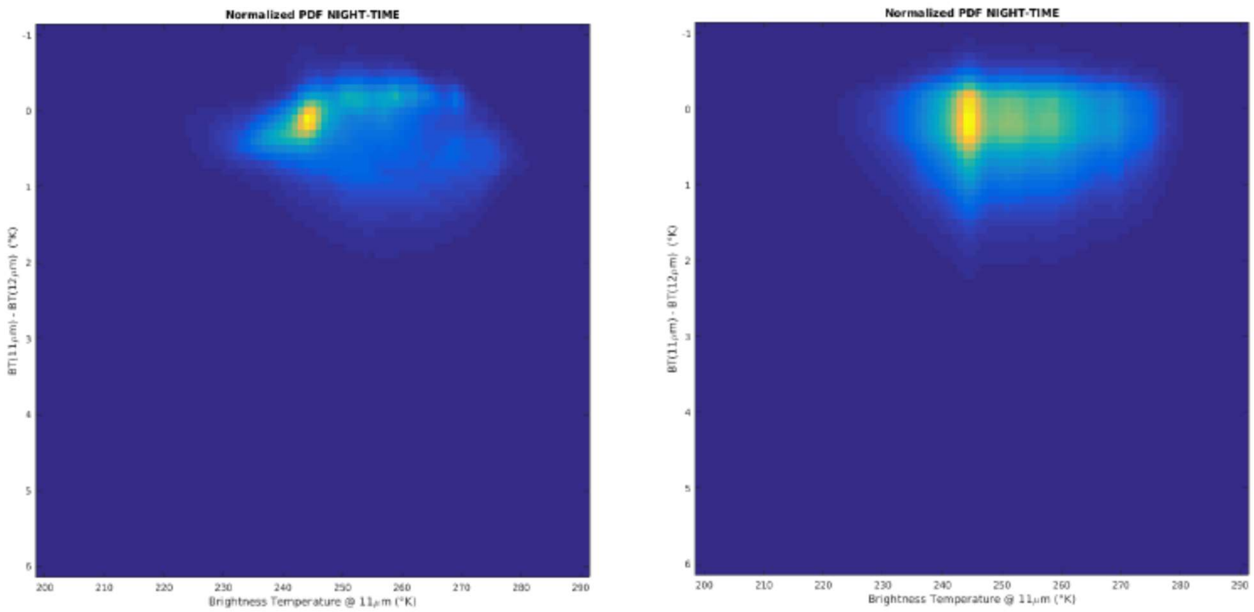

Fig.10 *Example of 2D* ***(BT11-BT12*** *vs* ***BT11)*** *PDF for CLD (left) and as obtained from the combination of 1D PDF's (right).*

Tab.7 *List of the combination used to generate the night-time PDFswith 4 variables.*

1	BT11-BT12	STD_BT12	BT11	BT11-BT3.7
2	BT11-BT12	STD_BT12	BT11	BT12-BT3.7
3	BT11-BT12	STD_BT12	BT12	BT11-BT3.7
4	BT11-BT12	STD_BT12	BT12	BT12-BT3.7
5	BT11-BT12	STD_BT3.7	BT11	BT11-BT3.7
6	BT11-BT12	STD_BT3.7	BT11	BT12-BT3.7
7	BT11-BT12	STD_BT3.7	BT12	BT11-BT3.7
8	BT11-BT12	STD_BT3.7	BT12	BT12-BT3.7

Tab.8 *List of the combination used to generate the daytime PDFswith 7 variables.*

1	R0.8	R1.3	BT11-BT12	STD1.6	BT11-BT3.7	BT11	NDSI
2	R0.8	R1.3	BT11-BT12	STD1.6	BT11-BT3.7	BT11	NDVI
3	R0.8	R1.3	BT11-BT12	STD1.6	BT11-BT3.7	BT11	R1.6
4	R0.8	R1.3	BT11-BT12	STD1.6	BT11-BT3.7	BT11	R2.1
5	R0.8	R1.3	BT11-BT12	STD1.6	BT11-BT3.7	BT12	NDSI
6	R0.8	R1.3	BT11-BT12	STD1.6	BT11-BT3.7	BT12	NDVI
7	R0.8	R1.3	BT11-BT12	STD1.6	BT11-BT3.7	BT12	R1.6
8	R0.8	R1.3	BT11-BT12	STD1.6	BT11-BT3.7	BT12	R2.1
9	R0.8	R1.3	BT11-BT12	STD1.6	BT12-BT3.7	BT11	NDSI
10	R0.8	R1.3	BT11-BT12	STD1.6	BT12-BT3.7	BT11	NDVI
11	R0.8	R1.3	BT11-BT12	STD1.6	BT12-BT3.7	BT11	R1.6
12	R0.8	R1.3	BT11-BT12	STD1.6	BT12-BT3.7	BT11	R2.1
13	R0.8	R1.3	BT11-BT12	STD1.6	BT12-BT3.7	BT12	NDSI
14	R0.8	R1.3	BT11-BT12	STD1.6	BT12-BT3.7	BT12	NDVI
15	R0.8	R1.3	BT11-BT12	STD1.6	BT12-BT3.7	BT12	R1.6
16	R0.8	R1.3	BT11-BT12	STD1.6	BT12-BT3.7	BT12	R2.1
17	R0.8	R1.3	BT11-BT12	STD_BT3.7	BT11-BT3.7	BT11	NDSI
18	R0.8	R1.3	BT11-BT12	STD_BT3.7	BT11-BT3.7	BT11	NDVI
19	R0.8	R1.3	BT11-BT12	STD_BT3.7	BT11-BT3.7	BT11	R1.6
20	R0.8	R1.3	BT11-BT12	STD_BT3.7	BT11-BT3.7	BT11	R2.1
21	R0.8	R1.3	BT11-BT12	STD_BT3.7	BT11-BT3.7	BT12	NDSI
22	R0.8	R1.3	BT11-BT12	STD_BT3.7	BT11-BT3.7	BT12	NDVI
23	R0.8	R1.3	BT11-BT12	STD_BT3.7	BT11-BT3.7	BT12	R1.6
24	R0.8	R1.3	BT11-BT12	STD_BT3.7	BT11-BT3.7	BT12	R2.1
25	R0.8	R1.3	BT11-BT12	STD_BT3.7	BT12-BT3.7	BT11	NDSI
26	R0.8	R1.3	BT11-BT12	STD_BT3.7	BT12-BT3.7	BT11	NDVI
27	R0.8	R1.3	BT11-BT12	STD_BT3.7	BT12-BT3.7	BT11	R1.6
28	R0.8	R1.3	BT11-BT12	STD_BT3.7	BT12-BT3.7	BT11	R2.1
29	R0.8	R1.3	BT11-BT12	STD_BT3.7	BT12-BT3.7	BT12	NDSI
30	R0.8	R1.3	BT11-BT12	STD_BT3.7	BT12-BT3.7	BT12	NDVI
31	R0.8	R1.3	BT11-BT12	STD_BT3.7	BT12-BT3.7	BT12	R1.6
32	R0.8	R1.3	BT11-BT12	STD_BT3.7	BT12-BT3.7	BT12	R2.1
33	R0.8	R1.3	BT11-BT12	STD_BT12	BT11-BT3.7	BT11	NDSI
34	R0.8	R1.3	BT11-BT12	STD_BT12	BT11-BT3.7	BT11	NDVI
35	R0.8	R1.3	BT11-BT12	STD_BT12	BT11-BT3.7	BT11	R1.6
36	R0.8	R1.3	BT11-BT12	STD_BT12	BT11-BT3.7	BT11	R2.1
37	R0.8	R1.3	BT11-BT12	STD_BT12	BT11-BT3.7	BT12	NDSI
38	R0.8	R1.3	BT11-BT12	STD_BT12	BT11-BT3.7	BT12	NDVI
39	R0.8	R1.3	BT11-BT12	STD_BT12	BT11-BT3.7	BT12	R1.6
40	R0.8	R1.3	BT11-BT12	STD_BT12	BT11-BT3.7	BT12	R2.1
41	R0.8	R1.3	BT11-BT12	STD_BT12	BT12-BT3.7	BT11	NDSI
42	R0.8	R1.3	BT11-BT12	STD_BT12	BT12-BT3.7	BT11	NDVI
43	R0.8	R1.3	BT11-BT12	STD_BT12	BT12-BT3.7	BT11	R1.6
44	R0.8	R1.3	BT11-BT12	STD_BT12	BT12-BT3.7	BT11	R2.1
45	R0.8	R1.3	BT11-BT12	STD_BT12	BT12-BT3.7	BT12	NDSI
46	R0.8	R1.3	BT11-BT12	STD_BT12	BT12-BT3.7	BT12	NDVI
47	R0.8	R1.3	BT11-BT12	STD_BT12	BT12-BT3.7	BT12	R1.6
48	R0.8	R1.3	BT11-BT12	STD_BT12	BT12-BT3.7	BT12	R2.1

7. PDFs generation. Phase II: Optimization

The second phase of the PDFs generation process consisted in producing the PDFs on the basis of the information from a larger (one year) MODIS dataset. **Table 9** reports the number of pixels used to produce the PDF at this stage.

PDF's were generated according with the definition of variable range and classes, parameters and combinations described in the previous section (**Table 5-6**).

Figure 11 shows examples of 2D representation of a 4D (***STD_BT12, BT11-BT12, BT11-BT3.7, BT11***) night-time PDF.

A large set of PDFs (Night: 8x10x11=880, Day:48x10x9=4320) was generated during this phase.

Once generated, an analysis of the PDFs dataset was performed in order to:

- Select the variables combination with better classification skills
- Optimize the range and class definition of each variable
- Optimize the number of needed classes of parameters

This optimization phase was performed using the following tools:

- Analysis of statistical properties of the produced PDFs;
- Visual analysis of a set of study cases (Section 9)
- Quantitative comparison against independent Sea Ice Concentration products (Section 10)

Table 9 *Number of MODIS pixels used to generate the PDF's. * For the scene involving solar channels the largest value is reported. If the combination includes the 1.6 µm channel roughly 50% of the pixels are used.*

	NIGHT	DAY*	DUAL VIEW	SUNGLINT*	TWILIGHT*
CLD	4069226969.	2393875423.	277104	223566888.	694895725
ICE	3977098453.	789747027.	17304	44378743.	670593196
SEA	218117743.	98373123.	36684	17794335.	43648470
TOT	8264443165.	3281995673.	331092	285739966.	1409137391

Figures 12-13 show the total number of pixels for DAYTIME and NIGTHTIME as a function of the parameters (i.e. the number of pixels used to generate the PDFs). Each panel is relative to an SST. In the DAYTIME (**Fig.12**) differences arise from the fact that the 1.6 µm channel was not available for Aqua observations, therefore PDFs for variable combinations including such channel will be based on a reduced (~50% of the larger one) statistical dataset.

This section describes the phase of the study dedicated to the selection of the final set of PDF's starting from the whole set of PDF's produced.

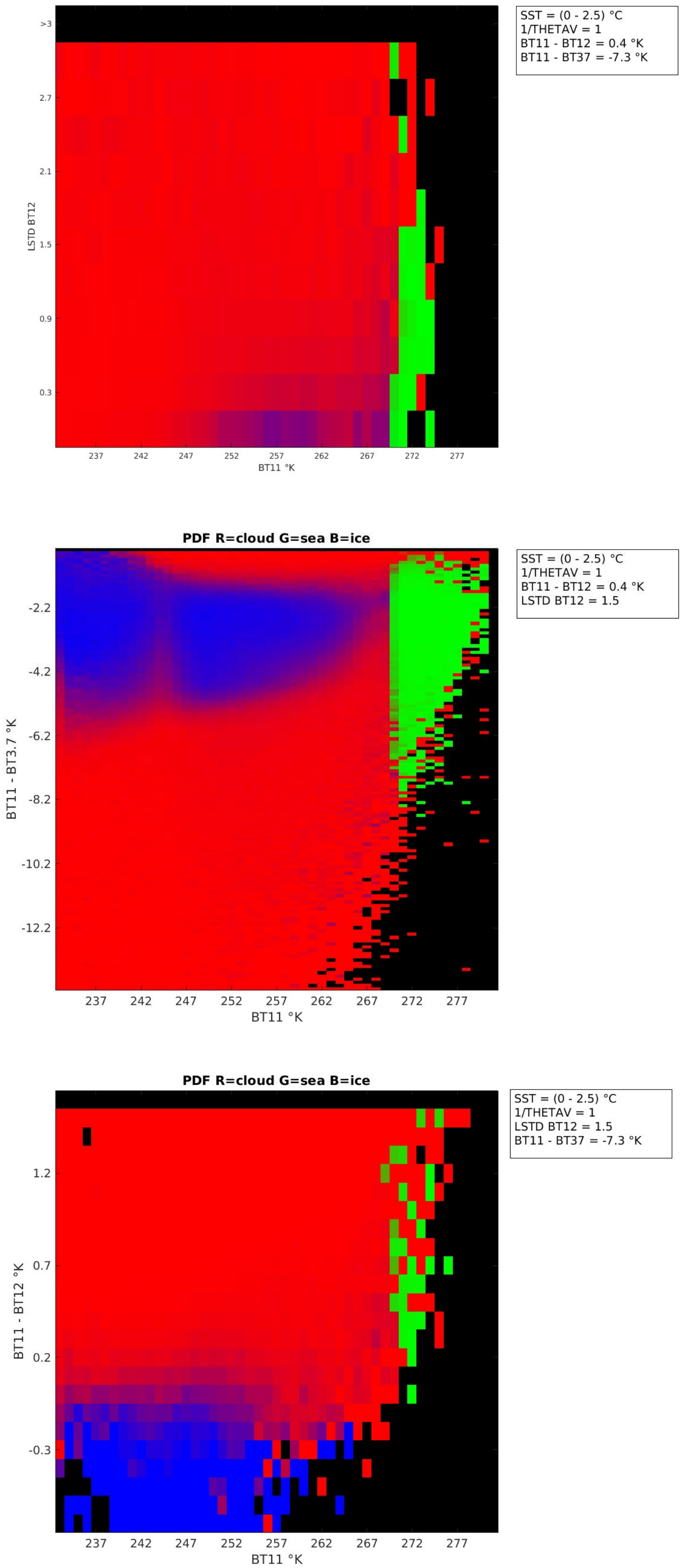

Fig.11. *Examples of night-time PDF: SST=0-2.5°C,* $cos^{-1}\theta_v$*=1-1.1. 2D representation obtained for fixed values of the other variables as reported on the box for each panel. Colours function of the probability of occurrence of* ***CLD***, ***SEA***, ***ICE***. *Upper to lower panel:* ***STD_BT12, BT11-BT12, BT11-BT3.7*** *vs* ***BT11***

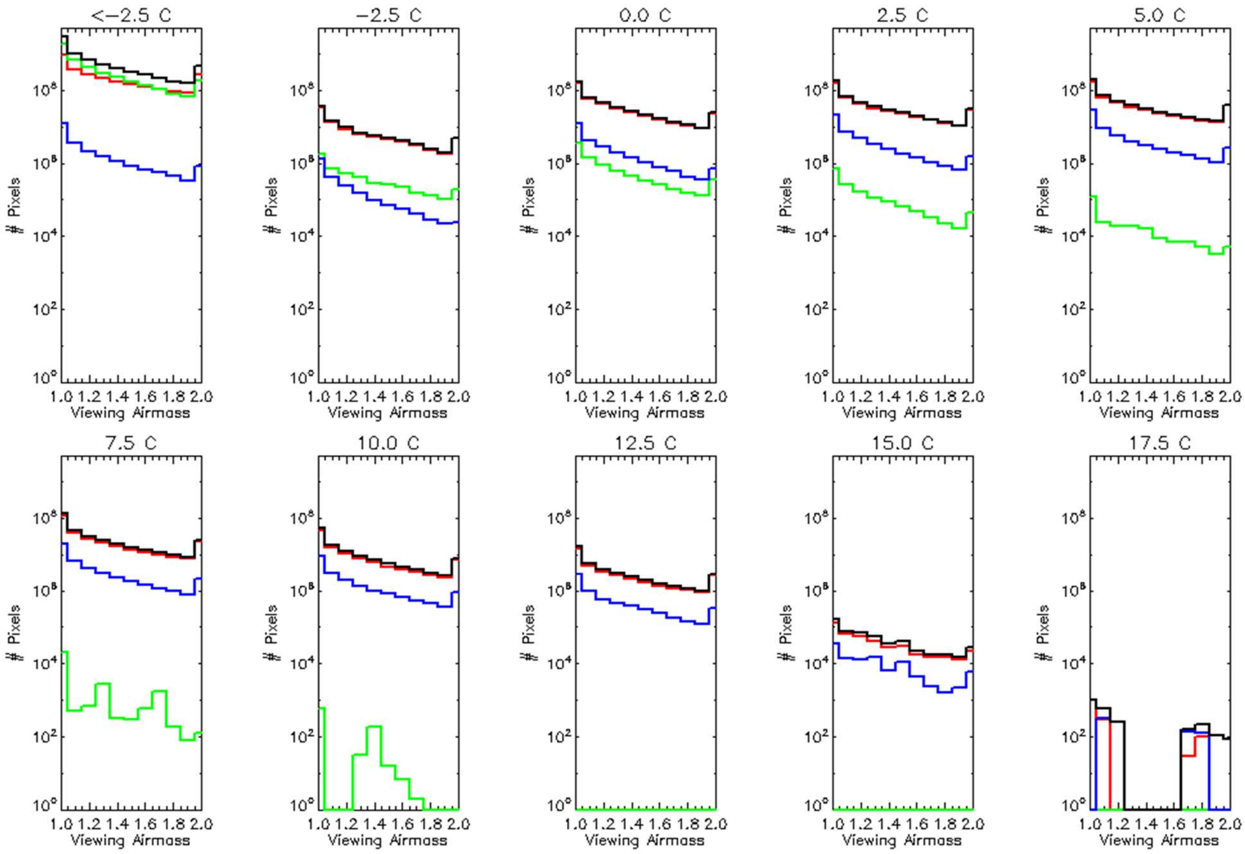

Fig.12 *Number of pixels as a function of SST classes ('<2.5°C' ice contaminated pixels according to AMSRE) and of the viewing airmass.* ***R****=CLD,* ***G****=ICE,* ***B****=SEA,* ***Black****=Total. Night time cases.*

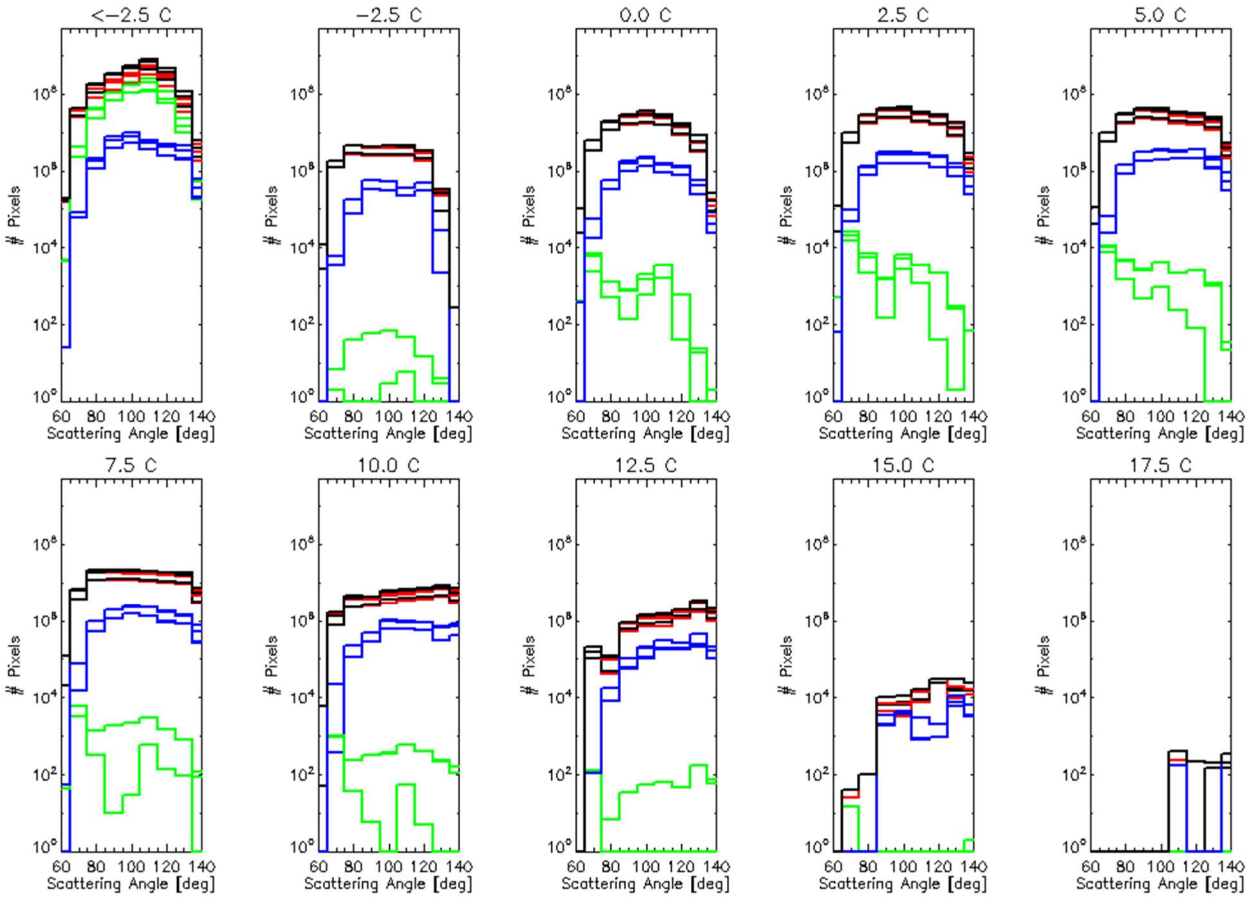

Fig.13 *Same as Fig7.for Daytime cases with observation geometry variable equal to the scattering angle.*

7.1 Range

Possibility to reduce the variable range is investigated by analyzing the population of the boundary classes in the larger dataset histogram. In particular, the initial range and class definition was based on the assumption, estimated from a reduced statistical set, that if above (below) a certain value the majority of the cases would fall in a unique class then the range was limited to the first value were only one scene type dominated the population. Analyzing the final dataset, if classes contiguous to boundary classes are found to be still populated in large majority by a unique scene type then the boundary class can are removed to reduce the total size of the PDFs.

Figs.14-15 show the histograms of distribution for night-time and daytime dataset integrated over the SST and geometry classes.

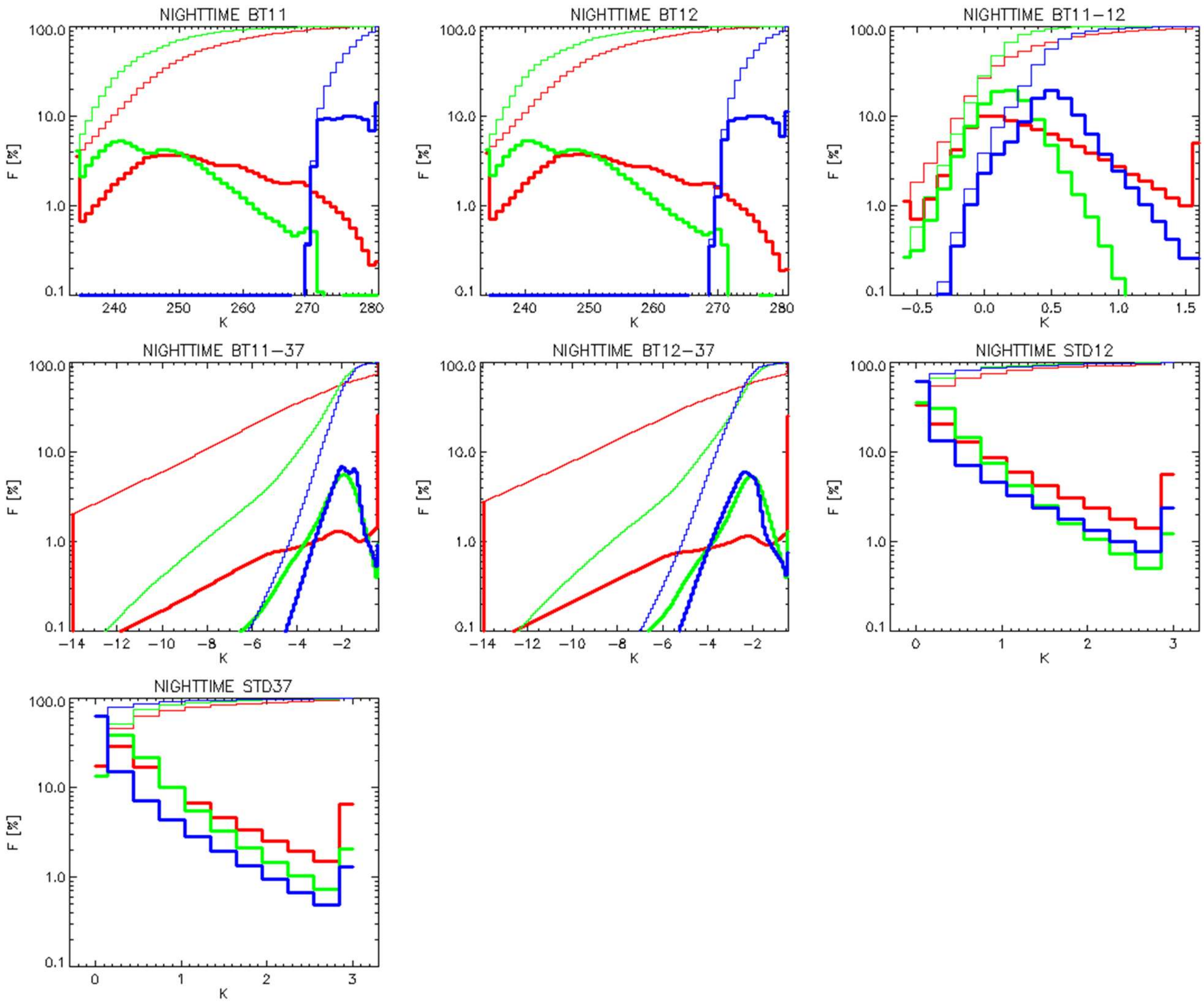

***Fig.14** Histogram of distribution for night-time dataset with the preliminary range and class definition (thin lines represent cumulative histogram). **R**=CLD, **G**=ICE, **B**=SEA*

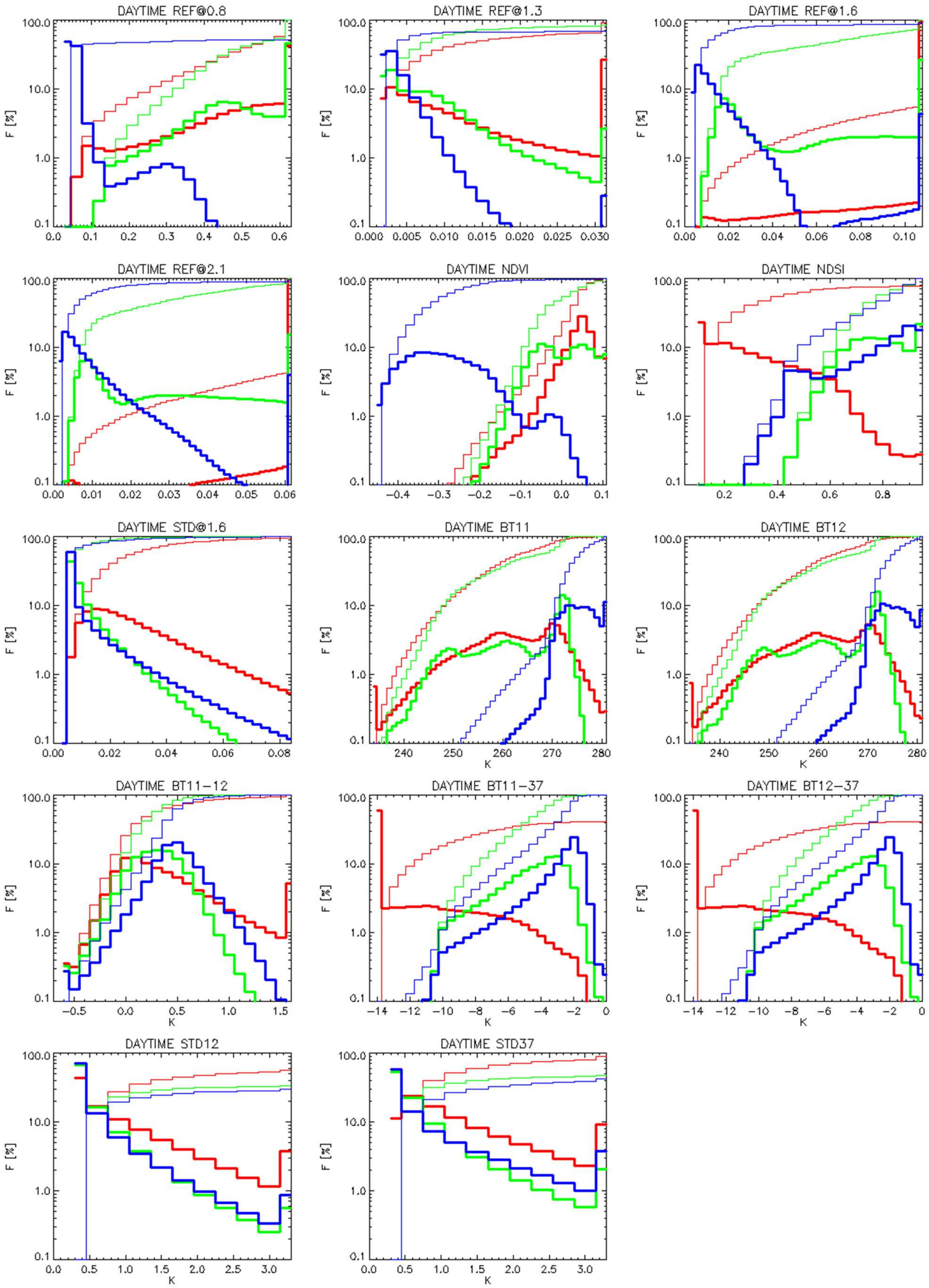

Fig.15 *Histogram of distribution for daytime dataset with the preliminary range and class definition (thin lines represent cumulative histogram).* ***R****=CLD,* ***G****=ICE,* ***B****=SEA*

7.2 Observation Geometry

The definition of classes for the observation geometry was optimized taking into account of:

- the effective occurrence in the larger dataset,
- the sensitivity of the variables as well
- the need to avoid artefacts clearly due to changes in the PDF used for classification.

For the scattering angle (DAYTIME) firstly the smallest values (<70°) are, in general, poorly populated (**Fig.13**) and, as expected, correlated to the SST values. Similar considerations apply for the upper class (>140°). For this reason the upper and lower limits of, respectively, the first and the last class were changed from 60°-140° to 80°-120°. Also the class widths remain nominally of 10° but practically each new class contains at least 20° of observed data as reported in **Tab.10**

Table 10. *Updated definition of the scattering angle classes*

Class Name	Effective Scattering Angle Range
80°	<90°
90°	80°-100°
100°	90°-110°
110°	100°-120°
120°	110°-130°
130°	>120°

Table 11. *Updated definition of the airmass classes*

Class Name	Effective Scattering Angle Range
1.1	1.0-1.1
1.3	1.1-1.3
1.5	1.3-1.5
1.7	1.5-1.7°
1.9	1.7-1.9°
2.0	>1.9

In addition to reducing the number of PDFs the new definition of observation geometry classes also solve partially the problem of missed classification. In fact, as mentioned in section 5, the convergence criteria to stop the generation of PDFs was based on the analysis of difference between different versions of the database base on overall variable histograms (geometry and SST cumulated statistics). However, particularly for the DAYTIME cases were we have 7 dimensions, there are still (internal) bins in the space defined by the variables that do not contain any MODIS information. The program we used to test the PDFs if the position in the PDF defined by the variable/parameters does not contain any data, leaves the pixel unclassified (black dots in the classification examples reported in Sect.9). By reducing the geometry classes (and creating an overlap) we also reduce the number of unclassified pixels..

For the observation angle, the sensitivity of changes of 0.1 airmass, for relatively dry and cold atmospheres is within the class width of the majority of the variables. Consequently, driven by the necessity to compact the PDFs we adopted a new definition of air mass classes that except for the first and last class the other one are 20° width (see **Tab.11**).

7.3 SST Classes

Regarding the possibility to reduce the number of SST classes, we examined two issues:

The first one was the reduction of the upper limit SST class. Conservatively the class including the warmer pixels was set with the relatively warm lower limit of 17.5°C. As expected, such class is poorly populated and there are no ice. We compacted all warmer classes to a single one SST>7.5°.

The second SST related issues is about the use of ancillary data (i.e. SST, sea ice occurrence) in the SLSTR product to select the PDF to be used for the classification. We identified a possible bias introduced by the use, in the classification, of the PDFs strictly according with the information contained in the ancillary data. In particular, if the SLSTR auxiliary data indicate occurrence of Sea Ice then use for the classification the PDF generated with all pixels classified as ICE from AMSRE.

As shown in figs.13-13, the majority sea ice pixel (green curves) occurred, as expected, when AMSRE classified its SST product as Sea Ice contaminated (53.5% of the pixels). On the other hand, we observe, that a portion of MODIS sea ice classified pixels occurs even for the SST class of 5°C. We also observe that the class with colder SST values (<0°C) labelled as -2.5°C shows an overall lower probability of occurrence of Sea Ice compared to classes with warmer SST. This is partly due to the limited size, and consequently statistical representativeness, of this class because of the effective range of SSt that is less than 2.5°C. In order to obtain a more realistic relation between SST value and probability of Sea Ice occurrence, we merged the -2.5°C and the sea ice one (labelled <2.5°) in a unique class.

7.4 Scene

In addition to DAY and NIGHT scene type, PDFs were generated also for TWILIGHT and SUNGLINT. The rationale for introducing this two additional scene types is the fact that solar channels are expected to contain, even in this critical situations, useful information for surface type classification compared to thermal ones. The planned test to check for their effective need consists in performing the classification using all scene type and comparing it against what obtained when using the corresponding (in terms of SST and geometry) NIGHT (DAY) PDF for TWILIGHT (SUNGLINT).

While conditions of twilight are relatively frequent, the occurrence of sun-glint conditions, given the overpassing local time of Sentinel3 are expected to be scarce (for MODIS overpassing times sunglint contaminated pixels are about 8% of the daytime uncontaminated data). Moreover, given the geometrical definition of sunglint contaminated pixels in MODIS data, we expect the corresponding PDF's to contain also case, with low local wind conditions, with very low sunglint contamination, as well as we noticed the occurrence in the DAY PDFs of values that can be associated to sunglint.

7.5 PDF missed combinations

Since the first classification tests we observed the occurrence in the produced images of unclassified pixels. This was due to the fact SLSTR observations would define positions in the PDF arrays that were not be filled (or scarcely filled <10) by corresponding MODIS data. The occurrence of missing PDF values is obviously larger the larger is the overall dimension (number of variables and variables classes) of the PDF. This was partly reduced by increasing the MODIS dataset, however residual missing values were still found even after analysing a full year of MODIS data. In order to eliminate the occurrence of unclassified cases, internal position in the PDF with missing data for any class were filled with the values corresponding to the one of the nearest neighbour. Given the fact that most of the unclassified cases seems to occur for clear ocean pixels, we suspect also the possibility that this could be partly due to the MODIS-SLSTR different spectral response function

7.6 Summary

Following the analysis described in the previous subsections we defined a new set of PDF with the characteristics summarized in **Tabs 12-13**

Table 12. *Final definition of class limits and width for the candidate variables. [1]First class includes all valid values lower than the minimum one [2]Last class includes all valid values larger than the maximum one*

Variable	min[1]	MAX[2]	Width
R0.8	0.06	0.6	0.03
R1.3	0.0015	0.03	0.0015
R1.6	0.009	0.105	0.003
R2.1	0.0045	0.06	0.0015
NDVI	-0.25	0.09	0.02
NDSI	0.3	0.9	0.05
STD1.6	0.003	0.081	0.003
TB11 [K]	234	280	1
TB12 [K]	234	280	1
TB11-TB12 [K]	-0.6	1.5	0.1
TB11-TB3.7 [K]	-11 -7	-0.5 -0.5	0.5 0.1
TB12-TB3.7 [K]	-11 -7	-0.5 -0.5	0.5 0.1
STDTB12 [K]	0.3	3	0.3
STDTB3.7 [K]	0.3	3	0.3

Table 13. *Optimized definition of class limits and width for the external parameters. [1]First class includes all valid values lower than the minimum one [2]Last class includes all valid values larger than the maximum one. [3]First class includes all valid values that according to AMSRE products are ice contaminated. [4]See text. [5] See Tab.9*

Parameter	Min[1]	MAX[2]	Width	
SST[4] [°C]	-2.5[3]	12.5	2.5	AMSR-E Derived SST (and ICE occurrence)
GAMMA [°]	90	120	10[5]	Scattering angle (Daytime)
$m=1/COS(\theta_v)$	1.1	1.9	0.2	Viewing air mass (Nigthtime)

8. Neural Network

During the tuning (Sect.7) and validation phase (Sect.10) of the PDF's classification approach the need of a significant processing time has been observed. This could be a limitation for operational applications. Having already faced this type of constraints, our team has developed different methodologies to speed up application of remote sensing algorithms. In particular, Neural Networks (NNs) have proven their effectiveness to produce results for applications with severe constraints on processing time, providing comparable accuracy to other methods. Examples of those applications are reported in different works published by the team and regarding the retrieval of temperature and humidity profiles (Del Frate and Schiavon, 1999) as well as the volcanic ash monitoring (Picchiani et al., 2011 & 2014).

Since the generation of the PDFs required collecting a large and representative set of cases, we have already a dataset suitable for training the NNs algorithm. In addition to the activities foreseen in the original job tasks structure, we decided to test the effectiveness of the alternative approach (NN) on a subset of possible cases (night-time), which represents the most challenging one.

In this experiment, Multilayer Perceptron NNs (MLP NNs) have been applied exploiting their capability to perform over a wide range of problems. MLP NNs belong to the ensemble of supervised algorithms, this means that the information is transferred from a given dataset, called training set, to the NNs architecture so that the algorithm can approximate a non-linear functional between the input and output quantities. In this study, the training set has been composed by the same inputs, MODIS observations, used to generate the PDFs (Sect.6).

The MLP NNs has been designed considering the *tanh* activation function and the Levenberg-Marquardt backpropagation algorithm for the training phase. The latter has been performed in Matlab 2016b exploiting the multicore capability of a workstation (Intel I7 6700; 64 GB of RAM) to reduce the training time. In the night-time case the training set has been computed considering the PDF combination 1 (**STDTB12, TB11, TB11-TB12, TB11-TB37, θ_v, SST**). The choice has been guided by the better performance achieved by this combination with respect the other ones in the tuning phase of the PDF approach. Further analysis should be performed in order to identify the best subset of variables for the classification task for all possible cases (daytime, twilight and night-time).

Since the PDF inputs represent the statistics of an extended period of observation, the NN should be trained considering the whole dataset but the dimension of this data set is extremely large (total number of patterns is about 300.32 10^6 for the night-time case). In order to prevent a very slow training phase and to avoid the possibility to incur in the overfitting problem, the training set was generated by randomly subsampling the complete dataset. After several trials, we have found that 10% of the total number of samples is sufficient to reach the best performances with the given set of inputs, provided that the random sampling reproduces the proportions between the examples of the different classes. This is a relevant advantage of the NNs technique since it reduces the memory occupation and the computational time.

Once randomly sampled 10% of the overall dataset, the resulting number of patterns has been divided considering the 60%, 20% and 20% of the available points to obtain three datasets: the training, the test and the validation ones. The training and test sets are employed to train the network applying the early stopping criteria, i.e. the learning phase is interrupted when the performance on the test set starts decreasing (Bishop, 1995). The validation test is applied after the training phase to evaluate the overall classification performance on samples not included in the learning process. A simple heuristic method has been applied to select the best NNs topology for the night case. The architecture of the network providing the higher overall accuracy on the validation set, resulted as composed of two hidden layers of 15 and 10 neurons respectively. Anyway, a test performed varying the number of hidden layers and the number of neurons in each layer shows a good stability of the classification performance. This confirms that the training datasets are representative and, at least for the small topologies here considered, the NNs correctly address the classification task without incurring in the overfitting problem. Another strength of the NNs solution is the fast computation in the application phase. Indeed, to classify a single Sentinel 3 SLSTR granule, the algorithm employs about 0.87 s.

Table 14 reports the confusion matrix for the night NNs: the Target Class refers to the MODIS classification of each pixel, while the Output Class refers to NNs outputs. The three classes are 1 – SEA. 2 - ICE. 3 – CLD. Overall correctly classified cases correspond to 88.5 % of the set, while larger error in classification occurs for SEA pixels. Misclassification for each class are also reported, as well as the commission and omission errors (Richards and Jia, 1999) reported in the grey column/row of the matrix.

Examples of granules classified with the NN are reported in the next section to be compared with classification results from PDFs based method.

Table 14. Confusion matrix for the Night NN. Classes are 1 – SEA. 2 - ICE. 3 –CLD.

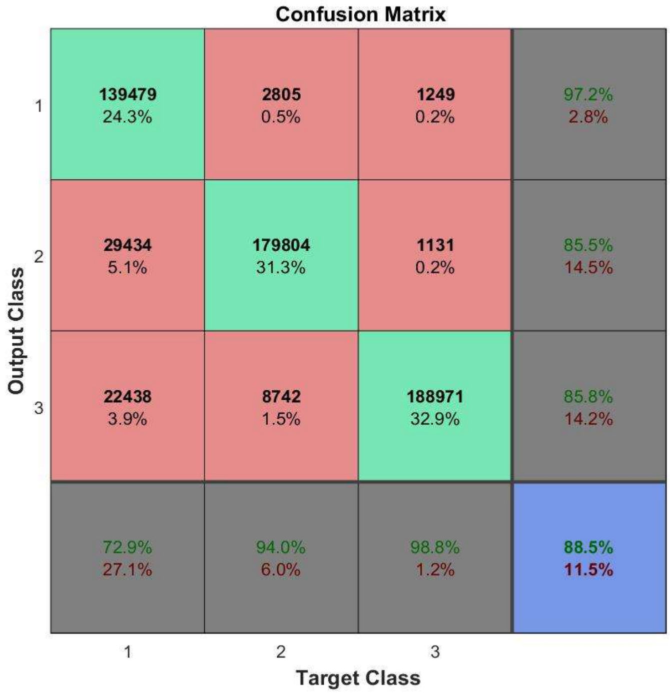

9. Examples of results

To tune and evaluate the classification algorithms, we selected manually a set of 95 granules (See Appendix 2) with the following criteria:

- area covered by the Sea Ice Concentration products (see **Fig.25**) used to quantitatively estimate the sea ice detection skill (Sect.10);
- granules close to the coast, with occurrence of both clouds and sea ice to focus on testing the ability to distinguish between sea-ice and clouds;
- sampling of different scene types: DAY, NIGHT and TWILIGHT

In addition to the limited geographical area, this sample of cases is also limited in terms of annual variation given the availability of SLSTR data (Nov. 2016 – May 2017).

This section shows some examples (**Figs.16-24**) from the selected cases to illustrate differences among different classification methods and common strengths and weaknesses. For each case, the following set of images are shown:

- a large image to show the context: for DAY and TWLIGHT, the RGB combination B=S1_radiance_an, G=S3_radiance_an, R=S5_radiance_an (**R5G3B1_LND**), for NIGHT the S8_BT_in. confidence_in_land mask (dark green colour) is applied (**S8_BT_in_LND**).
- an image of S8_BT_in with applied the confidence_in_land and summary_cloud (**CLD**).
- an RGB image with one of the following combinations: DAY/TWILIGHT B=S1_radiance_an, G=S4_radiance_an, R=S5_radiance_an (**R5G4B1**), or NIGHT B=S8_BT_in, G=S8_BT_in - S7_BT_in, R=S8_BT_in - S9_BT_in (**R8-9G8-7B8**).
- a series of images showing the results of the classification performed with different methods according to the Key reported in last column of Table.15 (**B-F, NN**).

***Table 15**. Classification algorithm tested. Column 1: name, Columns 3-5 Variables, Column 6: additional characteristics, Column 6: Key used to distinguish algorithms for **Figs.16-24**.*

METHOD	VARIABLES				Key
	DAYTIME	NIGHT-TIME	TWILIGHT	COMMENTS	
6VDCD14VN	**R0.8 R1.3 BT11-BT3.7 BT11 R16 STD1.6**	**BT11-BT12 STD_BT12 BT11-BT3.7 BT11**	//	SINGLE VIEW	A1
6VDCD24VN	**R0.8 BT11-BT12 BT11-BT3.7 BT11 R16 STD1.6**	**BT11-BT12 STD_BT12 BT11-BT3.7 BT11**	//	SINGLE VIEW	A2
5VD3VN	**R0.8 R1.3 BT11-BT3.7 BT11 R16**	**BT11-BT12 BT11-BT3.7 BT11**	//	SINGLE VIEW	B
5VD4VN	**R0.8 R1.3 BT11-BT3.7 BT11 R16**	**BT11-BT12 STD_BT12 BT11-BT3.7 BT11**	//	SINGLE VIEW	C
5VD3VN5VT	**R0.8 R1.3 BT11-BT3.7 BT11 R16**	**BT11-BT12 BT11-BT3.7 BT11**	**R0.8 R1.3 BT11-BT3.7 BT11 R16**	SINGLE VIEW	D
5VD4VN (NN)	//	**BT11-BT12 STD_BT12 BT11-BT3.7 BT11**	//	NEURAL NETWORK	NN
5VD4VN (DV)	**R0.8 R1.3 BT11-BT3.7 BT11 R16 +DBT_DV**	**BT11-BT12 STD_BT12 BT11-BT3.7 BT11 +DBT_DV**	//	DUAL VIEW	DV

Figure 16. *Night-time Example. Granule:*
S3A_SL_1_RBT____20170125T192921_20170125T193221_20170125T214713_0179_013_313_1439_SVL_O_NR_002.SEN3

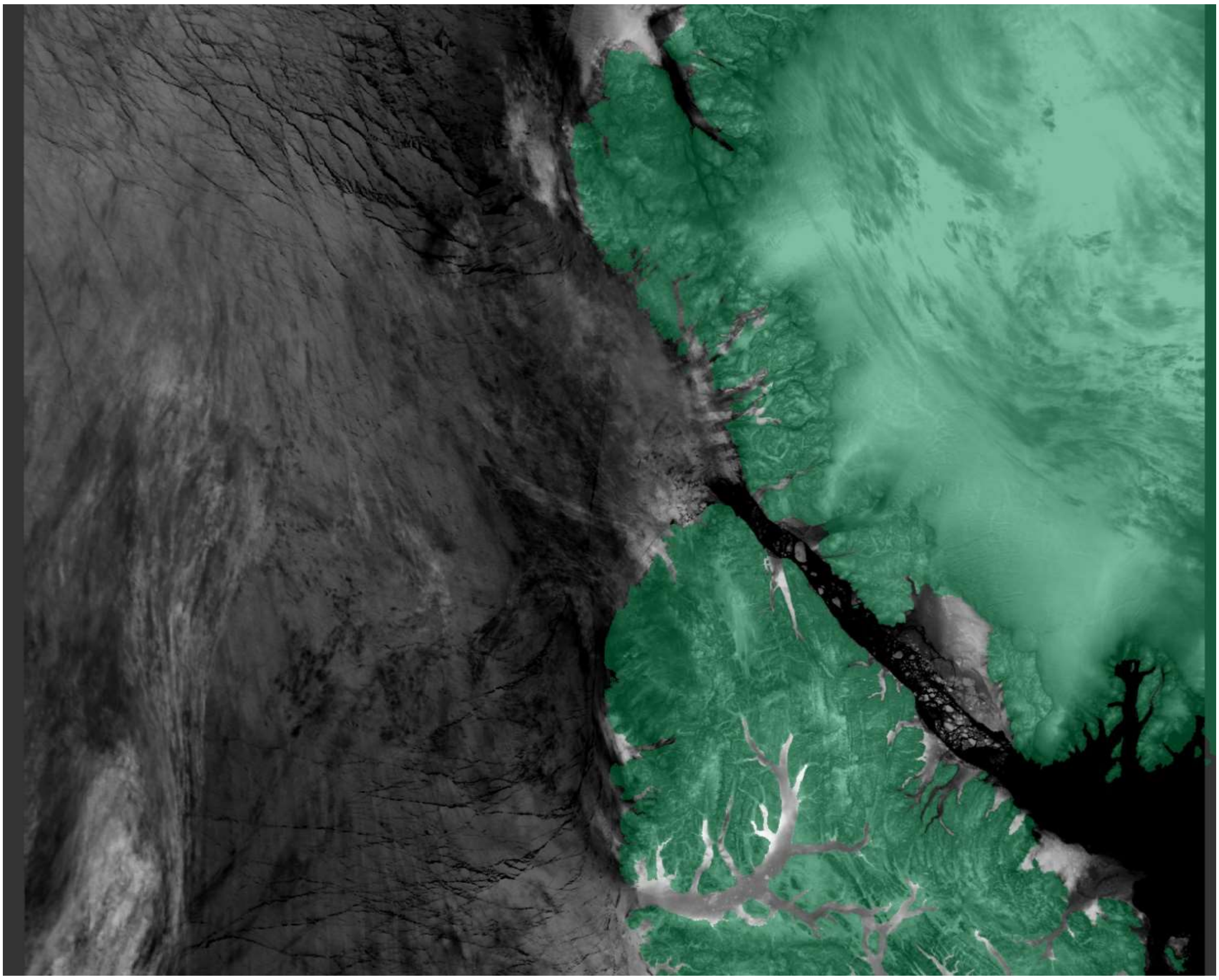

S8_BT_in_LND

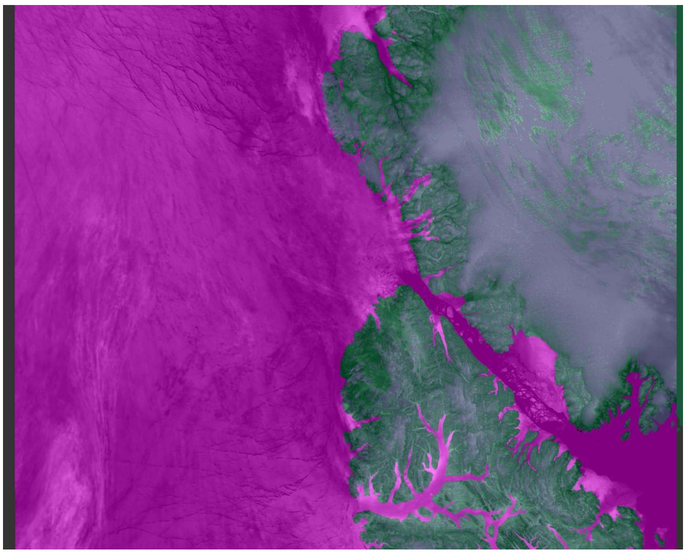

CLD

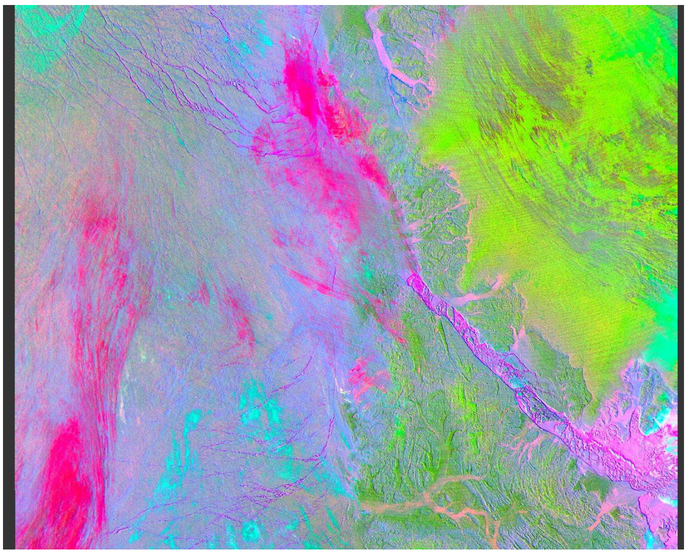

R8-9G8-7B8

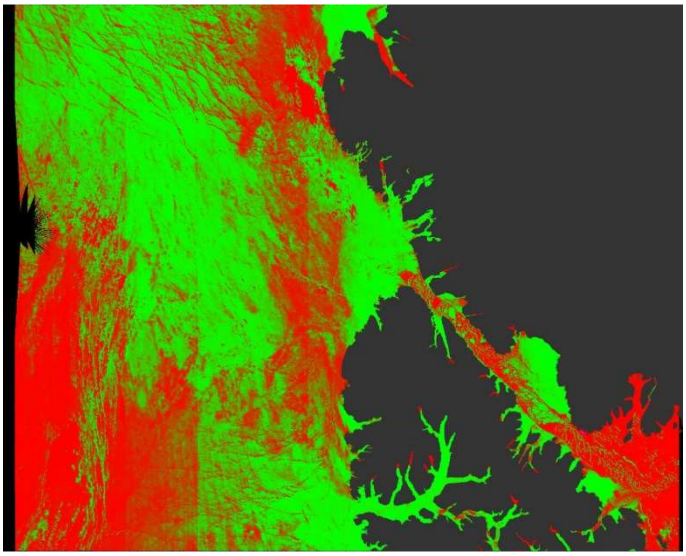

B

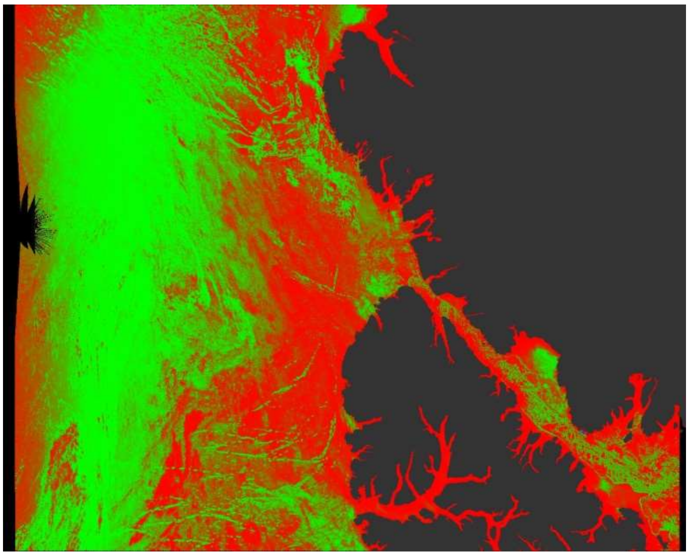

NN

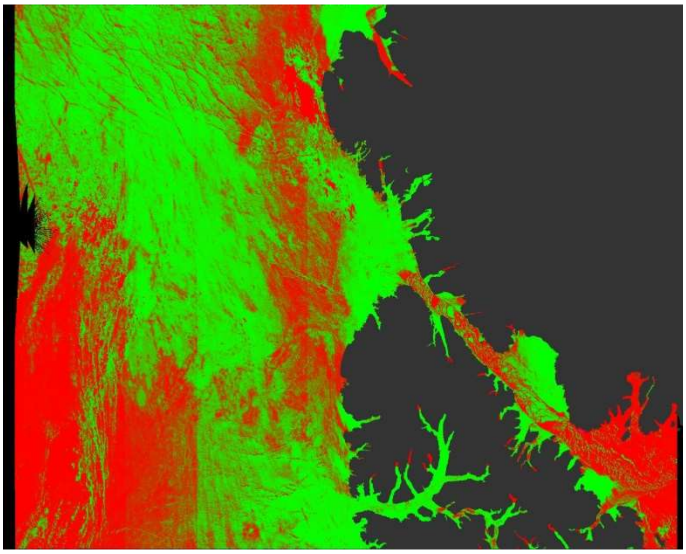

C

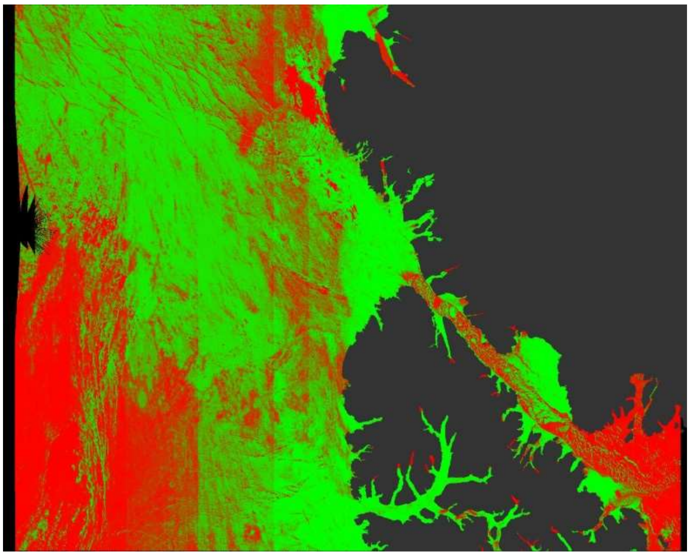

DV

Figure 17. *Night-time Example. Granule:*
S3A_SL_1_RBT____20170211T202612_20170211T202912_20170213T024901_0179_014_171_1260_LN2_O_NT_002.SEN3

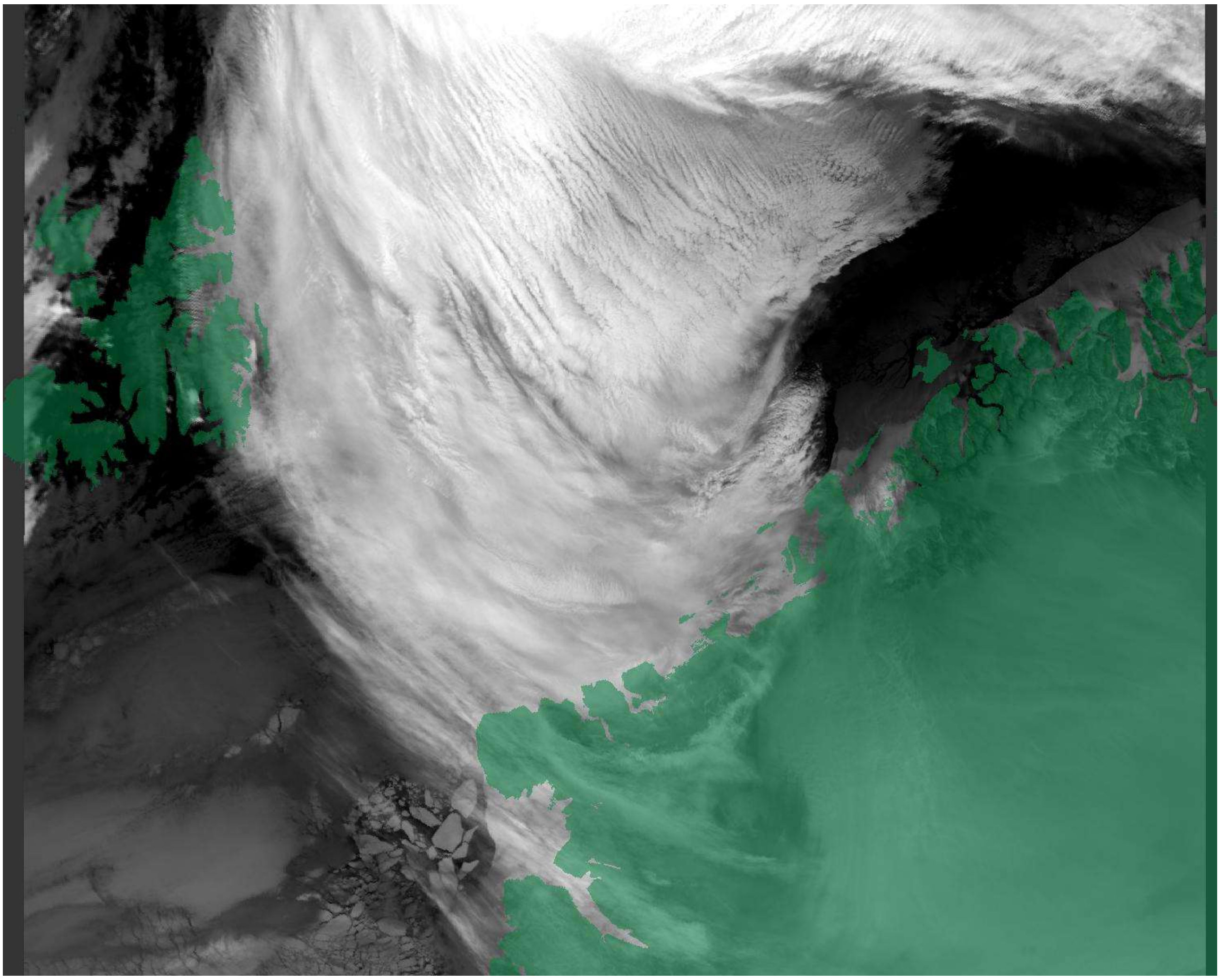

S8_BT_in_LND

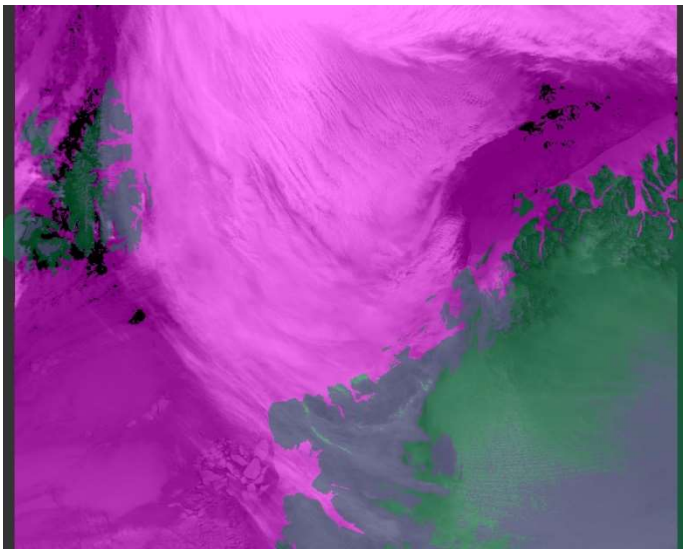

CLD

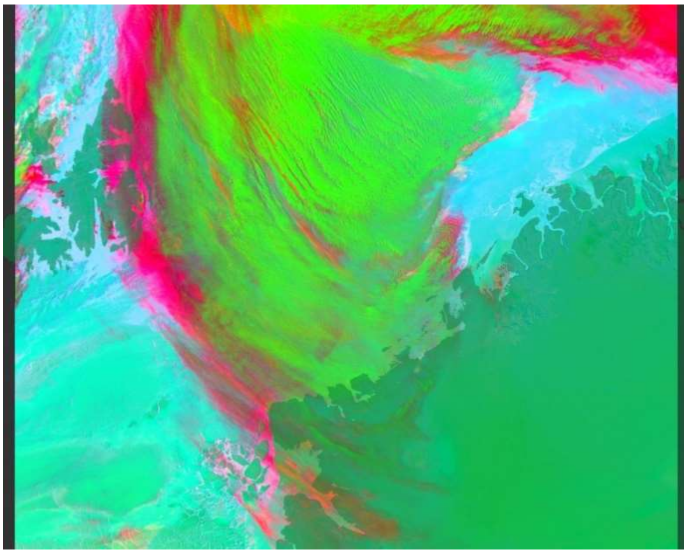

R8-9G8-7B8

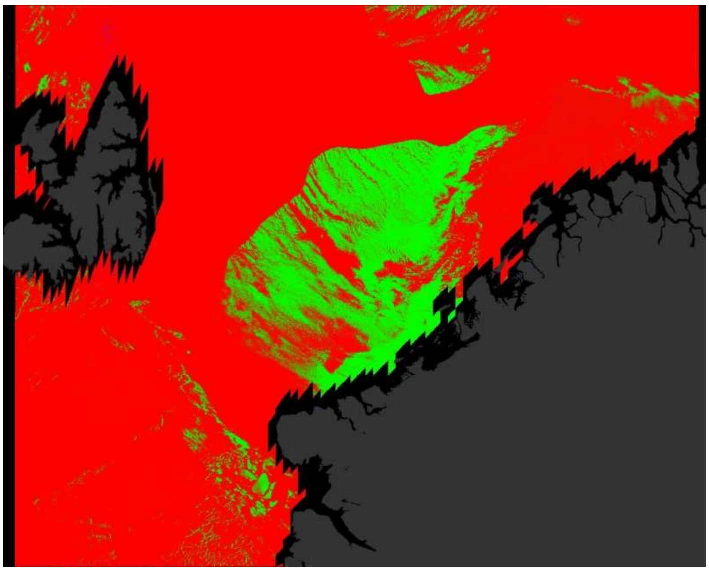

B

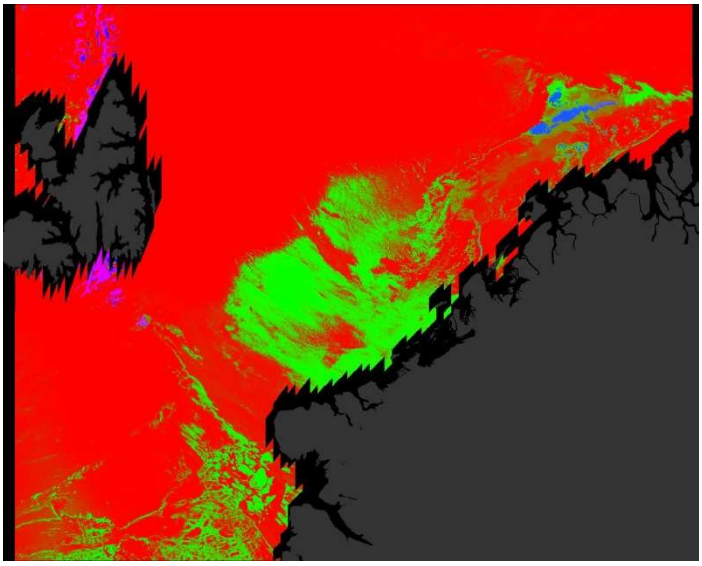

NN

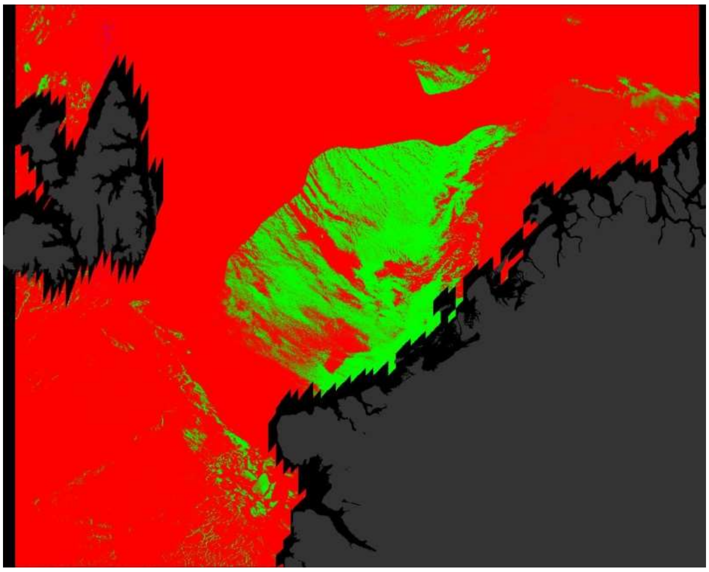

D

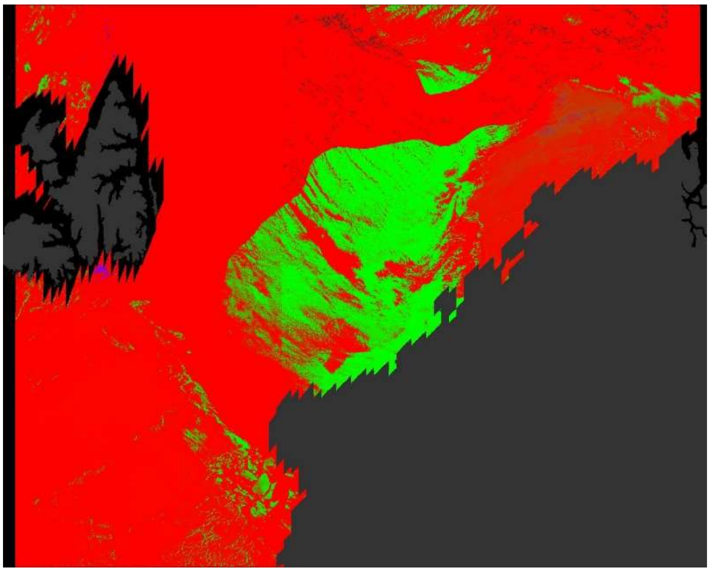

DV

***Figure 18**. Twilight Example. Granule:*
S3A_SL_1_RBT____20170401T155612_20170401T155912_20170403T111522_0179_016_097_1439_LN2_O_NT_002.SEN3

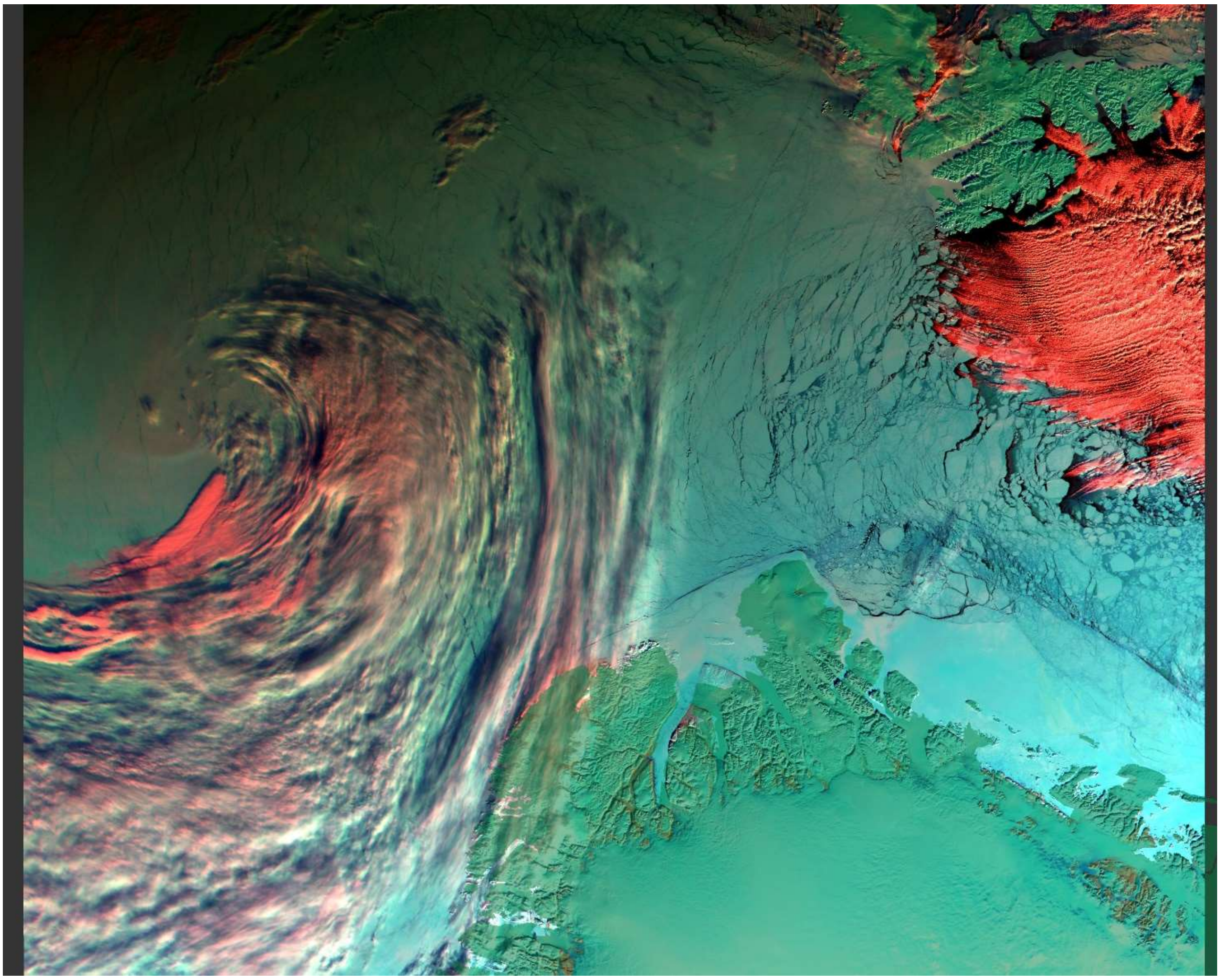

R5G3B1_LND

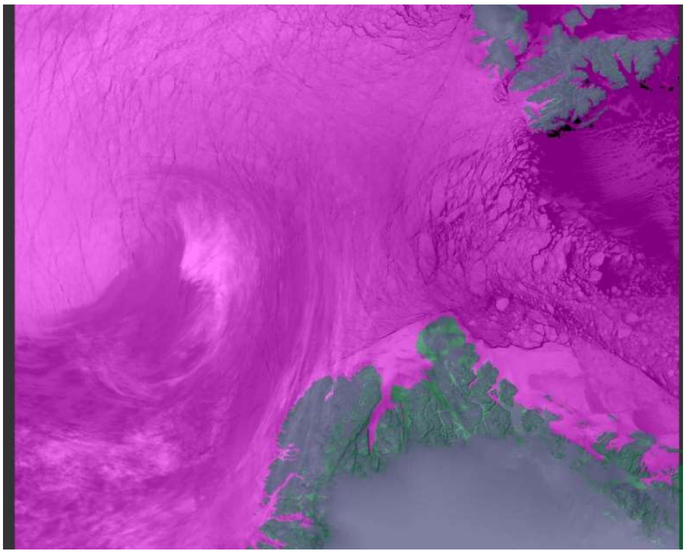

CLD

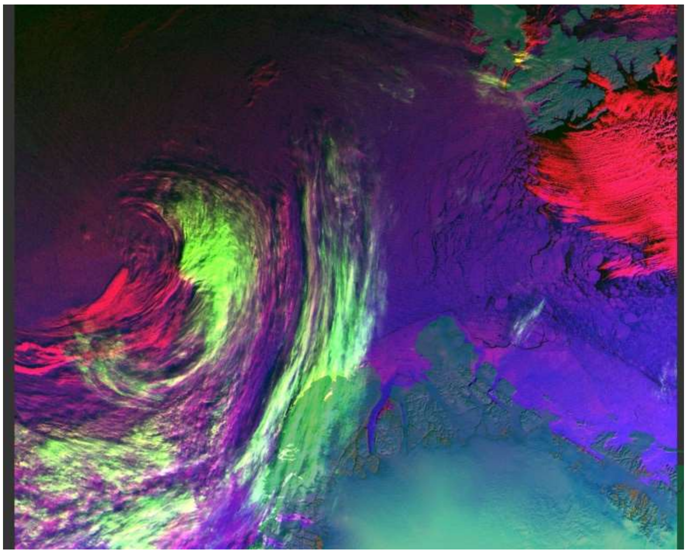

R5G4B1

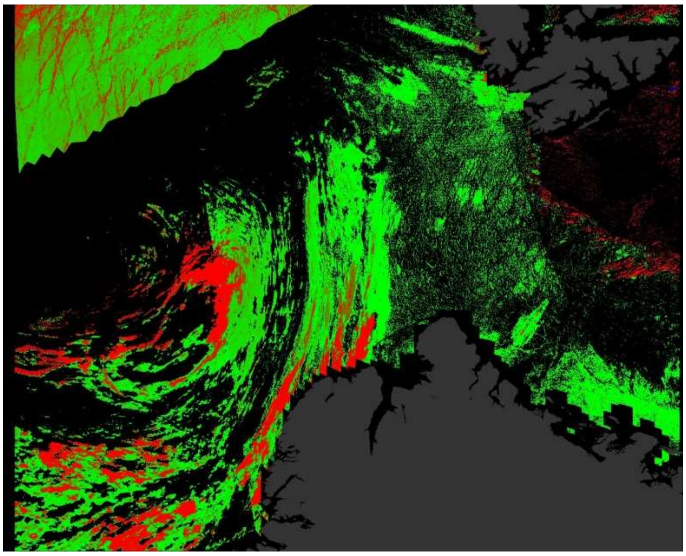

A1

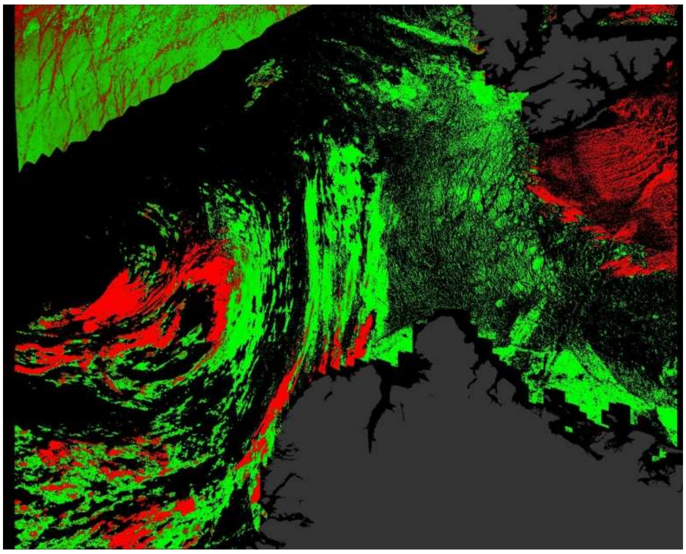

A2

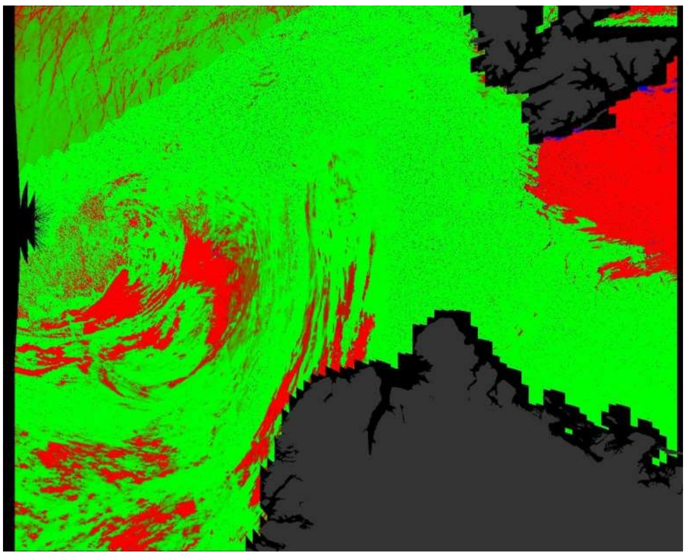

B

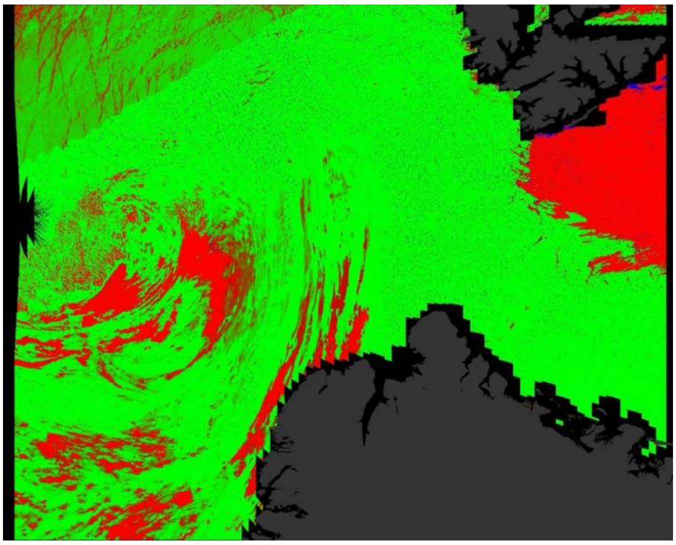

C

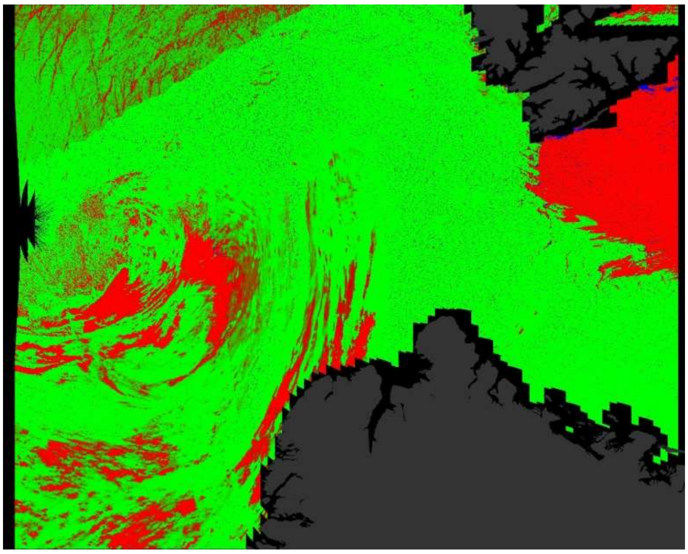

D

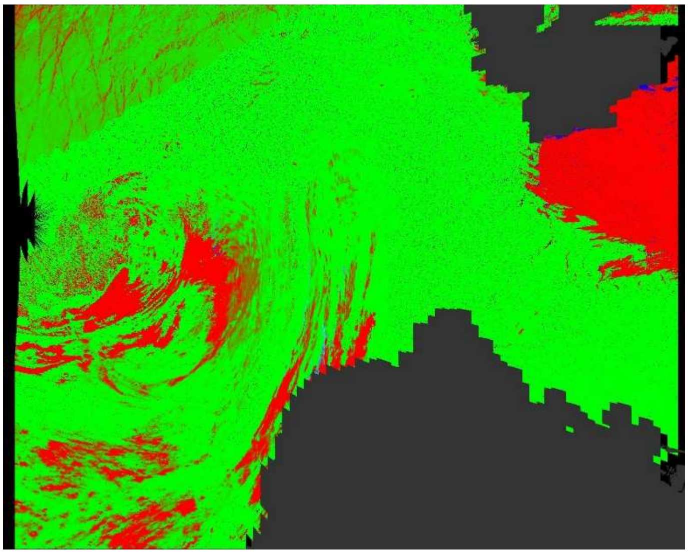

DV

Figure 19. *Daytime Example. Granule:*
S3A_SL_1_RBT____20170424T105959_20170424T110259_20170424T131246_0179_017_037_1620_SVL_O_NR_002

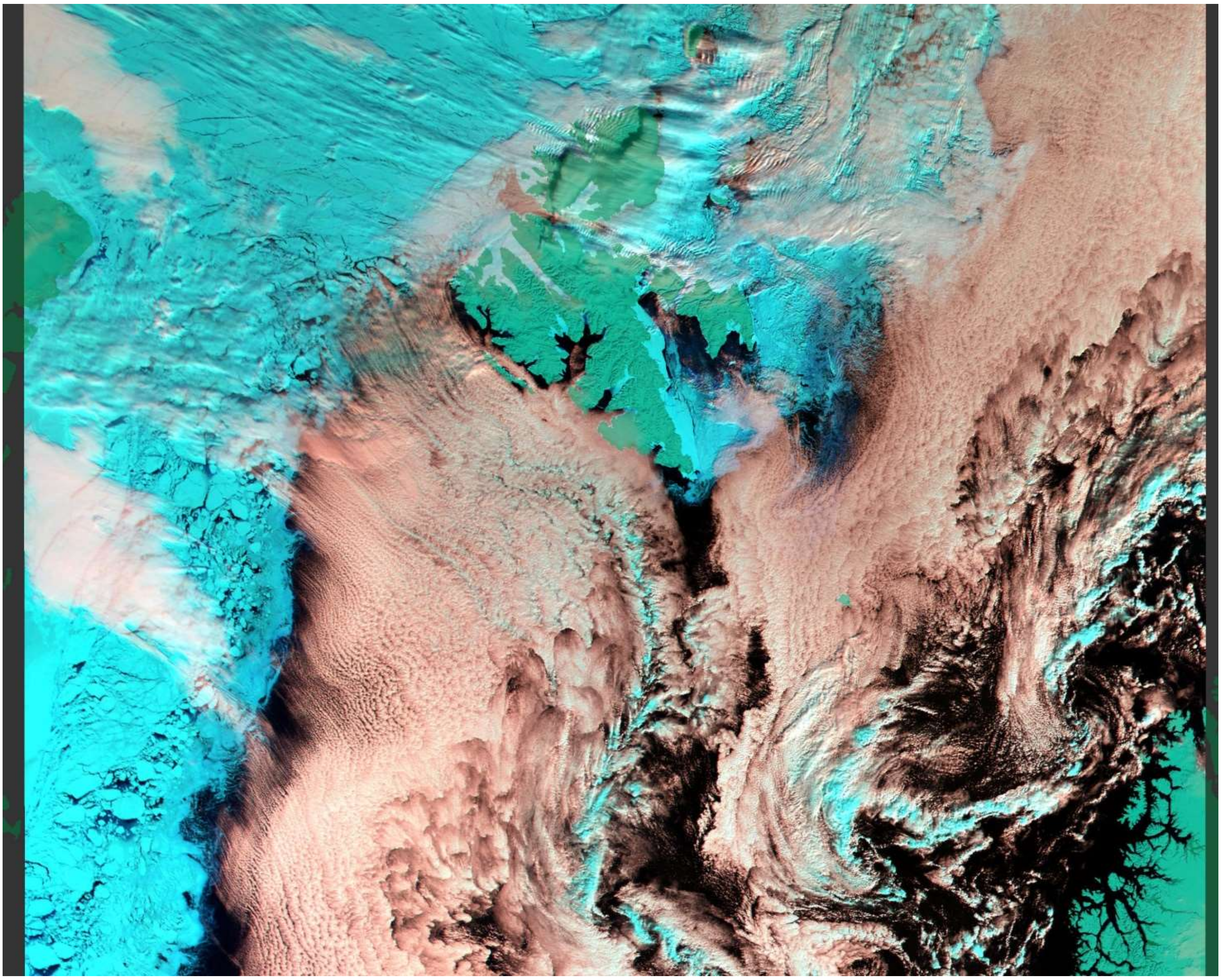

R5G3B1_LND

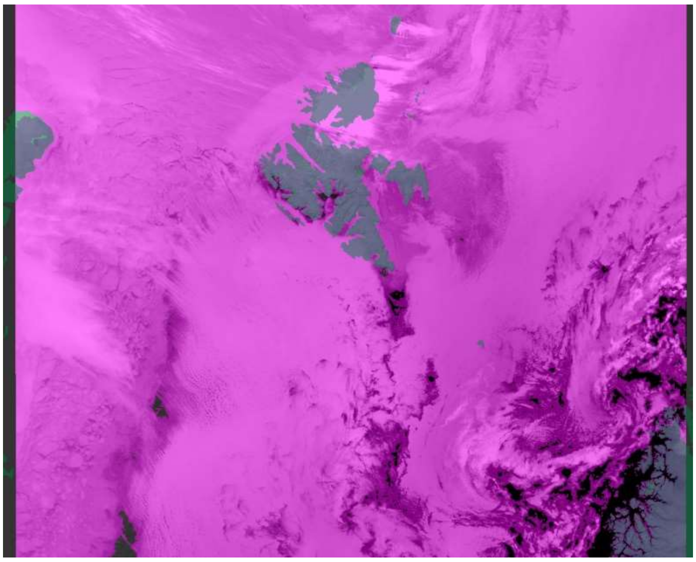

CLD

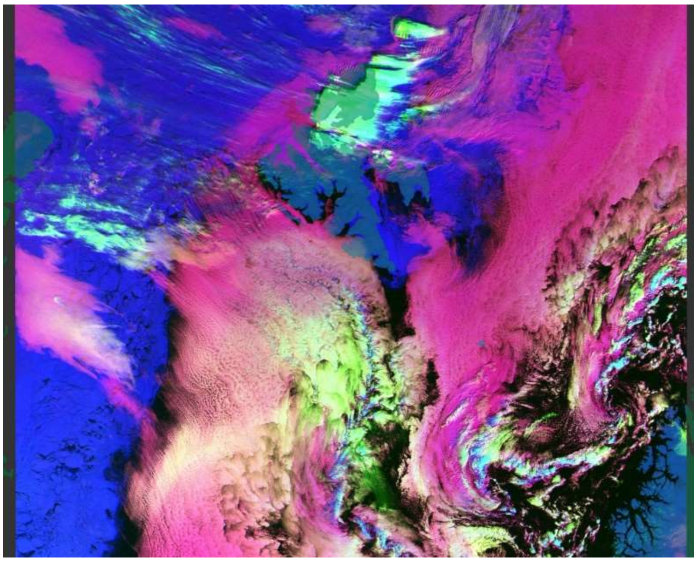

R5G4B1

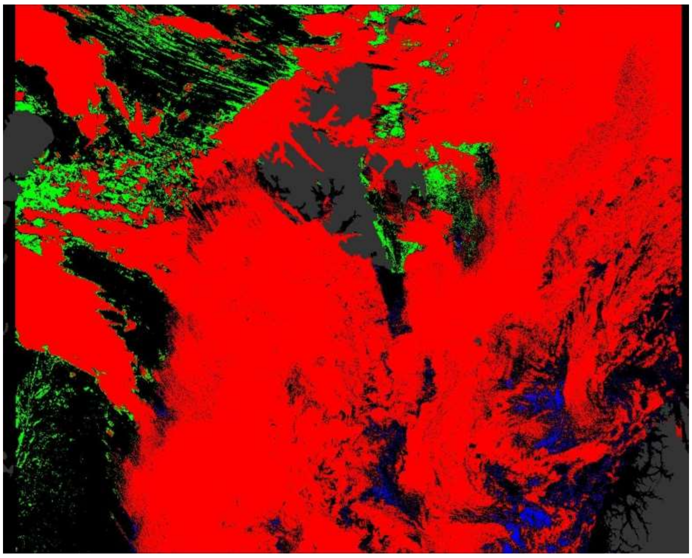

A1

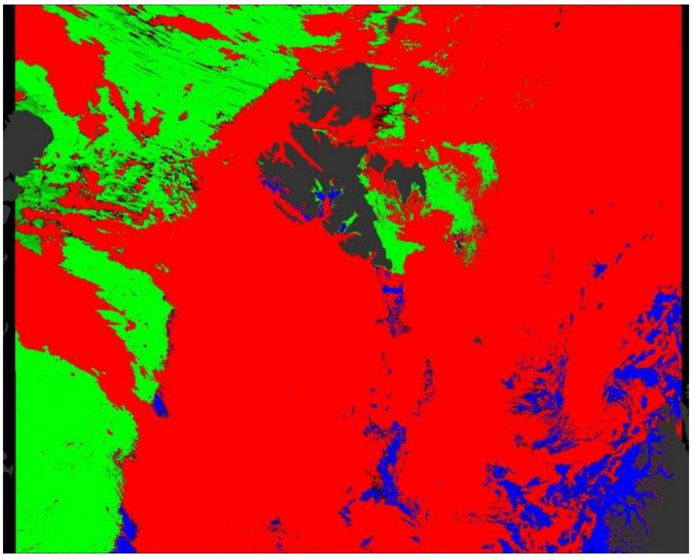

D

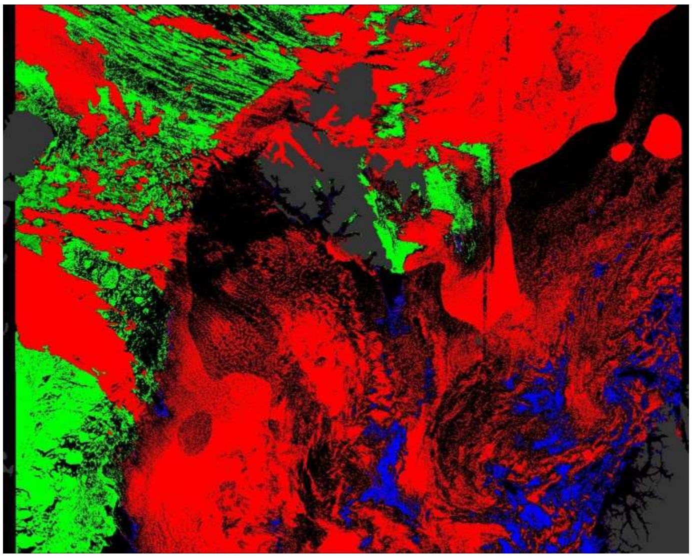

A2

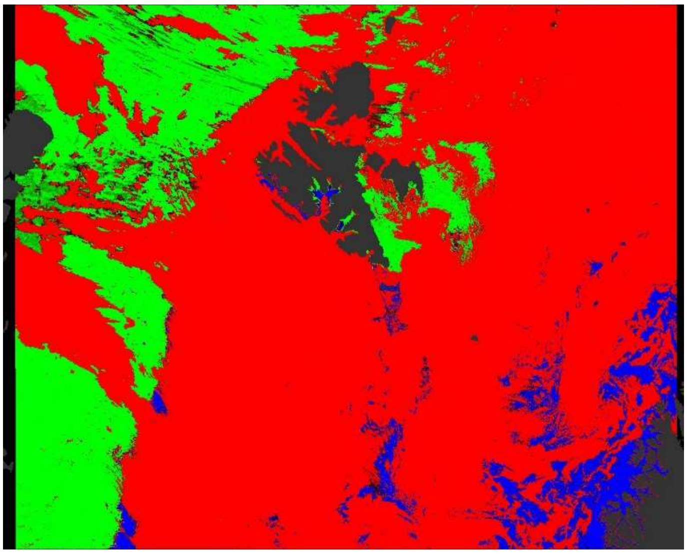

DV

***Figure 20**. Night-time Example. Granule:*
S3A_SL_1_RBT____20170119T202227_20170119T202527_20170119T224303_0179_013_228_1260_SVL_O_NR_002.SEN3

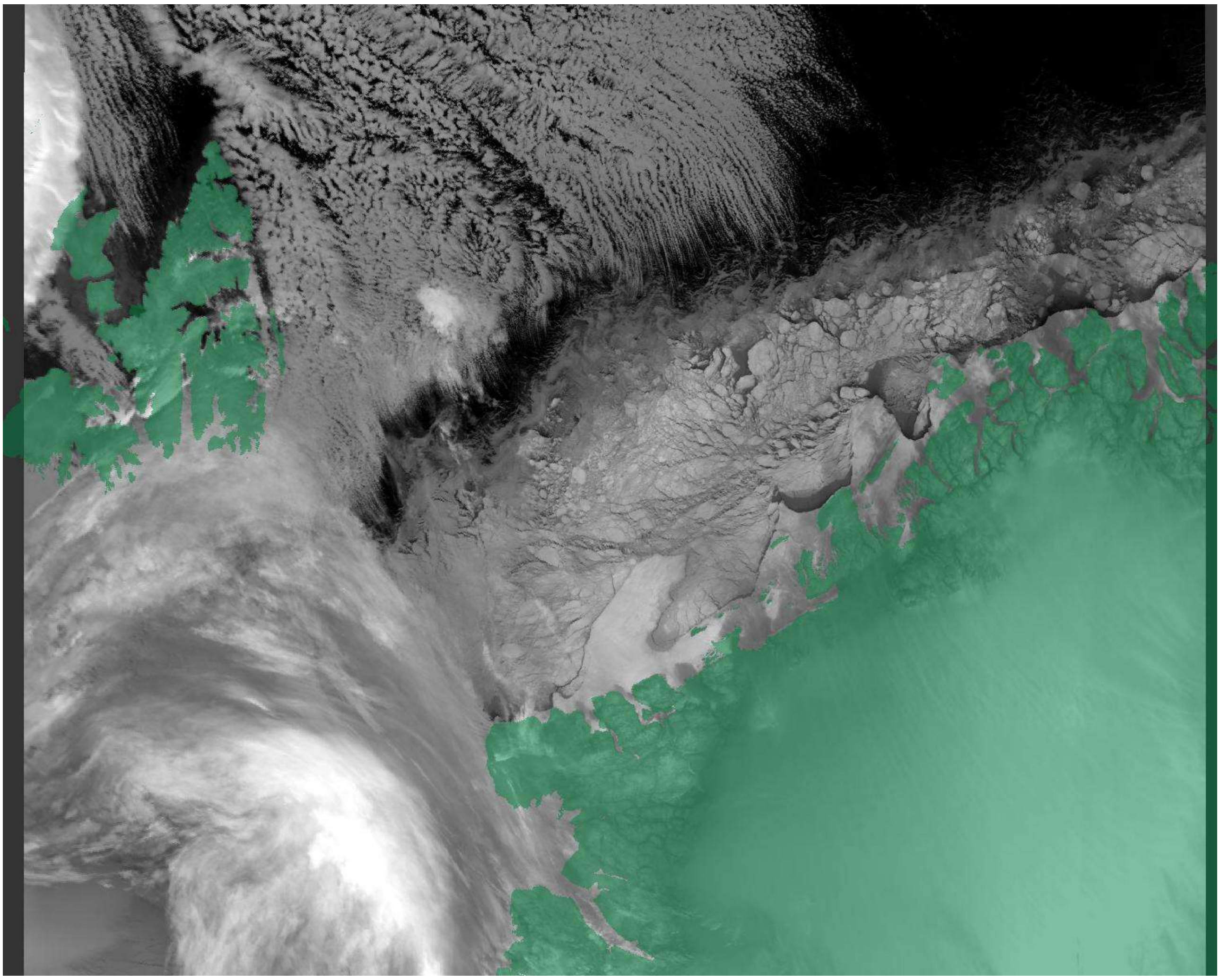

S8_BT_in_LND

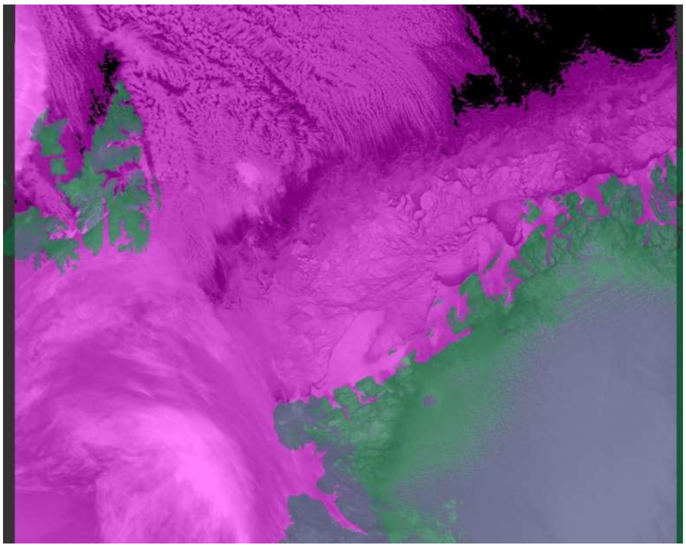

CLD

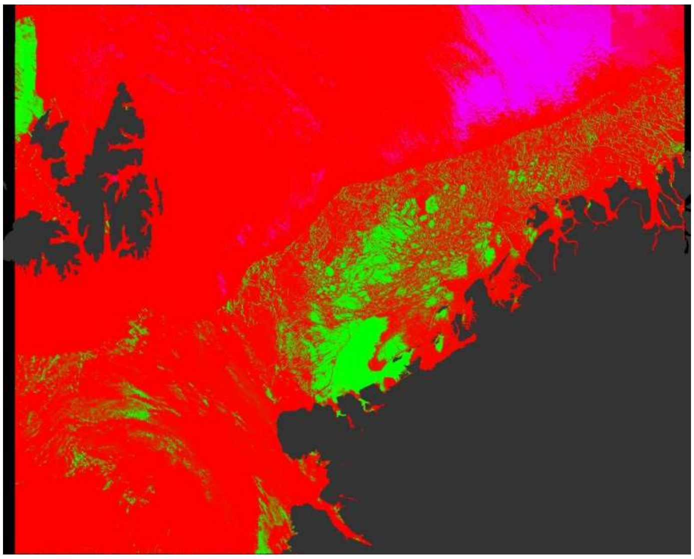

B

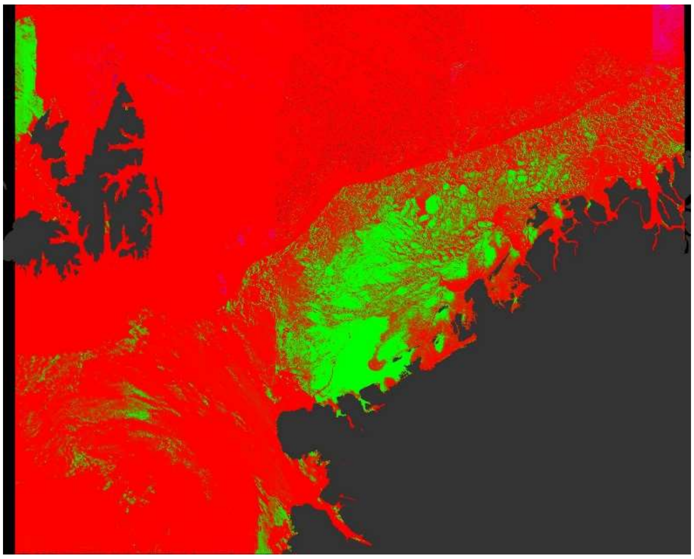

DV

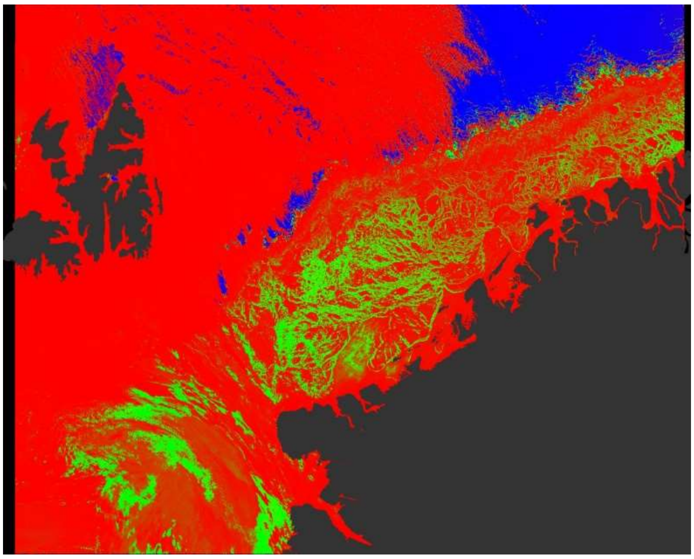

NN

Figure 21. *Night-time Example. Granule:*
S3A_SL_1_RBT____20170212T181902_20170212T182202_20170214T005338_0179_014_184_1260_LN2_O_NT_002.SEN3

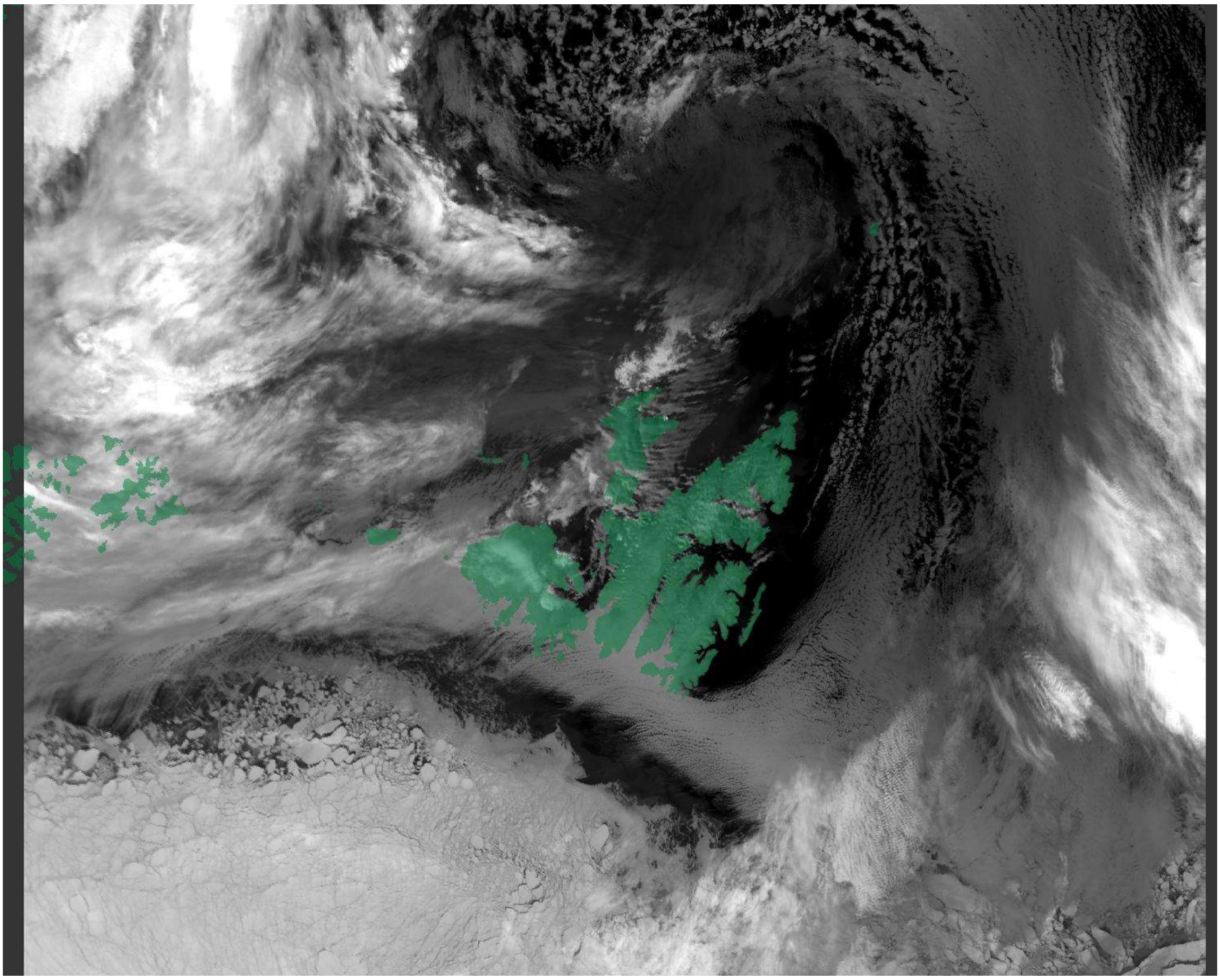

S8_BT_in_LND

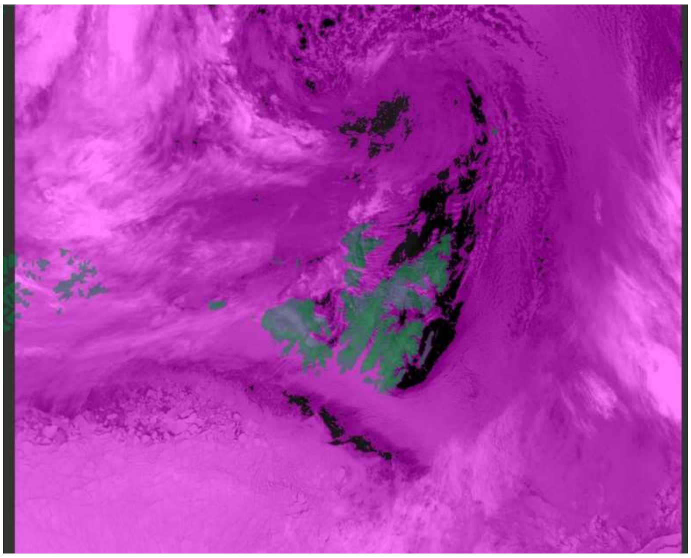

CLD

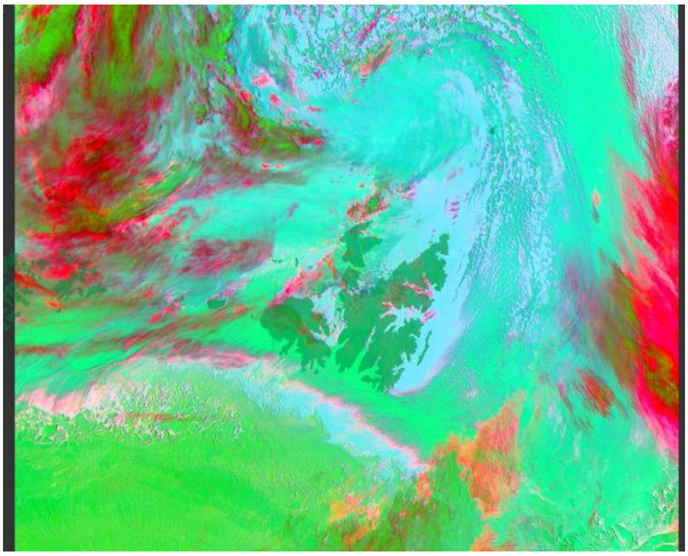

R8-9G8-7B8

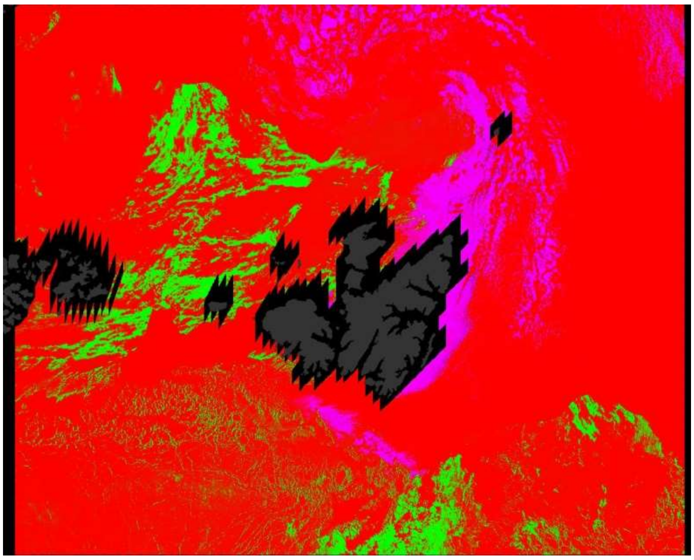

B

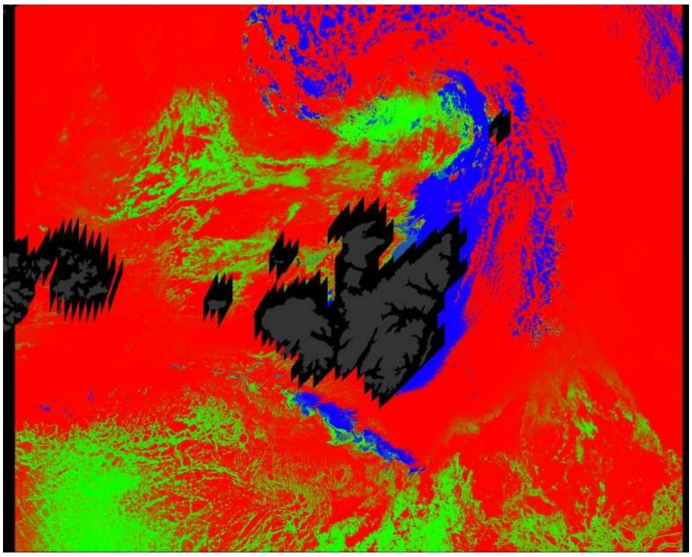

NN

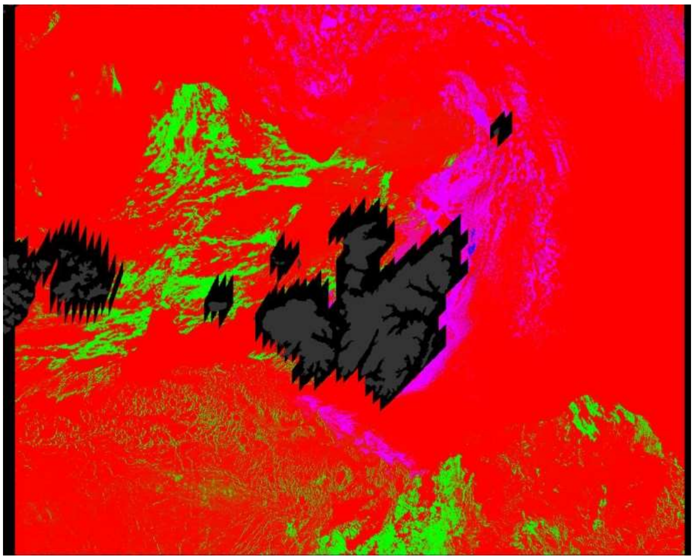

C

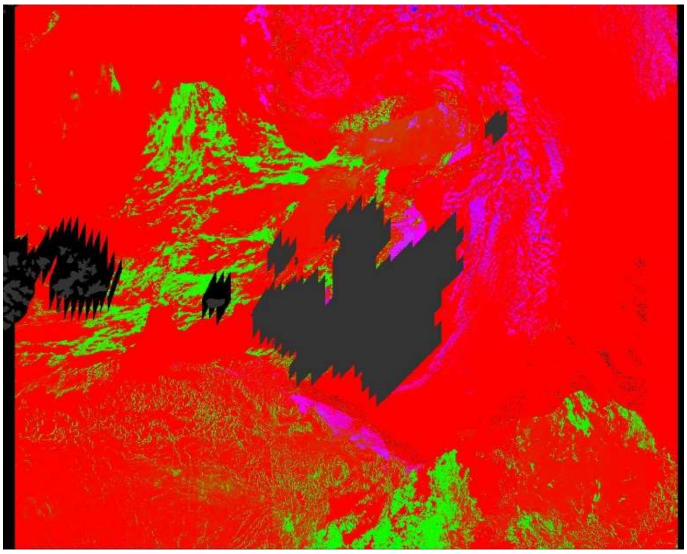

DV

***Figure 22**. Night-time Example. Granule:*
S3A_SL_1_RBT____20170308T161536_20170308T161836_20170309T224125_0180_015_140_1259_LN2_O_NT_002.SEN3

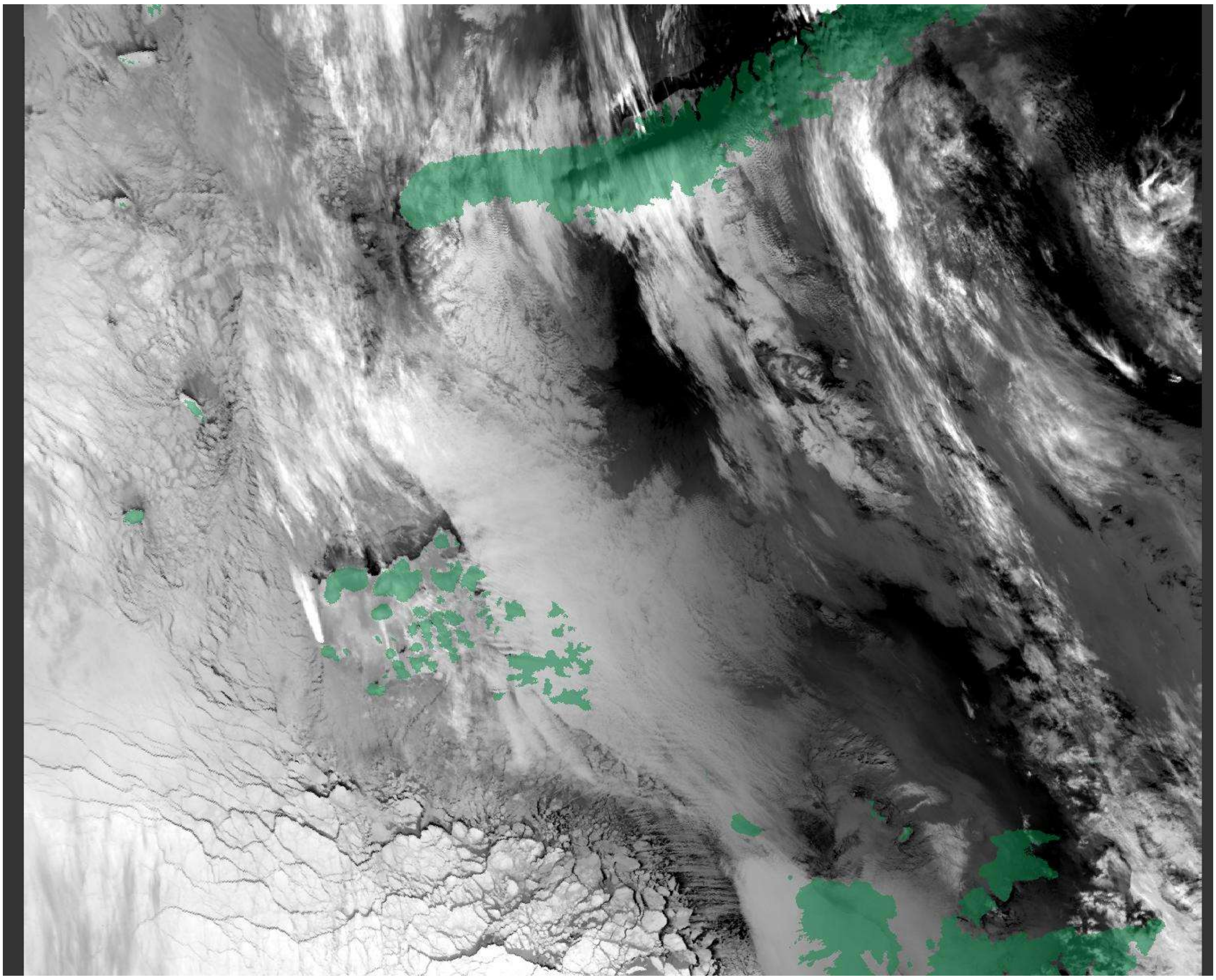

S8_BT_in_LND

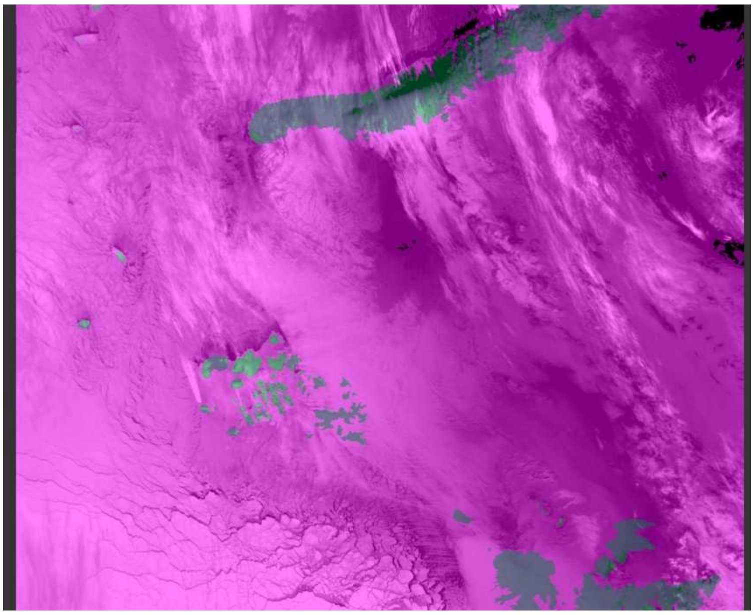

CLD

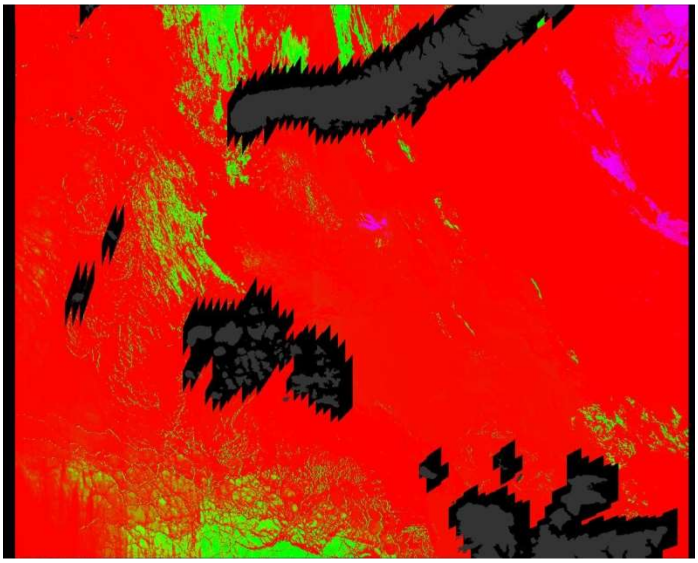

B

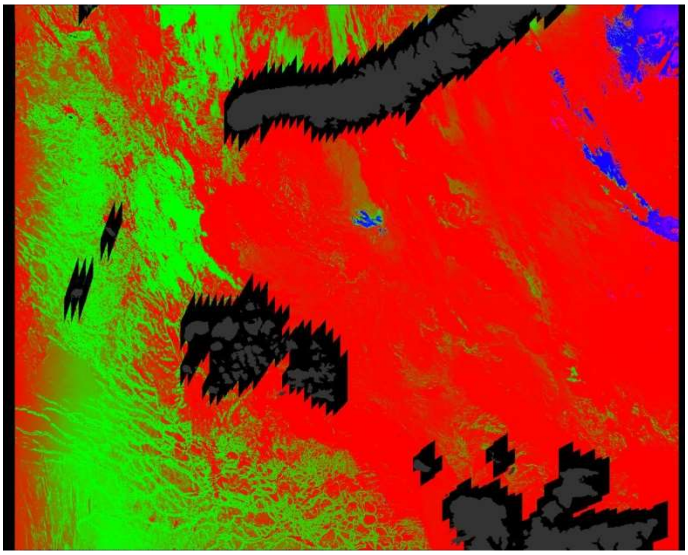

NN

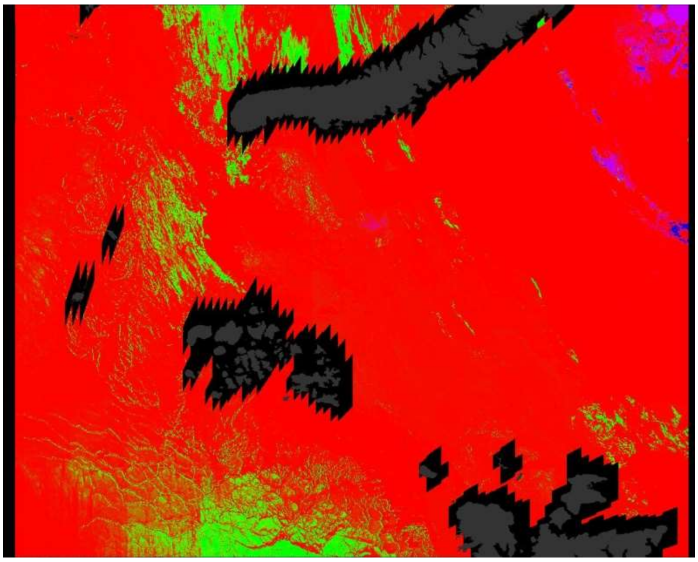

C

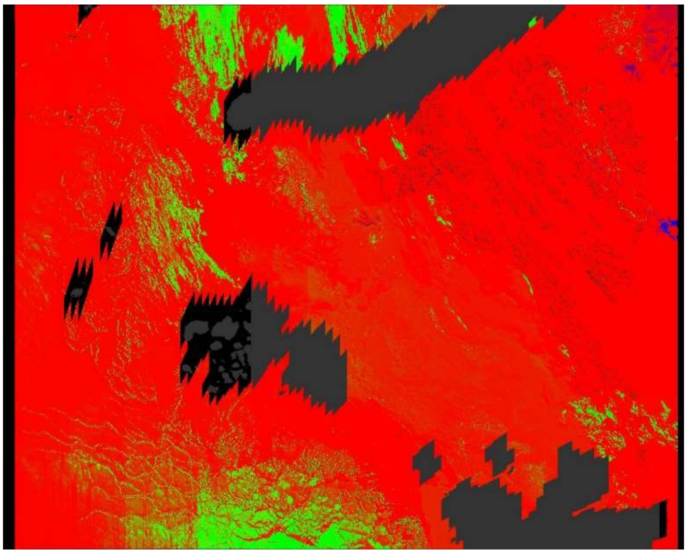

DV

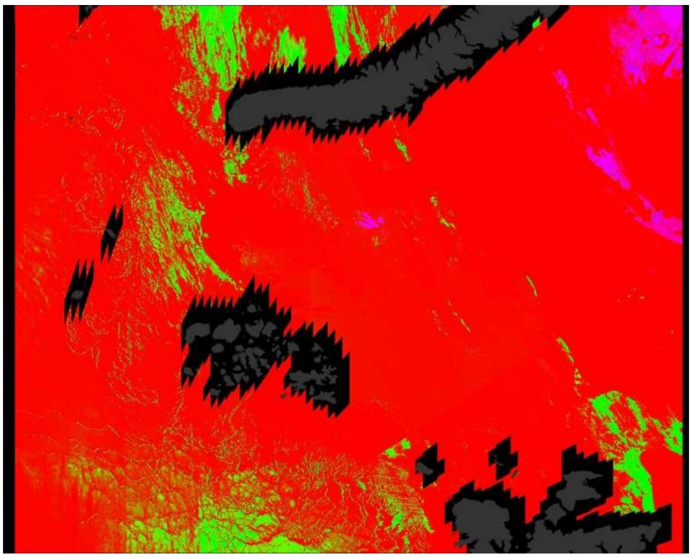

D

***Figure 23**. Twilight Example. Granule:*
S3A_SL_1_RBT____20170326T233616_20170326T233916_20170328T131650_0179_016_016_1439_LN2_O_NT_002.SEN3

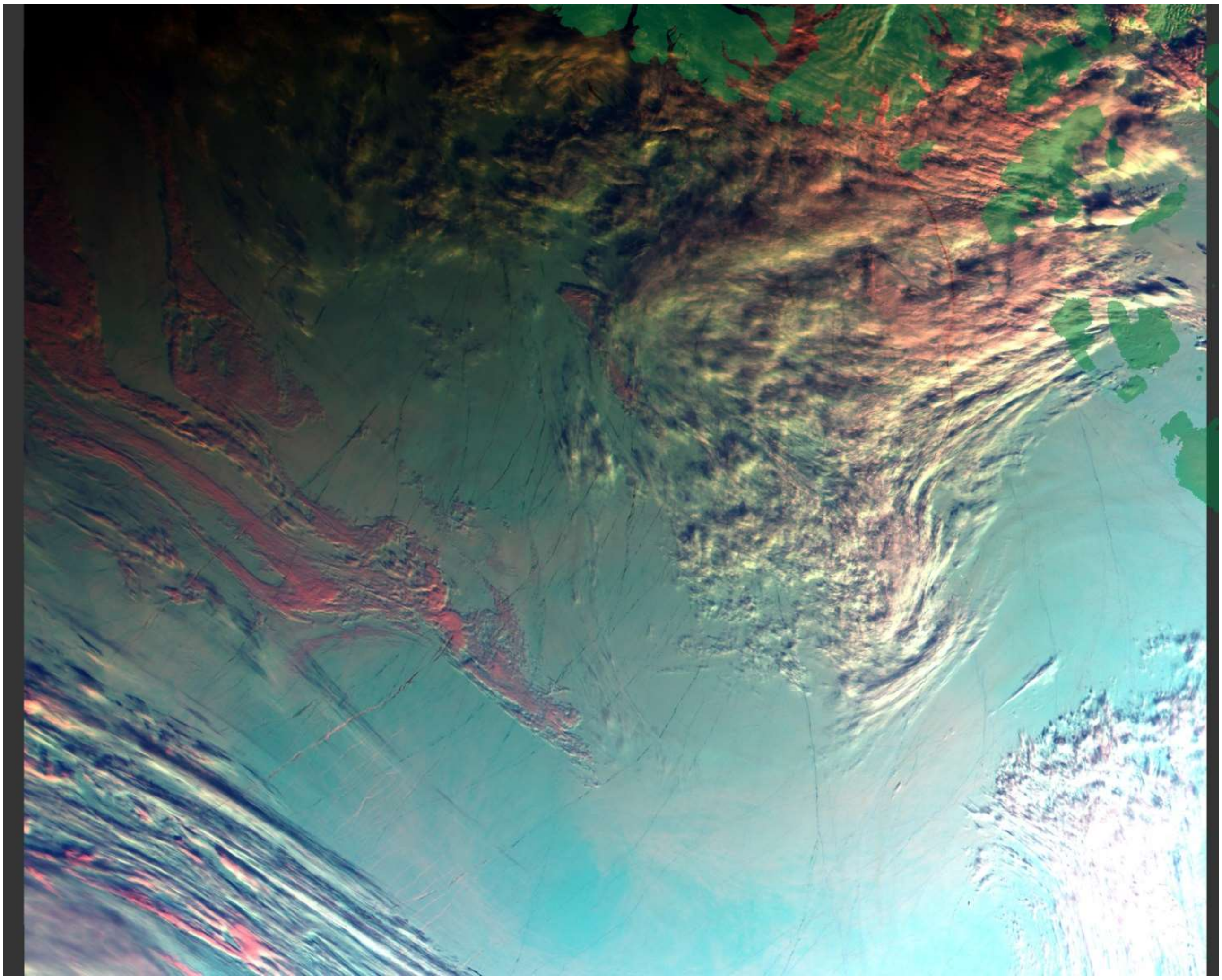

R5G3B1_LND

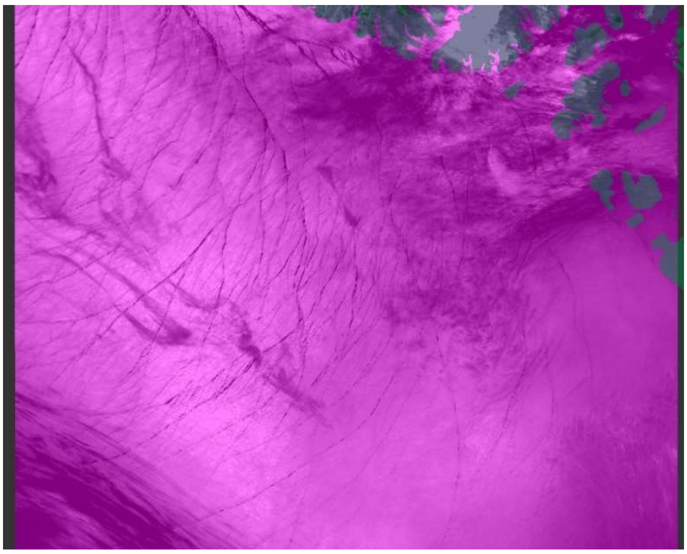

CLD

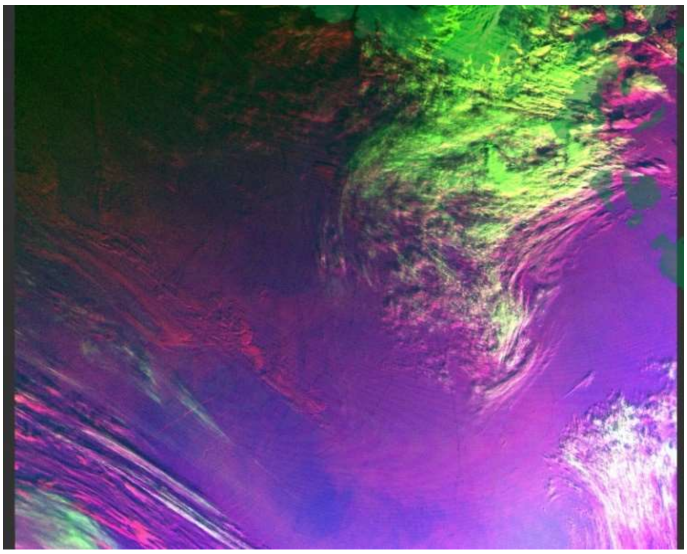

R5G4B1

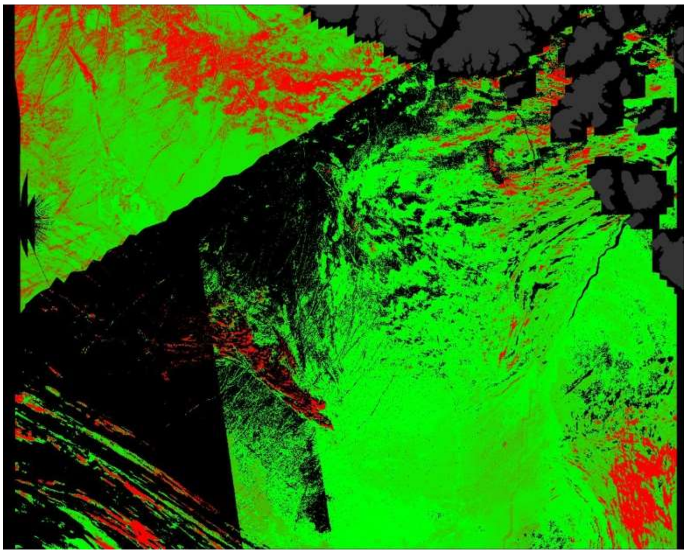

A1

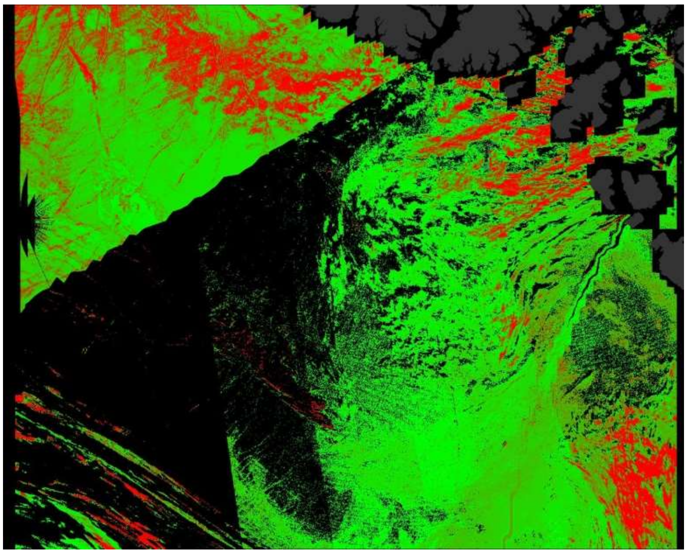

A2

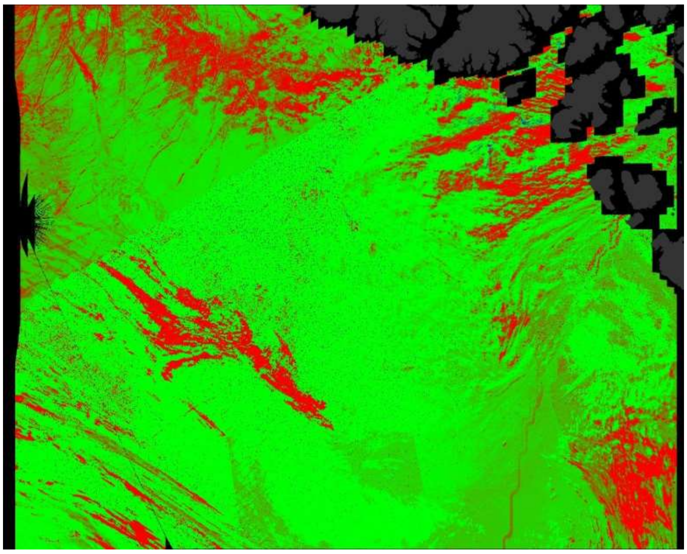

B

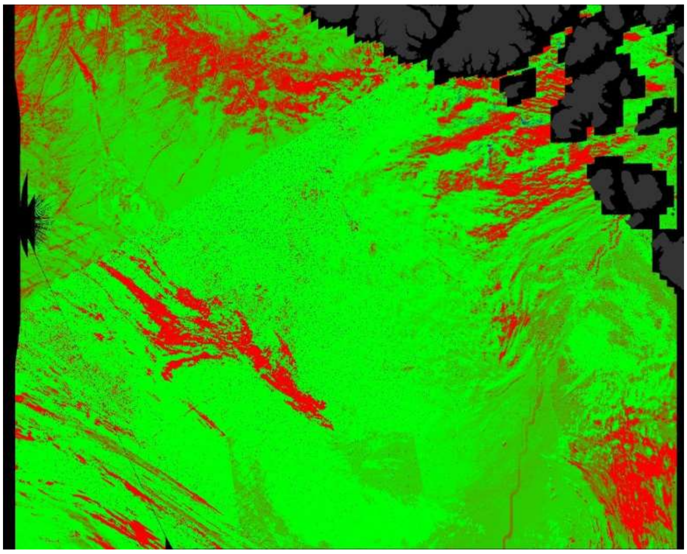

C

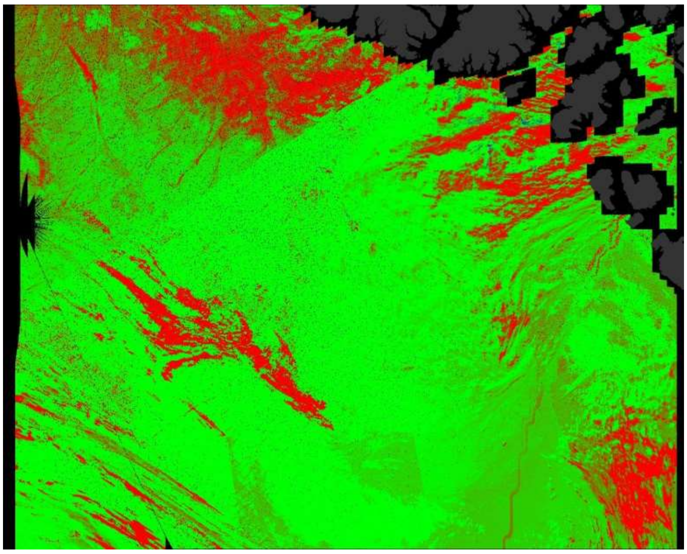

D

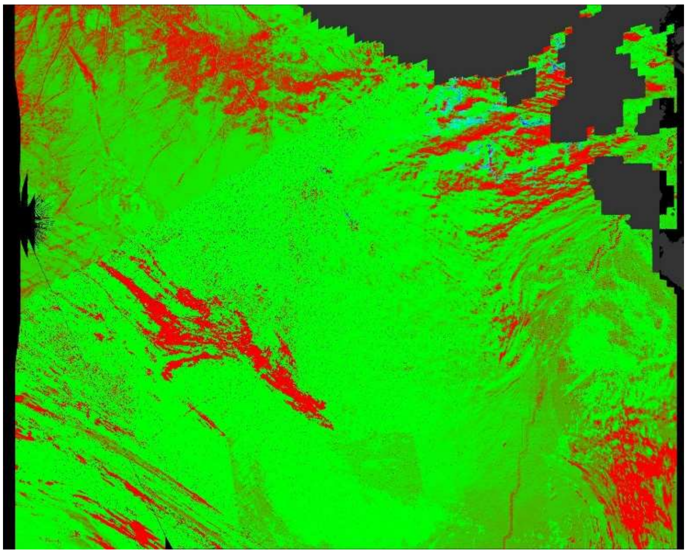

DV

Figure 24. *Daytime Example. Granule:*
S3A_SL_1_RBT____20170505T125556_20170505T125856_20170506T181054_0180_017_195_1619_LN2_O_NT_002.SEN3

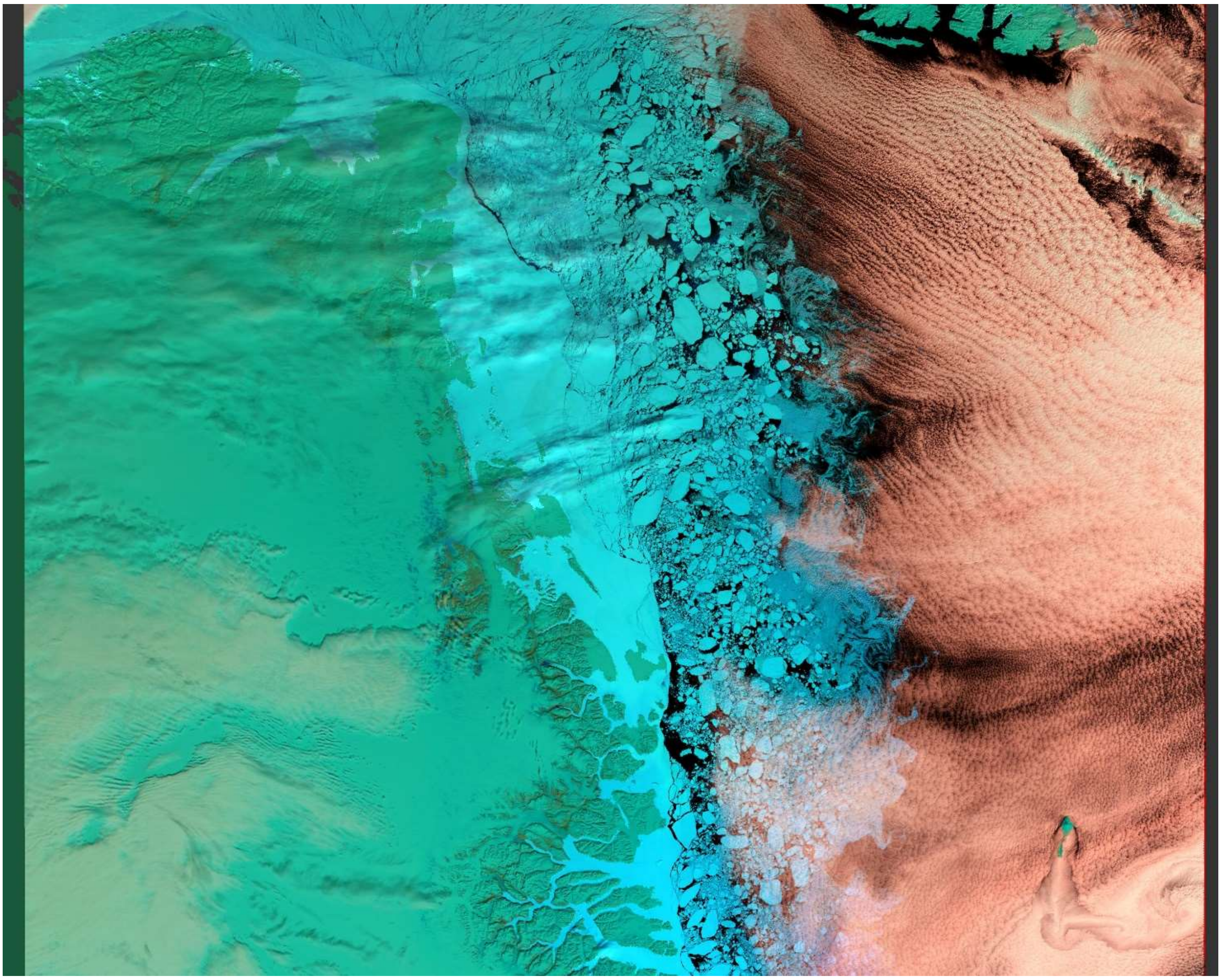

R5G3B1_LND

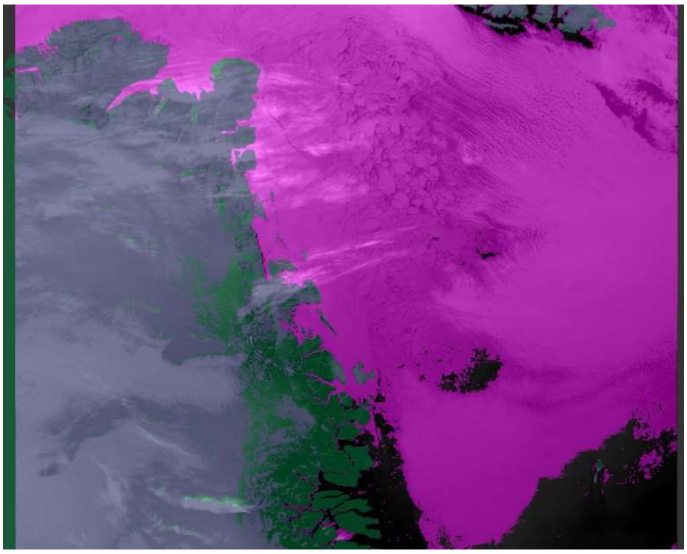

CLD

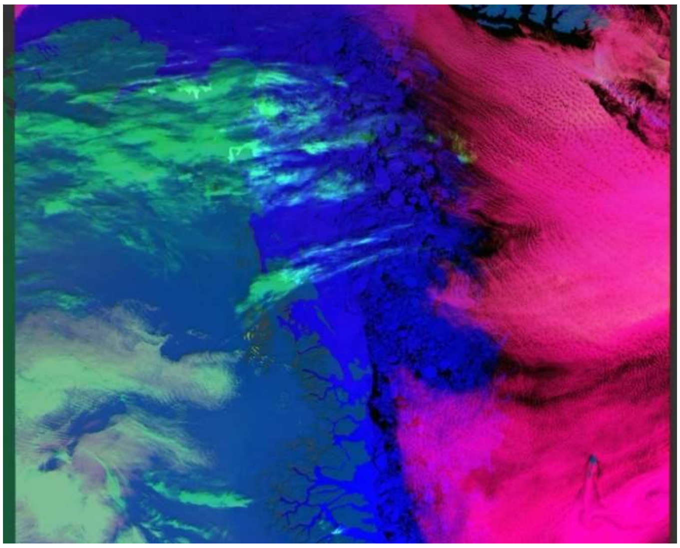

R5G4B1

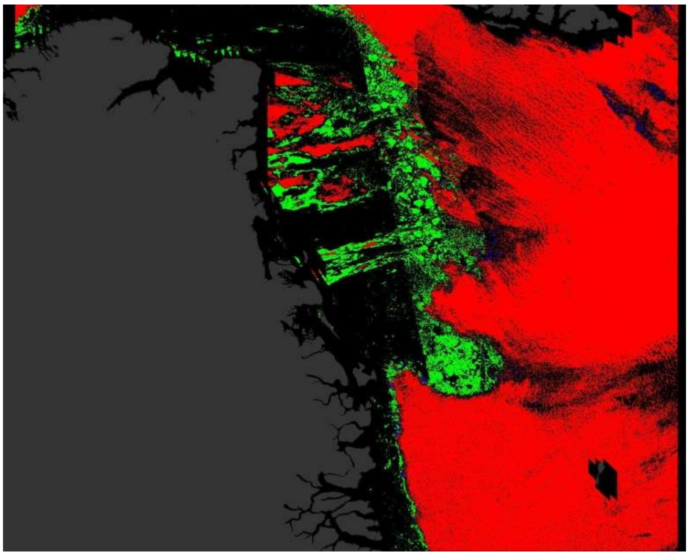

A1

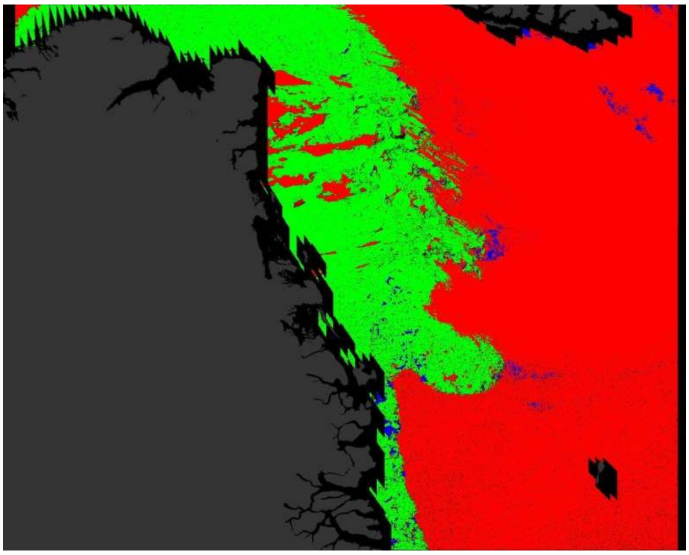

D

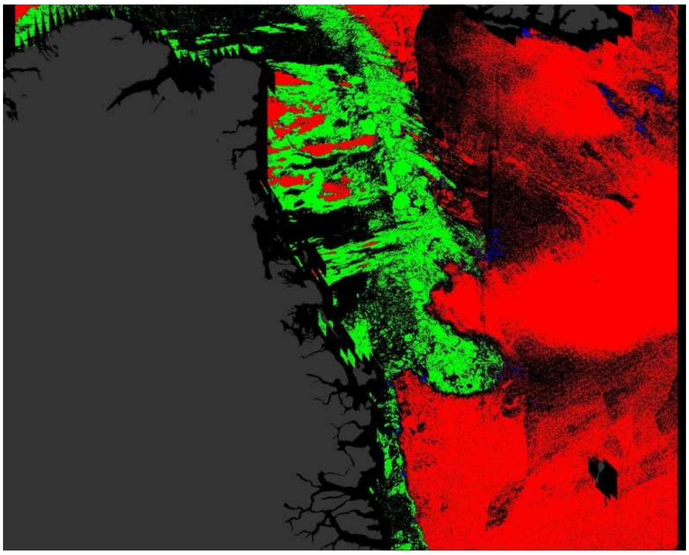

A2

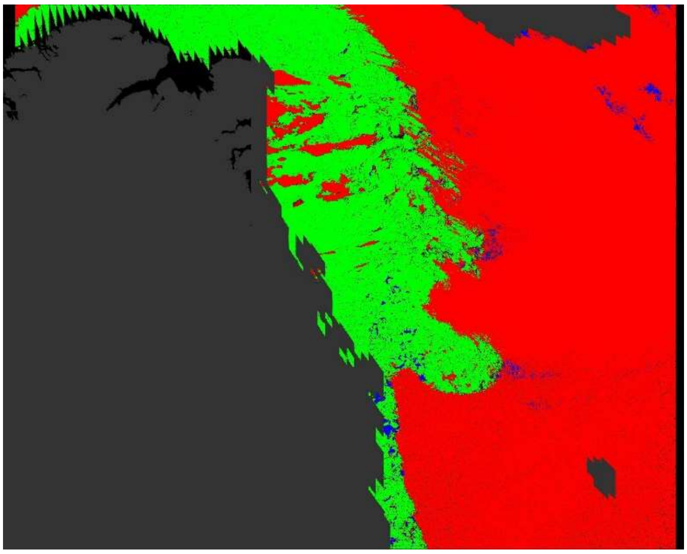

DV

10. Comparison against Synthetic Aperture Radar (SAR) product

To estimate the ability to detect sea ice we performed a quantitative comparison against sea ice cover as reported by the regional sea ice product SEAICE_ARC_SEAICE_L4_NRT_OBSERVATIONS_011_002 distributed by the CMEMS Sea Ice, SST and Wind Thematic Ensemble Centre (OSI TAC):

This product is obtained by manual interpretation of satellite data. The satellite data used are Synthetic Aperture Radar data from Sentinel-1 (A/B), RADARSAT and Envisat (during its lifetime). In addition, when available, data from MODIS and NOAA solar and thermal channels are also used. The product is released daily at 15:00 UTC in a polar-stereographic projection covering the area: 80°W-80°E, 60°N-85°N with a resolution of 1000m x 1000m (see example in **Fig.25**).

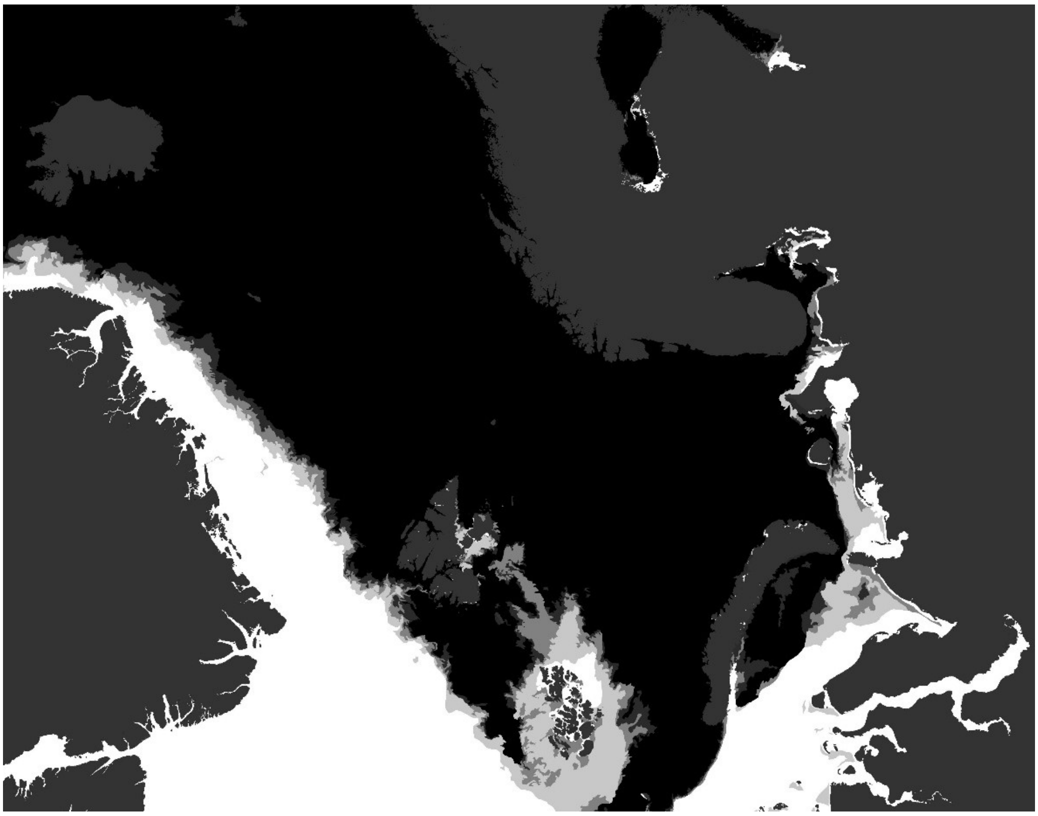

Fig.25 *Example of sea-ice concentration product 19/01/2017 (`ice_conc_svalbard_201701191500.nc`)*

The product follows the WMO Concentration Color code for sea ice, where the concentration classes are defined by concentration intervals:

- Fast ice: 10/10
- Very Close Drift Ice: 9-10/10
- Close Drift Ice: 7-8/10
- Open Drift Ice: 4-6/10
- Very Open Drift Ice: 1-3/10
- Open Water: < 1/10

These concentration intervals are converted to fixed concentration values in the gridded product described by the "`sea_ice_area_fraction`" variable:

- Fast ice: 100
- Very Close Drift Ice: 95
- Close Drift Ice: 75
- Open Drift Ice: 50
- Very Open Drift Ice: 20
- Open Water: 5
- Clear Ocean: 0

The dataset, described in the previous section, of 95 manually selected cases, representing a wide range of situations, was used to compare the *sea_ice_area_fraction* against the probability given by the PDF classification of occurrence of sea ice. SLSTR observations were analysed using different sets of PDFs (see Tab.15), including a Neural Network (NN) based classifier trained with the same MODIS dataset used to generate the PDF's.

Tabs.16-17 show two examples of contingency tables obtained from the comparison between the two classification products. To normalize for the different size of the matching dataset, we report the percent values of pixels for each class combination. The examples shown are relative to the same classification method (5VD4VN) and scene type (DAY) but they differ for the maximum probability of CLD allowed to be compared. This is due to the fact that, while the *sea_ice_area_fraction* product, being mostly based on SAR data, is insensitive to the presence of cloud, SLSTR is able to classify a pixel as ICE only if CLD+SEA<1. Consequently, the interpretation of the contingency tables in terms of classification skills through standard statistical indicators (e.g. http://www.cawcr.gov.au/projects/verification/#Skill_score) is not straightforward. In fact, in addition to the difference in the definition of variables estimating the sea ice coverage (probability vs concentration), a portion of off-diagonal bins can be still considered correctly classified: in presence of cloud the SLSTR classification may underestimate the SAR derived sea ice estimation and still be correct in case the cloud covers a portion of sea-ice.

For this reason, we performed the comparison by selecting only pixels with a given maximum probability of being cloudy (CLD_max). We used two threshold values: 0.1 (practically Clear Sky pixels) and 0.5.

To compare the classification skills for the different methods adopted, we introduced two different set of indices.

- The Cramer's *V* index defined as:

$$V = \sqrt{\frac{\varphi^2}{\min(k-1, r-1)}} = \sqrt{\frac{\chi^2/n}{\min(k-1, r-1)}}$$

$$x^2 = \sum_{i,j} \frac{(n_{i,j} - \frac{n_i n_j}{n})^2}{\frac{n_i n_j}{n}}$$

Where:

- $n_{i,j}$: is the population of the bin represented by matching of classes i and j;
- n_i (n_j): is the overall population of the class i (j);
- n : is the total number of matching points
- k,r : are the dimensions of the contingency table (i.e. 11,7)

***Table 16**. Example of contingency table for the classification algorithm **5VD4VN** (see **Tab.15**) for Daytime cases and CLD<0.1 (1849651 matches).*

	0.0	0.1	0.2,	0.3	0.4	0.5	0.6	0.7	0.8,	0.9,	1.0
0	36.99	0.30	0.14	0.08	0.06	0.03	0.02	0.02	0.01	0.21	1.60
5	0.78	0.11	0.05	0.03	0.02	0.01	0.01	0.00	0.00	0.09	0.46
20	0.60	0.11	0.04	0.02	0.01	0.01	0.00	0.00	0.00	0.10	0.86
50	0.22	0.09	0.04	0.02	0.01	0.01	0.00	0.00	0.00	0.13	1.69
75	0.21	0.14	0.05	0.03	0.02	0.01	0.01	0.00	0.00	0.22	3.89
95	0.22	0.18	0.10	0.07	0.05	0.03	0.03	0.02	0.02	1.55	41.79
100	0.02	0.00	0.00	0.00	0.00	0.00	0.00	0-00	0.00	0.24	6.09

***Table 17**. Same as **Tab.16** for CLD<0.5 (2227951 matches).*

	0.0	0.1	0.2,	0.3	0.4	0.5	0.6	0.7	0.8,	0.9,	1.0
0	33.91	0.75	0.37	0.25	0.18	0.28	0.35	0.31	0.33	0.36	1.33
5	0.83	0.32	0.20	0.15	0.12	0.19	0.23	0.19	0.18	0.16	0.39
20	0.62	0.20	0.09	0.07	0.05	0.09	0.10	0.09	0.10	0.15	0.71
50	0.27	0.16	0.07	0.05	0.04	0.09	0.11	0.11	0.12	0.18	1.40
75	0.30	0.26	0.12	0.08	0.07	0.13	0.17	0.18	0.24	0.33	3.23
95	0.31	0.43	0.29	0.23	0.19	0.64	1.02	1.22	1.47	2.18	34.69
100	0.02	0.01	0.01	0.01	0.01	0.05	0.14	0.15	0.20	0.32	5.05

- The total percentage of matched points for the following categories, represented by different colors in the examples of contingency table reported (**Tab.16-17**):
  - 'correct' ice classification cases. In the hypothesis of correspondence between probability and coverage and approximating the correspondence between classes.
  - 'correct within one class'
  - 'clearly misclassified' for this classes the classification algorithm gives probability of ice coverage while SAR gives 0 or lower values of ice coverage
  - 'uncertain': underestimation of sea ice concentration can be correct as long as a portion of ice is below a cloud.

Table 18 summarize the results of the comparisons for different methods and scenario.

Table 18. *Summary of the comparison of sea_ice_concentration products for different classification methods and scenarios (D=DAY, N=NIGHT, T=TWILIGHT)*

#VAR	Type[1]	Scene D/N/T	CLD<	#Matches	1	2	3	4	1+2	Cramer's V
6VDCD14VN	S	**D**	0.1	790457	41.28	45.3	12.73	0.69	86.58	0.37
6VDCD14VN	S	**D**	0.5	957896	39.38	44.1	14.53	1.99	83.49	0.36
6VDCD24VN	S	**D**	0.1	473130	24.22	57.91	16.62	1.26	82.13	0.30
6VDCD24VN	S	**D**	0.5	598138	23.96	55.03	18.2	2.81	78.99	0.29
5VD4(3)VN	S	**D**	0.1	1849651	45.62	43.52	9.45	1.41	**89.14**	**0.39**
5VD4(3)VN	S	**D**	0.5	2227951	43.17	41.78	11.17	3.88	84.95	0.38
5VD4VN	DU	**D**	0.1	1850093	44.36	44.29	10.18	1.17	88.84	0.39
5VD4VN	DU	**D**	0.5	2224263	42.36	42.24	12.33	3.08	84.60	0.38
5VD3VN	S	**N**	0.1	149580	37.49	23.79	38.71	0.00	61.29	0.09
5VD3VN	S	**N**	0.5	804048	23.86	41.19	29.25	5.69	65.06	0.11
5VD4VN	S	**N**	0.1	167973	40.71	21.26	38.03	0.00	61.97	0.19
5VD4VN	S	**N**	0.5	871765	25.96	40.24	27.11	6.68	66.21	0.18
5VD4VN	DU	**N**	0.1	354248	33.79	31.00	35.21	0.00	64.79	0.16
5VD4VN	DU	**N**	0.5	1010541	27.25	39.34	28.43	4.98	66.59	0.20
5VD4VN	NN	**N**	0.1	633833	73.45	16.9	9.28	0.38	90.35	**0.40**
5VD4VN	NN	**N**	0.5	2825187	70.05	17.36	10.48	2.10	87.42	0.37
5VD3VN	S	**T**	0.1	49790	45.47	21.07	33.46	0.00	66.54	0.10
5VD3VN	S	**T**	0.5	269421	23.94	44.99	22.77	8.3	68.93	0.16
5VD3VN5VT	S	**T**	0.1	185766	34.72	11.22	54.06	0.00	45.94	0.17
5VD3VN5VT	S	**T**	0.5	786551	32.1	21.77	42.27	3.86	53.87	0.21
5VD4VN	S	**T**	0.1	65177	56.13	17.84	26.03	0.00	73.97	0.30
5VD4VN	S	**T**	0.5	318372	30.89	41.63	20.24	7.24	72.52	0.30
5VD4VN	D	**T**	0.1	100062	48.60	25.23	26.16	0.00	73.84	0.29
5VD4VN	D	**T**	0.5	377172	35.73	38.57	19.89	5.80	74.30	0.32

11. Conclusions

A set of PDFs differing for the number and type of input variables were generated. Based on the results of this study, the suggested combinations of variables are:

NIGTH-TIME:	**BT11-BT12, STD_BT12, BT11-BT3.7, BT11**
DAY-TIME:	**R0.8, R1.3, STD1.6, BT11-BT3.7, BT11, R1.6**

The possibility to test on a larger dataset the suggested PDFs, as well as the other PDFs generated during the project, should be considered before drawing conclusions on the PDF to be used in the processing chains. In principle, the procedure adopted allows to generate the PDFs, with other variables combinations, among the one considered as candidate in this study. This possibility can be used in case of channel failures or if successive findings on possible improvements of the classification method suggest other combinations.

PDFs, even after the optimization process, were generated keeping the maximum available information within the ICE class in order to allow the investigation on the potential use for Sea Ice Type classification, needed for Sea Ice Temperature estimation.

Keeping in mind that being based on MODIS products, PDFs are expected to reproduce their strengths and weaknesses, in the following we discuss the main findings obtained from this study and possible solutions for further research activities.

The need for specific PDFs for TWILIGHT conditions was tested. From the results of this study, it appears that pixels in twilight conditions ($95° < \theta_s < 85°$) can be classified with NIGHT PDFs without significant lost of classification skills. In particular, we found that adding the dual view variable improves the results, at least in terms of correct sea-ice classification (**Tab.18**). Even if, from a visual analysis it seems to be still useful information in the solar channels probably the variability and the high noise level translate on highly overlapping distributions for the three classes. On the other hand, the contribution of solar reflected radiance in the **BT11-BT3.7** variable does not seems to generate classification problems when using PDFs generated with nigthtime observations. This is very likely due to the fact the solar contribution act mostly on the CLD class (bright and elevated objects) that occupies an extreme of the distribution.

We generated also specific PDFs for the SUNGLINT scene type. The lack of SLSTR cases for which sunglint conditions occurred limited the possibility to test the need of specific PDF for sunglint conditions (in alternative to the use of DAY ones). Dedicated tests should be performed if occurrence of sunglint in Polar Regions reveals to be a frequent problem once a full year (verification was performed using cases from mid-November to beginning of May) of SLSTR data will be available.

Information content due to the dual view was investigated. Due to the relatively limited size and, consequently, limited statistical robustness, of the MODIS AQUA-TERRA matching dataset used to generate the PDFs we adopted the assumption to consider the PDF of the dual view variable as independent from the other ones. With the limits of validity of the results we can conclude that addition of the dual view information, with the exception of TWILIGHT scenes, does not improve significantly the classification skills. However, in addition to the limited sample of cases used to generate the PDFs there is also the possibility that residual nadir-oblique co-registration problems are responsible for the observed results.

As mentioned in Section 4 we limited the use of the dual view information to a variable based **BT11** and **BT12** observations in both geometries. In principle, we expect dual view observations of solar reflected radiation, when available, to contain useful information in terms of surface characterization however to generate PDFs with MODIS data including this variable would have been extremely time consuming. A dedicated study to explore the information content using available SLSTR data should be done. In addition to explore the information content in terms of sea-ice/cloud discrimination, this study should focus principally on the potential use for Sea Ice Type classification needed to correctly estimate the Sea Ice Temperature (e.g. Nolin et al. 2002, Hori et al. 2006).

From the visual analysis of a set of classified test cases and the quantitative comparison against independent sea-ice concentration products we conclude that PDFs based classification can improve the current operational cloud detection by:

- Discriminating between sea-ice and cloud to allow for successive sea ice temperature estimation
- Reduce partially the cloud cover overestimation that characterize the currently applied cloud detection scheme in Polar Regions.
- Introducing the probability of cloud/sea-ice contamination to be used to estimate the SST.

Despite the lack of information from the solar channels, even in night-time conditions classification skills are still satisfactory. Inclusion in the PDFs input variables of channels combinations sensitive to the differences of refractive indices allows the discrimination of water clouds over sea-ice surfaces. Possibility of incorrect discrimination between sea-ice and ice-cloud is still observed. Intrinsic limitations due to the limited available information content can be overcame with the help of ancillary information (this is already partly occurring) and adding a post processing analysis for example analyzing short time series of classified images referring to the same area. As an example, **Fig.26** shows a sequence of two granules observed the 19/01/2017 at 18:41:28 UTC (left) 20:22:27 (right) (see also **Fig.20** BT8 and **Fig.25** SAR) with an overlapping area.

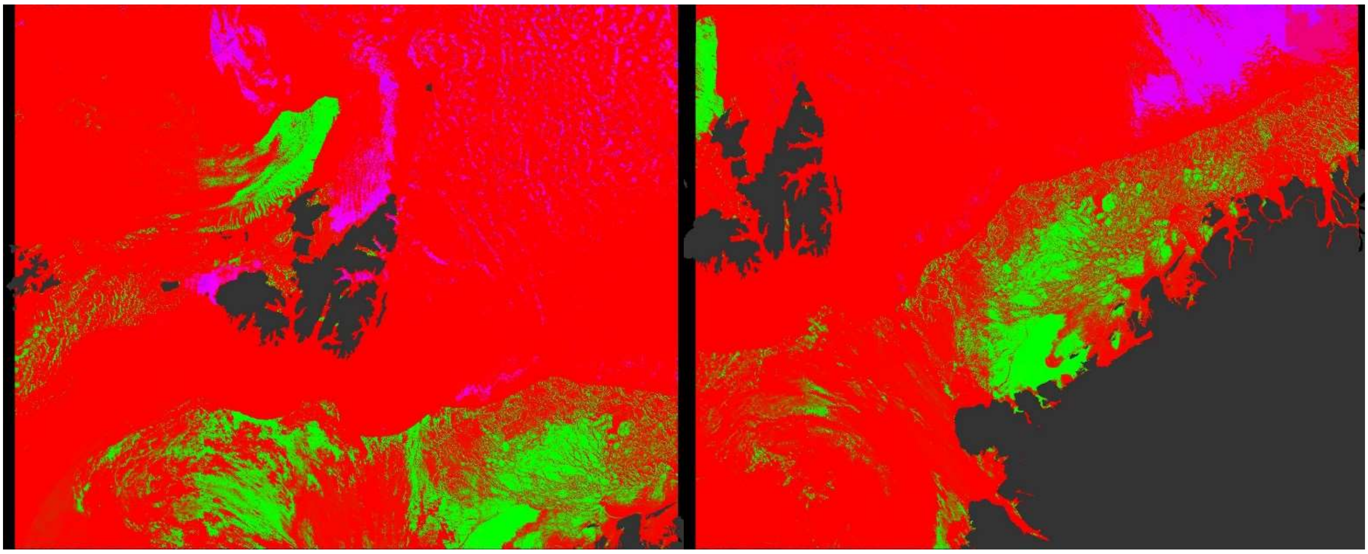

Fig.26 *Examples of overlapping granules classified within relatively short time (19/01/2017 at 18:41:28 UTC (left) 20:22:27 (right)) suitable for post-processing analysis .*

From the visual analysis of the study cases it seems that there is an underestimation of clear sky cases (SEA). According to Liu and Key (2016) we should expect roughly a mean cloud amount of about 70% (see **Fig.27**) and as a consequence, considering also the case of clear sky with sea ice, less than 30% of probability of clear ocean. Part of the observed clear ocean underestimation could be due to the criteria used to select the study cases that focused on testing the ability to distinguish between sea-ice and clouds. We searched for granules close to the coast, with occurrence of both clouds and sea ice and in the area covered by the Sea Ice Concentration product (see **Fig.25**) that being interested by the Gulf Current is particularly cloudy (Liu et al. 2012). In addition to the possible bias introduced by the criteria used to select the study cases, another possible reason for the observed clear sky underestimation could be the effect of the different spectral response characteristics of MODIS vs SLSTR channels (see Sect.2). In fact, for practically all variables the distribution of the SEA pixels is the narrowest one among the three classes. This is due to the relatively low variability of relevant geophysical variables (e.g. SST, surface roughness, TPWV) or of their impact in the measured radiance for clear sky ocean (SEA) with respect to the other two surface types. Spectral response differences can generate a shift, particularly for the variables given by brightness temperature differences, that has a larger impact in narrow distributions. This could be probably the explanation for the very low occurrence of SEA pixel for any night-time variables combination including the difference **BT12-BT3.7.** In case the clear sky underestimation will be confirmed by the analysis of routinely processed data, the impact of MODIS-SLSTR differences should be investigated in details. In absence of a robust assessment study, we suggest to test the classification skills by shifting empirically the input variables to contiguous classes and analyse the impact.

Impact of ancillary data is also observed and appears (see for example **Figs.17-24**) as large scale features. In general, the information on sea ice coverage is helpful to discriminate between sea ice and clouds while some negative impact, particularly for occurrence of relatively warm SST values in the ancillary data was observed. The impact was minimized by grouping PDFs for relatively warm SST in a single class (SST>7.5°C).

Impact of residual channels co-registration problems at the boundaries of contrasting patterns were observed particularly for the first SLSTR cases analysed. Co-registration problems are responsible for introducing contribution in the BT differences due to the spatial variability of the scene.

Given partly to the requirements in the SoW, the analysis focused on the North Atlantic/Artic Area. In addition, also for this area results obtained of this study may be not be conclusive because of the limited sampling of seasonal cycle (Nov. 2016 – early May 2017) due to the current availability of SLSTR data. Given the different cloud regimes over Polar Oceans (see for example Wang & Key 2005) evaluation of the classification methods should be performed over the whole Polar Oceans with SLSTR dataset sampling at least a full annual cycle.

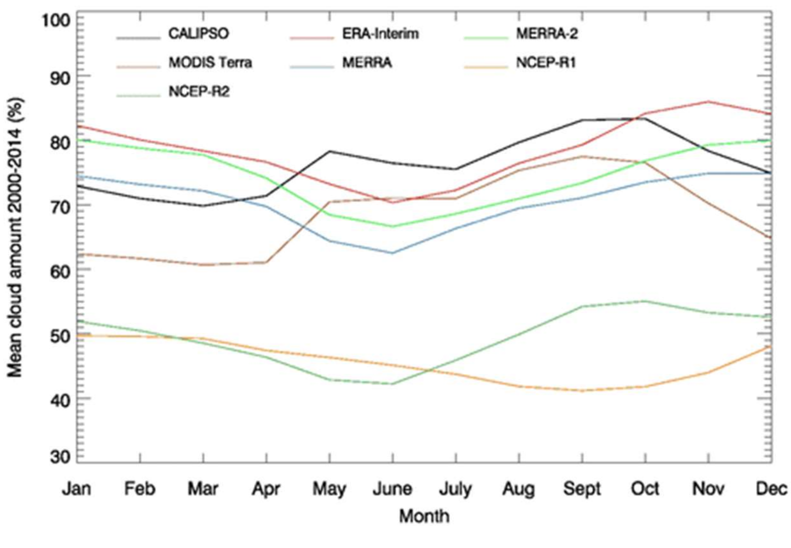

Fig.27 *Mean cloud amount over the Arctic (60°–90°N) from Terra MODIS, ERA-Interim, MERRA, MERRA-2, NCEP R1, and NCEP R2 during 2000–14 and from CALIPSO during 2006–14 (Liu & Key 2016).*

Having experienced the needs in terms of processing time for the PDFs based classification, taking advantage of a consolidated know-how on Neural Networks within the team and of the ready availability of a training dataset, we also tested the potential use of a NN based classification algorithm. The NN was trained with a dataset generated by randomly sampling 10% of the night-time cases. In addition to the expected gain in terms of processing time, performances in terms of classification skill are promising and a dedicated study should be done to:

- extend the NN classification to all possible scene;
- optimize the NN taking into account of the preliminary results obtained in this study and of the characteristics of the entire dataset to be used for the training;
- test the classification skills more extensively.

Acknowledgments

This study has been funded by the European Commission Copernicus programme and the results of the study are owned by European Commission.

A practical contribution to this study came from the students of the 4th year of the Liceo Scientifico "Louis Pasteur" (Rome, Italy): Elisa Ciotoli, Marius Bilhac, Giacomo Nicoletti, and of the 3rd /4th year of the Liceo Scientifico and "Isacco Netwon" (Rome, Italy): Lara Ammendola, Leonardo Fratocchi, Dario Furia, Daniele Giuliani, Juliette Liberti, Elena Parzanese, Alexander Winter. Within the frame of their stage of 'Alternanza Scuola Lavoro' they helped in selecting, classifying and organizing the study cases.

References

Bishop, C. M. Neural networks for pattern recognition. Oxford university press, 1995.

Cramér, Harald. 1946. *Mathematical Methods of Statistics*. Princeton: Princeton University Press, page 282 (Chapter 21. The two-dimensional case). ISBN 0-691-08004-6

Del Frate, F., Ortenzi, A., Casadio, S., and Zehner, C.: Application of neural algorithms for a real-time estimation of ozone profiles from GOME measurements, IEEE Transactions on Geoscience and Remote Sensing, 40 (10), 2263–2270, 2002.

Del Frate, F., and Schiavon, G.: Nonlinear principal component analysis for the radiometric inversion of atmospheric profiles by using neural networks, IEEE Transactions on Geoscience and Remote Sensing, 37, 2335–2342, 1999.

Hori, M., T. Aoki, T. Tanikawa, H. Motoyoshi, A. Hachikubo, K. Sugiura, T. J. Yasunari, H. Eide, R. Storvold, Y. Nakajima, F. Takahashi (2006). In-situ measured spectral directional emissivity of snow and ice in the 8–14 µm atmospheric window, *Remote Sens. Environ*, **100**, 4, 486-502.

Liu, Y., J. R. Key, R. A. Frey, S. A. Ackerman & W. P. Menzel (2004). Nighttime polar cloud detection with MODIS. *Remote Sens. Environ.*, **92**, 181–194.

Liu, Y. and J.R. Key, 2016: Assessment of Arctic Cloud Cover Anomalies in Atmospheric Reanalysis Products Using Satellite Data. *J. Climate,* **29**, 6065–6083,https://doi.org/10.1175/JCLI-D-15-0861.1

Liu, Y., J.R.Key, S.A.Ackerman, G.G.Mace & Q. Zhang, 2012. Arctic cloud macrophysical characteristics from CloudSat and CALIPSO, Remote Sensing of Environment, 124, 159-173, ISSN 0034-4257.

Nolin, A. W., F. Fetterer, and T. Scambos (2002), Surface roughness characterizations of sea ice and ice sheets: Case studies with MISR data, *IEEE Trans. Geosci. Remote Sens.,40*(7), 1605-1615.

Picchiani M, Chini M, Corradini S, Merucci L, Sellitto P, Del Frate F, Stramondo S. Volcanic ash detection and retrievals using MODIS data by means of neural networks. Atmospheric measurement techniques. 2011 Dec 1;4(12):2619.

Picchiani M, Chini M, Corradini S, Merucci L, Piscini A, Del Frate F. Neural network multispectral satellite images classification of volcanic ash plumes in a cloudy scenario. Annals of Geophysics. 2014.

Richards, J.A., Jia, X., (1999), Remote Sensing Digital Image Analysis: An Introduction. New York: Springer-Verlag

Pearson, K., O. Embury, C. Bulgin, C. J. Merchant (2014). Bayesian Cloud Detection Algorithm Theoretical Basis Document; EUM-BC-ATBD-003; *Univ. of Reading,*EUMETSAT Bayesian Cloud Detection, Final Issue 1, 1-56

Wang, X. J., & Key, J. R. (2005). Arctic surface, cloud, and radiation properties based on the AVHRR Polar Pathfinder dataset. Part I: Spatial and temporal characteristics. Journal of Climate, 18, 2558–2574

Warren, S.G. & R. E. Brandt, 2008. Optical constants of ice from the ultraviolet to the microwave: A revised compilation. J. of Geophysical Research, Vol. 113, D14220.

Wentz, F. J., C. L. Gentemann and P. D. Ashcroft, (2003), On-orbit calibration of AMSR-E and the retrieval of ocean products, paper presented at 83rd AMS Annual Meeting, Long Beach, CA.

Wentz, F. J., C. L. Gentemann and K. A. Hilburn, (2005), Three years of ocean products from AMSR-E: Evaluation and applications, paper presented at Proceedings of the 2005 IEEE International Geoscience and Remote Sensing Symposium,Seoul, Korea.

Wentz, F. J. and T. Meissner, (2000), AMSR Ocean Algorithm, Version 2, report number 121599A-1, 66 pp., Remote Sensing Systems, Santa Rosa, CA.

Wentz, F. J. and T. Meissner, (2007), AMSR-E Ocean Algorithms; Supplement 1, report number 051707, 6 pp., Remote Sensing Systems, Santa Rosa, CA.

Zavody, A.M., C. T.Mutlow & D.T. Llewellyn-Jones (2000). Cloud Clearing over the Ocean in the Processing of Data from the Along-Track Scanning Radiometer (ATSR). *J. Atmos. Ocean. Technol.* **17** 595-615.

Appendix: 1 NETCDF Use and format description

SLSTR data
Before using PDF stored in NETCDF files, some operations on SLSTR data must be done:

1. The following fields in SLSTR level1b data are required:

Word	Fields
confidence_in confidence_on	Coastline ocean land day twilight sun_glint summary_cloud
geodetic_in, geodetic_io, geodetic_tx	Latitude longitude
SX_quality_an (X = 1 to 6)	SX_solar_irradiance (X = 1 to 6)
geometry_tn, geometry_to	solar_zenith solar_azimuth sat_zenith sat_azimuth
met_tx	sea_surface_temperature_tx sea_ice_fraction_tx
SX_radiance_an (X = 1 to 6)	SX_radiance_an (X = 1 to 6)
SX_radiance_ao(X = 1 to 6)	SX_radiance_ao (X = 1 to 6)
SX_BT_in, SX_BT_io (X = 7,8,9)	SX_BT_in, SX_BT_io (X = 7,8,9)

2. The following SLSTR field must be derived by mean of an up-scaling (interpolation) at 500m resolution:

   solar_zenith_an = UPSCALING_500M (solar_zenith_tn)

   where UPSCALING_500M is a generic function to interpolate a field at 500m resolution (e.g. griddata in MATLAB language).

3. The following SLSTR field must be derived by mean of an up-scaling (interpolation) at 1000m resolution:

   sat_zenith_in = UPSCALING_1000M(sat_zenith_tn)
   solar_azimuth_in = UPSCALING_1000M(solar_azimuth_tn)
   sat_azimuth_in = UPSCALING_1000M(sat_azimuth_tn)
   sst_in = UPSCALING_1000M(sea_surface_temperature_tx)

   where UPSCALING_1000M is a generic function to interpolate a field at 1000m resolution (e.g. griddata in MATLAB language).

4. The following SLSTR field must be derived by mean of a down-scaling (averaging over a 2x2 box from 500m resolution field) at 1000m resolution:

solar_zenith_in = DOWNSCALING_1000M(solar_zenith_an)
SX_radiance_in = DOWNSCALING_1000M (SX_radiance_an) X = 1 to 6

where DOWNSCALING_1000M is a generic function to resample a field at 1000m resolution. In MATLAB language, the code should be, if A_500m is an image at 500m resolution:

```
B =  ones(2)/4;
A_1km = conv2(A_500m,B,'valid');
A_1km = A_1km(1:2:end,1:2:end);).
```

5. Using data from above, the following quantities must to be calculated:

 - Reflectance of visible band at 1km resolution
   SX_reflectance_in = π*SX_radiance_in/(cos(solar_zenith_in) * SX_solar_irradiance) (X = 1 to 6)

 - Normalized-Difference Snow Index and Normalized Difference Vegetation Index at 1km resolution:
   NDSI = (S1_reflectance_in - S5_reflectance_in) / (S1_reflectance_in + S5_reflectance_in)
   NDVI = (S3_reflectance_in – S2_reflectance_in) / (S3_reflectance_in + S2_reflectance_in)

 - Scattering angle:
   GAMMA = acos[-(cos(sat_zenith)*cos(solar_zenith) + sin(sat_zenith)*sin(solar_zenith)*cos(sat_azimuth))]

 - Air Mass:
   THETA = 1 / cos(sat_zenith)

File name convention

PDFs are stored in NETCDFv4 files. Files name are of the form:

pdf_XXX_SST_ANGLE.nc

with XXX:

- DAY (for pixel with solar zenith angle < 85 ° and with no sun-glint)
- SUNGLINT (for pixel with solar zenith angle < 85 ° and with sun-glint)
- NIGHT (for pixel with solar zenith angle ≥ 85 °)
- TWILIGHT (for pixel with 85°≤solar zenith angle ≤ 95 °)

SST (sea surface temperature) can be:

- -2.5 (for pixels with SST <= 0 °C)
- 0.0 (for pixels with 0 < SST <= 2.5 °C)
- 2.5 (for pixels with 2.5 < SST <= 5.0 °C)
- 5.0 (for pixels with 5.0 < SST <= 7.5 °C)
- 7.5 (for pixels with SST > 7.5 °C)

ANGLE for day time is the scattering angle (GAMMA) and can be:

- 80 (for pixels with GAMMA < 80°)
- 90 (for pixels with 80° <= GAMMA < 90°)
- 100 (for pixels with 90° <= GAMMA < 100°)

- 110 (for pixels with 100° <= GAMMA < 110°)
- 120 (for pixels with 110° <= GAMMA < 120)
- 130 (for pixels with GAMMA > 120°)

ANGLE for night time is the air mass THETA and can be:

- 1.0 (for pixels with 1 <= THETA < 1.1)
- 1.3 (for pixels with 1.1 <= THETA < 1.3)
- 1.5 (for pixels with 1.3 <= THETA < 1.5)
- 1.7 (for pixels with 1.5 <= THETA < 1.7)
- 1.9 (for pixels with 1.7 <= THETA < 1.9)
- 2.0 (for pixels with THETA > = 1.9)

N is the combination number and identifies the combination of variables used for the PDF according to tables 6 and 7. It could be 1 to 8 for night and 1 to 48 for day, sunglint and twilight scenarios.

File name example: pdf_night_00.0_1.30_comb_1.nc

where:

XXX = night (PDF for night time pixels)

SST = 0.0 °C (PDF for pixels with 0 < SST <= 2.5 °C)

THETA = 1.30 (PDF for pixels with 1.1 <= THETA < 1.3)

N = 1 means that variables used are:

1. Local Standard Deviation of Brightness Temperature @12μm (3x3 pixel area SLSTR band S9)
2. Brightness Temperature @ 10.95 μm (SLSTR band S8)
3. Brightness Temperature difference @ 10.95 – 12 μm (SLSTR band S8 and S9)
4. Brightness Temperature difference @ 10.95 - 3.74 μm (SLSTR band S8 and S7)

Global attributes

NETCDF file has 3 global attribute:

1. Date of creation: a string with the date of creation of the netcdf file.
2. Variables: a string with the short name of the variables used, as:
   LSTD @ 12, BT @ 10.95, BT @ 10.95-12, BT @ 10.95-3.74
3. for day time: Scattering Angle in decimal degrees, with the value of GAMMA (the same in the file name).
   For night time: Inverse of the cosine of the satellite zenith angle, with the value of THETA (the same in the file name).
4. Sea surface temperature in Celsius degree, with the value of the SST, (the same in the file name)

Dimensions and variables

Each NETCDF file has a certain number of NETCDF dimensions (6 for day time, twilight and sunglint condition and 4 for nigh time) with name and length. These dimensions are the SLSTR variables used for the classification. The values of these dimensions are contained in specific NETCDF variables.

The number of the variables in each NETCDF files is the sum of the dimensions (6 or 4) and the 3 PDF multidimensional array. The variables that describes the dimension's values have a short name (e.g. BT @ 10.95-12), a dimension length (e.g. 23) and a long name with a description of what SLSTR bands are used (e.g. Brightness Temperature difference @ 10.95 - 12 micrometre (SLSTR band S8 and S9)).

The values of these dimensions are stored as string in an attribute variable named 'Edge Values', that has to be understood as the edges of bins.

For example:

Edge Values = '-Inf -0.6 -0.5 -0.4 -0.3 -0.2 -0.1 0.0 0.1 0.2 0.3 0.4 0.5 0.6 0.7 0.8 0.9 1 1.1 1.2 1.3 1.4 1.5 Inf'

means the SLSTR brightness difference between channels S8 and S9 must be partitioned into bins with the bin edges specified by the vector above.

The value of the difference of a generic pixel is in the k-th bin if

BT @ 10.95-12 (k) ≤ S8-S9(i) < BT @ 10.95-12 (k+1).

BT @ 10.95-12 (1) is the left edge of the first bin, and BT @ 10.95-12 (end) is the right edge of the last bin.

For each SLSTR variable or combination of variables, this discretization provides the coordinates to obtain the probability of a pixel of being cloud, ice or sea.

For example, if

BT(S8)-BT(S9) = -0.31 K

then, according the bin edges above, bin = 4

The probability of a pixel being cloud, ice or sea is stored in 3 multidimensional variables. The short and long names are

Short name	Long Name
pdf_cloud	Probability of cloud pixel
pdf_sea	Probability of ice pixel
pdf_ice	Probability of sea pixel

The PDF values are multidimensional array with 6 dimensions for day time and 4 dimension for night time. The length of each of these dimension is the same of the length variables that contains the values of variables minus one.

Dump of the pdf_night_00.0_1.30_comb_1.nc file

Format: netcdf4

```
Global Attributes:
  Date of creation = '13-Apr-2017'
  Variables        = 'LSTD @ 12, BT @ 10.95, BT @ 10.95-12, BT @ 10.95-3.74'
  Air Mass { (cos(SAT_ZENITH))**-1 }       = 1.1
  Sea Surface Temperature (ancillary data) in Celsius Degree = -2.5
Dimensions:
  LSTD @ 12       = 11
  BT @ 10.95      = 48
  BT @ 10.95-12   = 23
  BT @ 10.95-3.74 = 67
Variables:
    pdf_cloud
  Size:       11x48x23x67
  Dimensions: LSTD @ 12,BT @ 10.95,BT @ 10.95-12,BT @ 10.95-3.74
  Datatype:   uint8
  Attributes:
     _FillValue = 0
     long_name  = 'Probability of cloud pixel'
    pdf_ice
  Size:       11x48x23x67
  Dimensions: LSTD @ 12,BT @ 10.95,BT @ 10.95-12,BT @ 10.95-3.74
  Datatype:   uint8
  Attributes:
     _FillValue = 0
     long_name  = 'Probability of ice pixel'
    pdf_sea
  Size:       11x48x23x67
  Dimensions: LSTD @ 12,BT @ 10.95,BT @ 10.95-12,BT @ 10.95-3.74
  Datatype:   uint8
  Attributes:
     _FillValue = 0
     long_name  = 'Probability of sea pixel'
    LSTD @ 12
  Size:       11x1
  Dimensions: LSTD @ 12
  Datatype:   single
  Attributes:
     long_name   = 'Local Standard Deviation of Brightness Temperature @                          12 micrometer (3x3
pixel area SLSTR band S9)'
     Edge Values = '-Inf 0.3 0.6 0.9 1.2 1.5 1.8 2.1 2.4 2.7 3 Inf'
    BT @ 10.95
  Size:       48x1
  Dimensions: BT @ 10.95
  Datatype:   single
  Attributes:
     long_name   = 'Brightness Temperature @ 10.95 micrometer (SLSTR band S8)'
     Edge Values = '-Inf  234  235  236  237  238  239  240  241  242  243  244  245  246  247  248  249  250  251  252
253  254  255  256  257  258  259  260  261  262  263  264  265  266  267  268  269  270  271  272  273  274  275
276  277  278  279  280  Inf'
    BT @ 10.95-12
  Size:       23x1
  Dimensions: BT @ 10.95-12
  Datatype:   single
```

Attributes:
long_name = 'Brightness Temperature difference @ 10.95 - 12 micrometer (SLSTR band S8 and S9)'
Edge Values = '-Inf -0.6 -0.5 -0.4 -0.3 -0.2 -0.1 1.110223e-16 0.1 0.2 0.3 0.4 0.5 0.6 0.7 0.8 0.9 1 1.1 1.2 1.3 1.4 1.5 Inf'
BT @ 10.95-3.74
Size: 67x1
Dimensions: BT @ 10.95-3.74
Datatype: single
Attributes:
long_name = 'Brightness Temperature difference @ 10.95 - 3.74 micrometer (SLSTR band S8 and S7)'
Edge Values = '-Inf -7 -6.9 -6.8 -6.7 -6.6 -6.5 -6.4 -6.3 -6.2 -6.1 -6 -5.9 -5.8 -5.7 -5.6 -5.5 -5.4 -5.3 -5.2 -5.1 -5 -4.9 -4.8 -4.7 -4.6 -4.5 -4.4 -4.3 -4.2 -4.1 -4 -3.9 -3.8 -3.7 -3.6 -3.5 -3.4 -3.3 -3.2 -3.1 -3 -2.9 -2.8 -2.7 -2.6 -2.5 -2.4 -2.3 -2.2 -2.1 -2 -1.9 -1.8 -1.7 -1.6 -1.5 -1.4 -1.3 -1.2 -1.1 -1 -0.9 -0.8 -0.7 -0.6 -0.5 Inf'

Appendix 2: List of granules used for SAR comparison

1. 20161110T203725
2. 20161117T105912
3. 20161117T191208
4. 20161117T205007
5. 20161118T103301
6. 20161119T114449
7. 20161119T114749
8. 20161119T150348
9. 20161119T200045
10. 20161119T214144
11. 20161120T193434
12. 20161120T211234
13. 20161121T204623
14. 20161122T121016
15. 20161122T220111
16. 20161126T120631
17. 20161127T114020
18. 20161127T213416
19. 20161129T204154
20. 20161130T120247
21. 20161130T215342
22. 20161130T215642
23. 20170102T192237
24. 20170104T183015
25. 20170112T182246
26. 20170113T111838
27. 20170113T193734
28. 20170117T161151
29. 20170119T151930
30. 20170119T170029
31. 20170119T184128
32. 20170119T202227
33. 20170120T132119
34. 20170121T125509
35. 20170124T095237
36. 20170124T113636
37. 20170124T213031
38. 20170125T111025
39. 20170125T125124
40. 20170125T143223
41. 20170125T174522
42. 20170125T192921
43. 20170126T140612
44. 20170127T115902
45. 20170127T134002
46. 20170128T113251
47. 20170128T131351
48. 20170128T204548
49. 20170129T124740
50. 20170130T085930
51. 20170130T104030
52. 20170130T122129
53. 20170130T140228
54. 20170131T041822
55. 20170202T223451
56. 20170207T121400
57. 20170211T202612
58. 20170212T181902
59. 20170213T060856
60. 20170213T130153
61. 20170213T143652
62. 20170307T165047
63. 20170308T043141
64. 20170308T075640
65. 20170308T093739
66. 20170308T111838
67. 20170308T112138
68. 20170308T125937
69. 20170308T130237
70. 20170308T144337
71. 20170308T161536
72. 20170321T225812
73. 20170326T225216
74. 20170326T233616
75. 20170326T234216
76. 20170331T130325
77. 20170331T163123
78. 20170331T194122
79. 20170401T155612
80. 20170401T173712
81. 20170402T122003
82. 20170404T194037
83. 20170408T111756
84. 20170408T125556
85. 20170410T134433
86. 20170410T220029
87. 20170424T105959
88. 20170427T112226
89. 20170429T202659
90. 20170430T200348
91. 20170501T225636
92. 20170502T104930
93. 20170503T102619
94. 20170503T120719
95. 20170505T125556